

Manuscript Number: GEOMOR-8878R1

Title: Predicting gully occurrence at watershed scale: comparing topographic indices and multivariate statistical models

Article Type: Research Paper

Keywords: Gully erosion susceptibility; Topographic indices; Multivariate Adaptive Regression Splines (MARS); Logistic Regression (LR)

Corresponding Author: Professor Christian Conoscenti, Ph.D.

Corresponding Author's Institution: University of Palermo, Italy

First Author: Christian Conoscenti, Ph.D.

Order of Authors: Christian Conoscenti, Ph.D.; Edoardo Rotigliano, Ph.D.

Abstract: In this study, the ability of five topographic indices to predict the gully trajectories observed in two adjacent watersheds located in Sicily (Italy) was evaluated. Two of these indices, named MSPI and MTWI, as far as we know, have never been employed to this aim. They were obtained by multiplying the stream power index (SPI) and the topographic wetness index (TWI), respectively, by the convergence index (CI). The predictive ability of the topographic indices was measured by using both cut-off independent (AUC: area under the receiver operating characteristic curve) and dependent statistics (Cohen's kappa index  $\kappa$ , sensitivity, specificity). These statistics were calculated also for 100 MARS (multivariate adaptive regression splines) and 100 LR (logistic regression) model runs, which used as predictors the topographic variables (i.e. contributing area, slope steepness, plan curvature and convergence index) combined into the five indices. Performance statistics of both topographic indices and statistical models were calculated using 100 random samples of 2 m grid cells, which were extracted only from flow concentration lines. This was done in order to focus the validation process on where gully erosion is more likely to occur. MSPI achieved the best predictive skill (AUC > 0.93;  $\kappa$  > 0.71) among the topographic indices and exhibited similar and better accuracy than local (i.e. trained and validated in the same watershed) and transferred (i.e. trained in one watershed and tested in the other one) LR models, respectively. On the other hand, MSPI performed similarly to transferred MARS runs (AUC > 0.92;  $\kappa$  > 0.71) but slightly worse than local MARS runs (AUC > 0.95;  $\kappa$  > 0.77). Based on the results of this experiment, it can be inferred that (i) including CI helps in detecting hollow areas where gullies are more likely to occur and (ii) MPSI can be a valid alternative to a data driven approach for mapping gully erosion susceptibility in areas where a gully inventory is not available, which is necessary to calibrate statistical models.

Research Data Related to this Submission

-----  
There are no linked research data sets for this submission. The following reason is given:

Data will be made available on request

Dear Editor, we have revised our work and manuscript in order to address comments and suggestions of the three reviewers.

---RESPONSES TO COMMENTS OF REVIEWER #1---

#### GENERAL COMMENT

This is a well-written article with clearly defined objectives, methods, results, and discussion. The study presents statistical and geospatial evaluation of the predictive performance of five topographic index models and two statistical modeling approaches. In addition to three standard TI models, two modified models were introduced by adding a convergence index CI to SPI and TWI models. This addition seemed to improve the gully predictions by adding sort of a "weighting" factor to each cell that would enforce channel incision. While this modification did not improve the TWI model's prediction, it drastically enhanced the prediction ability of the SPI model. The TWI model has a logarithmic form while the SPI model is a simple two factor product. The two statistical models (LR and MARS) unsurprisingly outperformed the TI models due to their extensive calibration on topographic attributes prior to their application to the watershed. It was interesting to learn that the thresholds for topographic index models and occurrence statistics were found to be in the range of the ones reported for Kansas, USA. With different soil types, land management, rainfall characteristics, etc, in two regions of the world, basic topographic features (slope, contributing area, curvature, convergence) appeared to yield similar results. Gullies provide sources of extensive erosion and their placement in the watershed is not yet fully understood, a development of predictive techniques is of paramount importance for watershed management and planning. I recommend the article to be published after minor comments below are addressed.

#### RESPONSE

Dear Reviewer, the authors wish to thank you for having read carefully our work and for having appreciated, as well as for your valuable suggestions. We have modified our manuscript to address your suggestions.

#### COMMENT #1

L. 148: "combine two or more primary topographic attributes". Which ones? Recommend providing examples.

#### RESPONSE #1

We added: "including contributing area, slope steepness, plan curvature and convergence index agree". These are the primary topographic attributes which were combined.

#### COMMENT #2

L. 149: Any topographic index modelling heavily relies on the quality of DEM. A more specific description of the locally-developed Lidar-based DEM would be appreciated, the URL refers to a site in Italian.

#### RESPONSE #2

We agree. We added more details, providing information about vertical accuracy of the DEM. Moreover, we provided a new URL (WMS server) which can be used to load the DEM in a GIS software.

#### COMMENT #3

L. 197: "where CI (m) is the convergence index (Köthe et al., 1996)." Although the basic description of the CI index is presented, the mathematical definition remains unclear. The citation refers to publication in German with no English translation. Since this index provides a significant improvement to the SPI model, providing mathematical and possibly graphical representation would be very helpful.

#### RESPONSE #3

Thanks for this comment. We definitely agree. We added more details about how CI is calculated. We hope that now is more clear.

**COMMENT #4**

Table 1 and Table 2. The values in the tables have 4 or 3 decimal places. Recommend maybe rounding up to the same number, say 3?

**RESPONSE #4**

We agree, 4 decimal places are too much. We rounded up the values of Table 1 to 3 decimal places. We also rounded to 1 or 2 decimal places large numbers of Table 2.

---RESPONSES TO COMMENTS OF REVIEWER #2---

GENERAL COMMENT

Dear Editor

I have read this article very carefully. Unfortunately I have the following concerns. I am not satisfy with present form of this article. I am not positive for my decision.

**RESPONSE**

Dear Reviewer, the authors wish to thank you for having read carefully our work and for having provided very useful suggestions and comments which helped us to improve our manuscript. We have modified our manuscript to address your suggestions/comments.

COMMENT #1

Highlights (for review)

In the first highlight, please remove word of "we".

**RESPONSE #1**

Ok, done. We rephrased the point to: "The ability of five topographic indices to predict gullies was evaluated"

COMMENT #2

Headers

Headers aren't according to reference format, for example " ABSTRACT" isn't correct, please replace with "Abstract"

**RESPONSE #2**

Ok, done. We changed the title of the abstract paragraph according to the suggestion.

COMMENT #3

In general, please remove word of "we" from all of text. This isn't suitable for international publications.

**RESPONSE #3**

The active voice we + verb was changed to the passive voice.

COMMENT #4

Line 16: five or four indices?

**RESPONSE #4**

(Line 16) - We changed line 16 and we hope that now is more clear. The topographic indices are five. These are made by different combinations of four primary topographic attributes (i.e. contributing area, slope steepness, plan curvature and convergence index).

COMMENT #5

In general, abstract is so vague... it is important to clear this part very carefully.

**RESPONSE #5**

We changed some parts of the abstract and we hope that now is less vague. Indeed, it provides information about the indices and the statistical models employed to predict the gullies, the validation strategy, the metrics employed to measure the predictive performance, the results and the conclusions.

COMMENT #6

1. Introduction

Line 42: "Gullying" isn't a correct word. Please edit it.

Lines 113-116: these paragraph isn't suitable for introduction.

#### RESPONSE #6

(Line 42) - We are sorry but the term “gullying” is often used as a synonym of “gully erosion” in a number of very important publications. For example: “Gully Erosion: Procedures to Adopt When Modelling Soil Erosion in Landscapes Affected by Gullying” (Poesen, Torri, Van Wallegem, 2011) or “Badlands and gullying” (Howard, 2009).

(Lines 113-116) – We agree. The paragraph was moved to the methods section (lines 291-294).

#### COMMENT #7

2.1. Study area and gully inventory

Lines 135-137: authors just used from GE images? Any field surveys?

Line 139: please introduce source a 2-m raster DEM.

#### RESPONSE #7

(Lines 135-137) - Actually, the gully inventory was prepared by analyzing the GE image dated 3 May 2015, but also field surveys to check the inventory were performed. Now we specify it in the text. However, we specified that most of the gully channels in the drainage basins are ephemeral and are usually filled in by tillage within few months after their initiation. Thus not all the mapped gullies were visible in the field or in more recent GE images.

(Line 139) - We added more details about the DEM and a new URL (WMS server) which can be used to load the DEM in a GIS software. (Lines 116-117)

#### COMMENT #8

2.2. Topographic indices

Eq. 2, *PLANC* is plan curvature... please write plan curvature in text.

Eqs. 4 and 5: I am not satisfy from these two indices because they are using from *CI* and this index used from *AS* and *S*... So, I think authors used from double *AS* and *S*. Is this correct?

#### RESPONSE #8

(Eq. 2) – *PLANC* is explained just below the equation, as done for *As* (specific contributing area) and *S* (slope gradient). Moreover, *PLANC* is employed in many other papers to refer to “plan curvature”.

(Eqs. 4 and 5) – Now we explained better how *CI* is calculated (Lines 190-195). This attribute is calculated from slope aspect (not from *As* and/or *S*).

#### COMMENT #9

2.3. Statistical modelling

It is better to authors separate description of models from multicollinearity test. In general, I think methodology needs to write better than previous to remove some vague.

Line 228: how many gully locations do you find in two watersheds? Authors written 1928 and 717 cells. How many gully locations?

#### RESPONSE #9

In the 2.3 section, we explain that the topographic attributes *As*, *S*, *PLANC* and *CI*, were used as independent variables of *MARS* and *LR* models. Since these statistical techniques require absence of multicollinearity, we simply verified that there was no strong relationship between the topographic attributes employed as predictors. We do not consider this as a result of the research, that's why we reported it in the methods section.

(Line 228) – Thanks for this comment, we realized that we did not provide this important information. In the revised version of the manuscript, we specify in line 141 that “The inventory includes 115 gullies (83 in W1, 32 in W2)”.

#### COMMENT #10

##### 2.5. Gully prediction maps

Line 290: the four ensemble statistical models? Ensemble models?

In general, I think it is important to add a flowchart of used methodology. Really, methodology is written difficult to understand it.

#### RESPONSE #10

(Line 290) – Dear Reviewer, thanks for this comment. We followed your suggestion and added a flow chart (new Fig. 1) to schematically explain the methodology. We hope that it helps to understand the following steps: 1) random selection of 100 calibration samples for W1 and 100 for W2, each including 25% of the gully pixels and the same number of non-event pixels; 2) Each of this sample was used to calibrate one LR and one MARS model, thus we have calibrated 100 LR and 100 MARS models; 3) random selection of 100 validation samples for W1 and 100 for W2 (each including 25% of the gully pixels and the same number of non-event pixels); 4) for both LR and MARS, calculation of gully probability for the pixels of each validation sample by averaging the score provided by the 100 model runs. Thus we have for one validation pixel 100 probability values, which were averaged to provide one value of gully probability. As explained in line 262 (and in the flow-chart), the “LR and MARS ensemble models” are prepared by averaging the score of the 100 model runs.

We report here the following text taken from Kotu and Deshpande, 2015 (citation added to the manuscript), which explain well what an ensemble model is: “Ensemble modeling is a process where multiple diverse models are created to predict an outcome, either by using many different modeling algorithms or using different training data sets. The ensemble model then aggregates the prediction of each base model and results in once final prediction for the unseen data.” <https://www.sciencedirect.com/topics/computer-science/ensemble-modeling>

In our case, the ensemble model is prepared “using different training data sets” and calculating the average value of probability.

#### COMMENT #11

##### 3. Results

This part started by sub-header "predictive performance measured..."

I think author at first have to write about gully prediction maps and then add validation and other things.

#### RESPONSE #11

Dear Reviewer, we first present the results of the validation process because these serve as premise to understand the reliability of the models which were applied to all the study area to prepare the gully erosion susceptibility maps.

#### COMMENT #12

##### 4. Discussion

This part written the same with introduction, indeed it isn't a discussion (Lines 374-390).

I don't know why authors presented text without and with figures... any reason?

#### RESPONSE #12

Dear Reviewer, we added this part because we think that a comparison with the results found in other areas by applying the same indices could be very useful (as also highlighted by Reviewer #1).

We believe that the figure showing the kernel density plots of *CI* and *PLANC* is useful in the discussion section, because it supports the hypothesis that the contribution of *CI* in increasing the ability to discriminate between non-gully and gully cells is higher than that provided by *PLANC*.

#### COMMENT #13

Figures:

What is your reason for adding Fig. 2? You don't use from these factors in your analysis.

In Fig. 3, contour lines are 10-m, but in Fig. 4 they are 2-m. which one?

I cant understand Fig. 7. Please present gully erosion map for each watershed separately.

#### RESPONSE #13

Dear Reviewer, we believe that the maps shown in Fig. 2 (Fig. 3 in the revised version) could be useful for the reader. Indeed, the elevation map (DEM) is used to derive the topographic variables; slope angle is included in the topographic indices and is used as predictor variable of LR and MARS models; Lithology and Soil use maps (as well as elevation and slope) may help in understanding the geomorphological setting of the area.

We used different contour intervals because Fig. 3 (Fig. 4 in the revised version) shows the entire area whereas Fig. 4 (Fig. 5 in the revised version) shows at larger scale a small portion of the area to highlight the correspondence between flow lines and gully trajectories.

Fig. 7 (Fig. 8 in the revised version) shows two small portions of the catchments W1 and W2, corresponding to the GE views shown in Fig. 3 (Fig. 4 in the revised version).

#### ---RESPONSES TO COMMENTS OF REVIEWER #3---

##### GENERAL COMMENT

I read the manuscript carefully. I found it interesting and practical. However, there are some unclear points and drawbacks in the manuscript.

I have provided some minor comments to improve the manuscript.

##### RESPONSE

Dear Reviewer, the authors wish to thank you for having read carefully our manuscript and for having provided very useful suggestions. We have modified our manuscript in order to address your comments.

#### COMMENT #1

It's interesting that you have used two indices (MSPI and MTWI) for the first time in this field of study. I'm not sure that they have developed by authors or they are previously available. If the later is correct, please add their original citations. In addition, these indices are the main part of the study and readers expect to get some information regarding them. Please describe these indices in detail and say how they can reflect gully erosion (direct and indirect impacts).

##### RESPONSE #1

Thanks for this comment. As far as we know, the two indices, which we called MSPI and MTWI, have never been proposed or used before. We added more details about how MSPI and MTWI are calculated and about the expected relationship with the spatial distribution of the gullies.

#### COMMENT #2



Literature review should be improved. There are some studies that used data-mining and machine learning models for gully-erosion susceptibility mapping. Please consider them in the introduction and discussion sections.

**RESPONSE #2**

Dear reviewer, in the revised version of our manuscript we consider also the contribution of other recent studies which employed data-mining and machine learning models to map gully-erosion susceptibility.

**COMMENT #3**

I agree with this sentence in the manuscript "MPSI can be a valid alternative to a data driven approach for mapping gully erosion susceptibility in areas where a gully inventory is not available" but authors have improperly proposed this point in the Highlight section. Data-mining and machine learning always perform better than a single index when a gully erosion inventory is available.

**RESPONSE #3**

We agree, thus we changed the highlight point to: "*MSPI* can be an alternative to a data-driven approach if gullies are not yet mapped"

- The ability of five topographic indices to predict gullies was evaluated
- Two of these indices, named *MSPI* and *MTWI*, have never been used to predict gullies
- Among the indices tested, *MSPI* ( $= SPI \cdot CI$ ) exhibited the best accuracy
- The convergence index (*CI*) helps in detecting where a gully is more likely to occur
- *MSPI* can be an alternative to a data-driven approach if gullies are not yet mapped

# Predicting gully occurrence at watershed scale: comparing topographic indices and multivariate statistical models

Christian Conoscenti, Edoardo Rotigliano

## A B S T R A C T

In this study, the ability of five topographic indices to predict the gully trajectories observed in two adjacent watersheds located in Sicily (Italy) was evaluated. Two of these indices, named *MSPI* and *MTWI*, as far as we know, have never been employed to this aim. They were obtained by multiplying the stream power index (*SPI*) and the topographic wetness index (*TWI*), respectively, by the convergence index (*CI*). The predictive ability of the topographic indices was measured by using both cut-off independent (*AUC*: area under the receiver operating characteristic curve) and dependent statistics (Cohen's kappa index  $\kappa$ , sensitivity, specificity). These statistics were calculated also for 100 MARS (multivariate adaptive regression splines) and 100 LR (logistic regression) model runs, which used as predictors the topographic variables (i.e. contributing area, slope steepness, plan curvature and convergence index) combined into the five indices. Performance statistics of both topographic indices and statistical models were calculated using 100 random samples of 2 m grid cells, which were extracted only from flow concentration lines. This was done in order to focus the validation process on where gully erosion is more likely to occur. *MSPI* achieved the best predictive skill ( $AUC > 0.93$ ;  $\kappa > 0.71$ ) among the topographic indices and exhibited similar and better accuracy than local (i.e. trained and validated in the same watershed) and transferred (i.e. trained in one watershed and tested in the other one) LR models, respectively. On the other hand, *MSPI* performed similarly to transferred MARS runs ( $AUC > 0.92$ ;  $\kappa > 0.71$ ) but slightly worse than local MARS runs ( $AUC > 0.95$ ;  $\kappa > 0.77$ ). Based on the results of this experiment, it can be inferred that (i) including *CI* helps in detecting hollow areas where gullies are more likely to occur and (ii) *MPSI* can be a valid alternative to a data driven approach for mapping gully erosion susceptibility in areas where a gully inventory is not available, which is necessary to calibrate statistical models.

# 1 Predicting gully occurrence at watershed scale: comparing 2 topographic indices and multivariate statistical models

3 Christian Conoscenti <sup>a,\*</sup>, Edoardo Rotigliano <sup>a</sup>

4 <sup>a</sup>Department of Earth and Marine Sciences (DISTEM), University of Palermo, Via Archirafi 22, 90123 Palermo,  
5 Italy

## 6 ~~ABSTRACT~~

### 7 Abstract

8  
9 In this study, ~~we evaluated~~ the ability of five topographic indices to predict the gully trajectories  
10 observed in two adjacent watersheds located in Sicily (Italy) ~~); was evaluated~~. Two of these indices,  
11 named *MSPI* and *MTWI*, as far as we know, have never been employed to this aim. They were  
12 obtained by multiplying the stream power index (*SPI*) and the topographic wetness index (*TWI*),  
13 respectively, by the convergence index (*CI*). The predictive ability of the topographic indices was  
14 measured by using both cut-off independent (*AUC*: area under the receiver operating characteristic  
15 curve) and dependent statistics (Cohen's kappa index  $\kappa$ , sensitivity, specificity). These statistics  
16 were calculated also for 100 MARS (multivariate adaptive regression splines) and 100 LR (logistic  
17 regression) model runs, which used as predictors the topographic variables ~~combined in the five~~  
18 ~~indices~~ (i.e. contributing area, slope steepness, plan curvature and convergence index) ~~); combined~~  
19 ~~into the five indices~~. Performance statistics of both topographic indices and statistical models were  
20 calculated using 100 random samples of 2 m grid cells, ~~which were~~ extracted only from flow  
21 concentration lines. This was done in order to focus the validation process ~~on~~ where gully erosion is  
22 more likely to occur. *MSPI* achieved the best predictive skill ( $AUC > 0.93$ ;  $\kappa > 0.71$ ) among the

Formatted: Font color: Text 1

Formatted: Font color: Text 1

Formatted: Font color: Text 1,  
Border: : (No border), Pattern: Clear  
(White)

Formatted: Font color: Text 1

Formatted: Font color: Text 1

Formatted: Font color: Text 1

Formatted: Font color: Text 1

Formatted: Font color: Text 1, Italian  
(Italy)

Formatted: Font color: Text 1

Formatted: Font color: Text 1

Formatted: Font color: Text 1

Formatted: Font color: Text 1

Formatted: Font color: Text 1

Formatted: Font color: Text 1, Italian  
(Italy)

Formatted: Font color: Text 1

23 topographic indices and exhibited similar and better accuracy than local (i.e. trained and validated  
24 in the same watershed) and transferred (i.e. trained in one watershed and tested in the other one) LR  
25 models, respectively. On the other hand, *MSPI* performed similarly to transferred MARS runs  
26 ( $AUC > 0.92$ ;  $\kappa > 0.71$ ) but slightly worse than local MARS runs ( $AUC > 0.95$ ;  $\kappa > 0.77$ ). Based on  
27 the results of this experiment, ~~we infer~~ it can be inferred that (i) including *CI* helps in detecting  
28 hollow areas where gullies are more likely to occur and (ii) *MPSI* can be a valid alternative to a data  
29 driven approach for mapping gully erosion susceptibility in areas where a gully inventory is not  
30 available, which is necessary to calibrate statistical models.

31  
32 *Keywords:* Gully erosion susceptibility; Topographic indices; Multivariate Adaptive Regression  
33 Splines (MARS); Logistic Regression (LR); Geographic Information System (GIS)

34 ▲  
35 \* Corresponding author. Tel.: +39 09123864670; fax: +39 0916169908. E-mail address:  
36 christian.conoscenti@unipa.it (C. Conoscenti).

Formatted: Font color: Text 1, Italian (Italy)

Formatted: Font color: Text 1

Formatted: Font color: Text 1, Italian (Italy)

Formatted: Font color: Text 1

Formatted: Font color: Text 1

Formatted: Font color: Text 1, Pattern: Clear

Formatted: Font color: Text 1

38 **1. Introduction**

39 Gully erosion causes land degradation in a wide range of environmental conditions. The  
40 development of gullies in agricultural watersheds may induce high soil loss and reduction of water  
41 availability, leading to a significant decrease of soil quality and crop yield. Moreover, gully  
42 channels hamper the trafficability of the fields causing extra damages and costs to farmers (Poesen  
43 et al., 2003, 2011).

44 Gullying is a threshold phenomenon that is mainly controlled by rainfall, topography, soil, lithology  
45 and land use. Gullies occur only after a threshold of runoff erosivity and soil erodibility is  
46 exceeded. In addition to rainfall, runoff erosive power depends on topography which regulates  
47 discharge, concentration and velocity of overland flow (e.g., Moore et al., 1988; Desmet et al.,  
48 1999; Poesen et al., 2003; Valentin et al., 2005; Gómez-Gutiérrez et al., 2009a; Daggupati et al.,  
49 2013; Conoscenti et al., 2013). Morphology, density and development of gullies in a given  
50 landscape is also significantly controlled by parent material (Oostwoud Wijdenes et al., 2000;  
51 Vandekerckhove et al., 2001; Poesen et al., 2011). Furthermore, gully occurrence is controlled by  
52 resistance of soil, which is influenced by soil properties such as texture, bulk density, moisture  
53 conditions, organic matter content (Poesen et al., 2003). Soil erosion susceptibility is also related to  
54 crop type and stage, as well as tillage direction and conservation practices (Parker et al., 2007).  
55 Also, several studies have reported triggering of gullies or increasing of gully erosion rates as being  
56 caused by land use changes, intensification of farming activities and overgrazing (Poesen et al.,  
57 2003; Valentin et al., 2005; Zucca et al., 2006; Gómez-Gutiérrez et al., 2009b).

58 Planning of gully erosion control in agricultural watersheds requires either quantifying soil loss and  
59 predicting gully location. Several process-based models have been developed to quantify gully  
60 erosion (e.g., CREAMS, Knisel, 1980; EGEM, Merkel et al., 1988; GLEAMS, Knisel, 1993;  
61 Sidorchuk, 1999; REGEM, Gordon et al., 2007). However, these models require physical input  
62 variables that are difficult to measure at the watershed scale. Soil loss due to gully erosion can be  
63 also evaluated by using empirical models which are based on relationships established between

Formatted: Font color: Text 1, Italian (Italy)

Formatted: Font color: Text 1

Formatted: Font color: Text 1, Italian (Italy)

Formatted: Font color: Text 1

64 volume and length of the gully channels (e.g., Nachtergaele et al., 2001; Capra and Scicolone, 2002;  
65 Capra et al., 2005; Caraballo-Arias et al., 2014, 2015).  
66 Prediction of gully location can be achieved by identifying a topographic threshold that has to be  
67 exceeded for a gully to form. A number of studies have proposed topographic threshold lines  
68 defined on a log-log plot of local slope gradient ( $S$ ) versus upslope contributing area ( $A$ ) measured  
69 at gully heads (e.g., Patton and Schumm, 1975; Montgomery and Dietrich, 1992; Nachtergaele et  
70 al., 2001b; Zucca et al., 2006; Nazari Samani et al., 2009). Both these topographic attributes are  
71 indeed widely considered to play the role of controlling factors in the gully formation process as  
72 they act as proxies for flow velocity and discharge, respectively. The approach based on  $S$ - $A$   
73 threshold lines assumes that for a given  $A$ , a critical  $S$  exists above which runoff erosivity is large  
74 enough to produce gully erosion. The  $S$ - $A$  threshold can be used to predict gullies by classifying a  
75 study area into non-event positions (below the threshold line) and event positions (on or above the  
76 threshold line). However, this approach tends to overestimate the likelihood of gully occurrence  
77 (Svoray et al., 2012; Gómez-Gutiérrez et al., 2015), providing a high number of false positives (i.e.  
78 non-gullied positions classified as gullied).

79 Furthermore, several topographic indices have been employed to predict gully location (e.g.,  
80 Thorne et al., 1986; Moore et al., 1988; Vandaele et al., 1996; Desmet et al., 1999). These models  
81 rely on the assumption that gully formation depends on a combination of primary topographic  
82 attributes (Wilson and Gallant, 2000) which reflect erosivity of concentrated overland flow; gully  
83 erosion occurs when the topographic index exceeds a critical threshold value. Daggupati et al.  
84 (2013), Sekaluvu et al. (2015) and Sheshukov et al. (2018) have compared the ability to  
85 discriminate between gullied and non-gullied areas of several topographic indices, which were  
86 applied using different thresholds. Their analyses revealed that gully predictions were not accurate  
87 without identifying an optimal threshold through local calibration. Indeed, they have observed that a  
88 low threshold causes high number of false positives whereas a high threshold produces high number  
89 of false negatives (i.e. gullied sites predicted as non-gullied).

Formatted: Font color: Text 1, Italian  
(Italy)

Formatted: Font color: Text 1

Formatted: Font color: Text 1, Italian  
(Italy)

Formatted: Font color: Text 1

90 Recently, accurate predictions of gully locations have been achieved by using statistical modeling  
91 and data mining techniques such as logistic regression, classification and regression trees,  
92 multivariate adaptive regression splines, stochastic gradient treeboost, artificial neural network,  
93 random forest, maximum entropy, etc. ~~(e.g., Meyer and Martínez-Casasnovas, 1999; Gómez-~~  
94 ~~Gutiérrez et al., 2009c; Eustace et al., 2011; Svoray et al., 2012; Conoscenti et al., 2014, 2018;~~  
95 ~~Dewitte et al., 2015; Angileri et al., 2016; Pourghasemi et al., 2017; Garosi et al., 2018, 2019)~~.(e.g.,  
96 Meyer and Martínez-Casasnovas, 1999; Gómez-Gutiérrez et al., 2009c; Eustace et al., 2011; Svoray  
97 et al., 2012; Conoscenti et al., 2014, 2018; Dewitte et al., 2015; Angileri et al., 2016; Pourghasemi  
98 et al., 2017; Rahmati et al., 2016, 2017a, 2017b; Garosi et al., 2018, 2019; Azareh et al., 2019;  
99 Choubin et al., 2019; Javidan et al., 2019). These techniques are able to analyze and model the  
100 relationships between gully locations and spatial variability of a set of environmental predictors  
101 related to topography, land use, parent materials and soils. Based on the identified statistical  
102 relationships, these techniques allow for calculating a probability of gully occurrence that ranges  
103 from 0 to 1, for each position (usually grid cell) in a given area. However, an important drawback in  
104 these procedures, which are data-driven, is that they generate prediction images which efficiently  
105 explain the gully distribution in the study area but tend to fail when exported to other areas, even if  
106 located at a close distance (Conoscenti et al., 2018).

107 This study focuses on investigating the topographic control of gully erosion caused by concentrated  
108 overland flow at watershed scale. The experiment was carried out in two small agricultural  
109 watersheds located in Sicily (Italy). The main goal of the study was to evaluate and compare the  
110 ability to predict the location of gullies achieved by using a set of topographic indices, which  
111 includes three indices previously proposed for predicting gully location and two modified versions  
112 of them. Predictive models of gully occurrence were prepared also by using logistic regression (LR;  
113 Hosmer and Lemeshow, 2000) and multivariate adaptive regression splines (MARS; Friedman,  
114 1991), two statistical modeling techniques which have been successfully used to this aim in  
115 previous studies (e.g., Vanwallegem et al., 2008; Gómez-Gutiérrez et al., 2009c; Svoray et al.,

Formatted: Font color: Text 1, Italian  
(Italy)

Formatted: Font color: Text 1



116 2012; Conoscenti et al., 2014, 2018; Dewitte et al., 2015). To further assess the ability to predict  
117 gully occurrence provided by the five topographic indices, their accuracy was compared with that  
118 achieved by LR and MARS models.

Formatted: Font color: Text 1, Italian (Italy)

Formatted: Font color: Text 1

## 120 2. Materials and Methods

Formatted: Font color: Text 1

121 ~~The statistical analyses~~In this study, the topographic analysis was carried out using a LiDAR-  
122 derived 2×2 m Digital Elevation Model (DEM; Regione Siciliana, 2010), with vertical accuracy of  
123 0.1–0.2 m. The GIS calculations were performed using SAGA-GIS software (Conrad et al., 2015).  
124 ~~The calibration of MARS and LR and the validation of both topographic indices and statistical~~  
125 ~~models~~ were performed using the R software (R Core Team, 2017) with the packages “raster”  
126 (Hijmans, 2017), “usdm” (Naimi, 2015), “splitstackshape” (Mahto, 2018), “pROC” (Robin et al.,  
127 2011), “ROCR” (Sing et al., 2005), “caret” (Wing and Kuhn, 2018) and “earth” (Milborrow, 2018).  
128 ~~The flow-chart of Fig. 1 shows a schematic overview of the methodology, which is described in~~  
129 ~~detail in the following sections.~~

Formatted: Font color: Text 1

Formatted: Font color: Text 1

## 131 3. Materials and Methods

Formatted: Font color: Text 1

### 132 3.1. Study area and gully inventory

133 The experiment was carried out in two adjacent agricultural watersheds located in central-western  
134 Sicily (Fig. 42), approximately 35 km south-east of the city of Palermo. The westernmost watershed  
135 (W1) drains an area of 621.7 ha whereas the easternmost one (W2) covers 901.4 ha. The study area  
136 experiences a typical Mediterranean climate with an average annual rainfall of 711 mm (time  
137 interval: 2002–2017; Camporeale rainfall station; Regione Siciliana – SIAS - Servizio Informativo  
138 Agrometeorologico Siciliano), with a minimum in July (5.6 mm) and a maximum in December  
139 (88.7 mm). Topography of the two investigated watersheds is slightly different (Fig. 2a3a–b):

Formatted: Font color: Text 1

Formatted: Font color: Text 1

140 elevation ranges from 185 to 576 m a.s.l. in W1 (mean = 303 m) and from 209 to 571 m a.s.l. in W2  
141 (mean = 345 m), whereas average slope gradient is  $10.1^\circ$  (SD =  $5.0^\circ$ ) and  $9.7^\circ$  (SD =  $6.9^\circ$ ),  
142 respectively. Soils are mostly regosols and vertisols with fine-medium texture (Fierotti, 1988).  
143 Lithologies are mainly eluvial-colluvial deposits, sands of the Late Miocene Terravecchia Fm.,  
144 clays of the Middle-Late Miocene Castellana Sicula Fm., silty-clays and sandy-silts of the  
145 Terravecchia Fm. (Fig. 2e3c). Primary land covers are arable lands (mainly cereal fields) and  
146 vineyards, which occupy 92% of W1 and 80% of W2 (Fig. 2d3d).

Formatted: Font color: Text 1

Formatted: Font color: Text 1

147 Both watersheds are affected by gully erosion which increases soil loss, causes landscape dissection  
148 and hampers the movement of farm machines. Most of the gully channels in the drainage basins are  
149 ephemeral and are usually filled in by tillage within few months after their initiation. Conoscenti et  
150 al. (2018) created a gully inventory of the watersheds by analyzing a Google Earth image acquired  
151 on 3 May 2015 (Fig. 3-4) and by carrying out field surveys. As their objective was to model gully  
152 erosion due to overland flow concentration, the inventory includes only gullies located on  
153 concentrated flow pathways. The latter were extracted from a ~~2-m raster Digital Elevation Model~~  
154 ~~(DEM; Regione Siciliana, 2010)~~ the DEM, by calculating for each cell the value of upstream  
155 contributing area. To ensure consistency between mapped gullies and contributing area, gully  
156 trajectories have been slightly modified in order to exactly match flow pathways and to ensure that  
157 contributing area increases along each gully from head to mouth (Fig. 45). The inventory includes  
158 115 gullies (83 in W1, 32 in W2) and reveals that gully erosion is more severe in W1 (gully density  
159 =  $0.73 \text{ km}^{-1}$ ) than in W2 ( $0.18 \text{ km}^{-1}$ ). Gullies mostly occur on eluvial-colluvial deposits and clays.  
160 As regards land cover, arable lands host most of the gully trajectories.

Formatted: Font color: Text 1

Formatted: Font color: Text 1

Formatted: Font color: Text 1

Formatted: Font color: Text 1

### 161 3.2. Topographic indices

162 In this experiment, ~~we assessed~~ the ability to predict gully location of five topographic indices ~~was~~  
163 ~~assessed. These indices,~~ which combine two or more primary topographic attributes (Wilson and  
164 Gallant, 2000). ~~These attributes), including contributing area, slope steepness, plan curvature and~~  
165 ~~convergence index,~~ were calculated for each grid cell of a ~~LiDAR-derived 2x2 m~~ the DEM (Regione

Formatted: Font color: Text 1

Formatted: Font color: Text 1

Formatted: Font color: Text 1

Formatted: Font color: Text 1

166 Siciliana, 2010), by using terrain analysis tools of SAGA-GIS software (Conrad et al., 2015).

Formatted: Font color: Text 1

167 Three topographic indices adopted here, namely stream power index (*SPI*), compound topographic  
168 index (*CTI*) and topographic wetness index (*TWI*), have been employed in previous studies to  
169 predict location of ephemeral gullies in cultivated watersheds (e.g., Vandaele et al., 1996; Parker et  
170 al., 2007; Daggupati et al., 2013, 2014; Sekaluvu et al., 2015; Sekaluvu and Sheshukov, 2016;  
171 Sheshukov et al., 2018).

172 The *SPI* (Moore et al., 1988, 1991) is a measure of erosive power of concentrated runoff and is  
173 calculated as:

174

$$175 \quad SPI = A_s \cdot S \quad (1)$$

176

177 where  $A_s$  ( $m^2 m^{-1}$ ) is the specific contributing area and  $S$  ( $m m^{-1}$ ) is the local slope gradient.  $A_s$  and  $S$   
178 are employed as surrogates for flow discharge and velocity.  $A_s$  was extracted from upslope  
179 contributing area ( $A$ ), which in turn was calculated by applying the single flow direction (also  
180 referred to as D8) algorithm (O'Callaghan and Mark, 1984), after filling sinks in the DEM. To  
181 obtain  $A_s$ ,  $A$  has to be divided by the contour width within the pixel (Desmet and Govers, 1996). As  
182 the contour width can be set to the average of the grid cell width (i.e., 2.0 m) and the grid cell  
183 diagonal (i.e., 2.8 m),  $A_s$  was calculated dividing  $A$  by 2.4.

Formatted: Font color: Text 1

184 The *CTI* (Thorne et al., 1986) is defined as:

185

$$186 \quad CTI = A_s \cdot S \cdot PLANC \quad (2)$$

187

188 where  $PLANC$  ( $m/100 m$ ) is the curvature of the contour line (Hengl and Reuter, 2008).  $PLANC$  is a  
189 measure of local flow convergence and divergence and thus reflects the degree of concentration of  
190 the runoff. *CTI* is employed in the USDA Agricultural Non-Point Source (AGNPS) modelling

Formatted: Font color: Text 1

191 system (Bingner and Theurer, 2001) to identify potential ephemeral gully locations throughout a  
192 watershed (Parker et al., 2007; Momm et al., 2012, 2013).

Formatted: Font color: Text 1

193 *TWI* (Moore et al., 1988; 1991) is a measure of soil saturation and is calculated as:

194

$$195 \quad TWI = \ln(A_s / S) \quad (3)$$

196

197 As *TWI* reflects zones of saturation in a watershed, it could also be an index of the potential location  
198 of ephemeral gullies. Indeed, gully heads often form where soils become very wet and lose their  
199 strength (Moore et al., 1988).

200 In addition to *SPI*, *CTI* and *TWI*, ~~we explored~~ the ability to predict gully locations of ~~other~~ two  
201 topographic indices ~~was explored~~. These indices are modified versions of *SPI* and *CTI* and are  
202 calculated as:

Formatted: Font color: Text 1

Formatted: Font color: Text 1

Formatted: Font color: Text 1

203

$$204 \quad MSPI = A_s \cdot S \cdot CI \quad (4)$$

205

$$206 \quad MTWI = \ln(A_s / S) \cdot CI \quad (5)$$

207

208 ~~where *CI* (m) is the convergence index (Köthe et al., 1996). *CI* measures to what extent neighboring~~  
209 ~~cells point to the center cell and is calculated by setting a search radius. Differently from *PLANC*,~~  
210 ~~which depends on local morphology, *CI* describes the general shape of the landscape up to a scale~~  
211 ~~that depends from the set search radius. In this experiment, the *CI* value of each cell was calculated~~  
212 ~~by averaging the values obtained by varying the search radius from 1 to 10 cells. As, *PLANC* and~~  
213 ~~*CI* calculated by SAGA-GIS have negative values on concavities (e.g. valley bottoms) and positive~~  
214 ~~values on convexities (e.g. ridges), a change in the sign of both parameters was performed before~~  
215 ~~using them to calculate the topographic indices employed to predict gully location.~~

216 where *CI* is the convergence index (Köthe et al., 1996; Kiss, 2004; Thommeret et al., 2010). *CI*

217 measures to what extent neighboring cells point to the center cell. *CI* is calculated as the average  
218 difference between actual aspect of surrounding cells within a moving square or circular window  
219 and the direction to the center cell, minus 90 degrees. The value ranges from -90 degrees (max  
220 convergence) by 0 (planar slopes) to 90 degrees (max divergence). *CI* provided by SAGA-GIS is  
221 normalized between -100 and 100. Differently from *PLANC*, which depends on local morphology,  
222 *CI* describes the general shape of the landscape up to a scale that depends from the size of the  
223 moving window. In this experiment, the *CI* value of each cell was calculated by averaging the  
224 values obtained varying the search radius of a circular moving window from 1 to 10 cells. As  
225 *PLANC* and *CI* calculated by SAGA-GIS have negative values on concavities (e.g. valley bottoms)  
226 and positive values on convexities (e.g. ridges), a change in the sign of both parameters was  
227 performed before using them to calculate the topographic indices employed to predict gully  
228 location.

229 *MSPI* and *MTWI* could help in predicting gully occurrence as they estimate runoff erosive power  
230 and potential soil saturation, respectively, and incorporate a weighting factor which reflects flow  
231 convergence/divergence (i.e. *CI*).

### 232 3.3. *Statistical modelling*

233 In our experiment, the location of the gullies was also predicted by employing two statistical  
234 techniques, namely logistic regression (LR; Hosmer and Lemeshow, 2000) and multivariate  
235 adaptive regression splines (MARS; Friedman, 1991).

236 LR is a generalized linear model with a logistic link function. LR is among the most common  
237 statistical technique for prediction of gully occurrence (e.g., Meyer and Martínez-Casasnovas, 1999;  
238 Lucà et al., 2011; Conoscenti et al., 2014; Dewitte et al., 2015; Selkimäki and González-Olabarria,  
239 2016). Conversely, MARS has been employed only recently to model gully erosion (Gómez-  
240 Gutiérrez et al., 2009a, 2009c, 2015; Arabameri et al., 2018; Garosi et al., 2018; Conoscenti et al.,  
241 2018). LR and MARS enable modelling of relationships between continuous and/or categorical  
242 independent variables and a dichotomous dependent variable (i.e. event or non-event). Both

Formatted: Font color: Text 1

Formatted: Font color: Text 1, Italian (Italy)

Formatted: Font color: Text 1

243 techniques consist of an additive combination of terms. LR has a linear structure with constant  
244 coefficients across the entire range of the predictor variables. Conversely, MARS uses piece-wise  
245 linear regressions with breaks at the knots to describe non-linear relationships between event  
246 occurrence and predictors. To reduce the complexity of the models, ~~we prepared~~ MARS models  
247 ~~were prepared~~ with terms made of single predictors ~~whereas;~~ as regards LR models, ~~we adopted~~ a  
248 bilateral stepwise strategy ~~that, which~~ selects only the most significant predictors, ~~was adopted~~.  
249 Please refer to Hosmer and Lemeshow (2000) and Friedman (1991) for further details about LR and  
250 MARS, respectively.

251 LR and MARS models were prepared by using as predictor variables the primary topographic  
252 attributes *S*, *A<sub>s</sub>*, *PLANC* and *CI*. Since both the employed statistical techniques require absence of  
253 multicollinearity, the degree of correlation among these four variables was evaluated before running  
254 the models. To this aim, ~~we used~~ the variance inflation factor (*VIF*) (Jebur et al., 2014; Heckmann  
255 et al., 2014; Bui et al., 2015; Conoscenti et al., 2016; Cama et al., 2017; Rotigliano et al., 2019;  
256 Vargas-Cuervo et al., 2019), ~~was employed. The results, which were interpreted~~ according to the  
257 “rule of 10<sup>22</sup>” ~~revealed absence of strong correlations among the predictor variables (*VIF* range: 1.0~~  
258 ~~– 1.1).~~

259 Calibration of the statistical models was carried out separately in W1 and W2, where 100 learning  
260 samples were prepared by randomly selecting the 25% of the total number of event pixels and the  
261 same number of non-event pixels. This percentage was chosen in order to achieve a compromise  
262 between the attempt to minimize the effects of spatial autocorrelation and the effort to obtain robust  
263 models, by using a sufficiently large number of cases. Since 1928 and 717 gully cells were  
264 identified in W1 and W2, respectively, the W1 learning samples include 964 pixels (i.e. 482 non-  
265 event + 482 event cells, the latter corresponding to 25% of 1928) whereas 358 pixels (i.e. 179 non-  
266 event + 179 event cells, the latter corresponding to 25% of 717) form the W2 samples. The learning  
267 samples were employed to perform 100 LR and 100 MARS model runs in each of the watersheds.  
268 Hereafter, MARS1 and LR1 are used to indicate model runs calibrated in W1 whereas MARS2 and

Formatted: Font color: Text 1

Formatted: Font color: Text 1

Formatted: Font color: Text 1

Formatted: Font color: Text 1

Formatted: Font color: Text 1

Formatted: Font color: Text 1

Formatted: Font color: Text 1

Formatted: Font color: Text 1

Formatted: Font color: Text 1

Formatted: Font color: Text 1

269 LR2 indicate model runs calibrated in W2.

#### 270 3.4. Validation strategy

271 The ability to predict gully occurrence of topographic indices and statistical models was measured  
272 on a network of flow lines which were identified separately in W1 and W2 by using two different  
273 thresholds of contributing area. The thresholds were set equal to the minimum ~~AA<sub>c</sub>~~ of W1 and W2  
274 gully cells, respectively, after discarding values below the 1<sup>st</sup> percentile which were regarded as  
275 outliers. By using this approach, ~~we measured and compared~~ the predictive performance of  
276 topographic indices and statistical models ~~focusing was measured~~ where drainage area is sufficient  
277 to trigger gully erosion, given the rainfall, soil, bedrock and land use characteristics which caused  
278 gully erosion in our study watersheds.

279 One hundred validation samples were prepared by randomly selecting pixels from flow lines of  
280 both W1 and W2. Like the calibration samples, also the validation samples include the 25% of the  
281 gully cells and a same number of non-gully cells. The value of the topographic indices was used  
282 directly as a score to predict the distribution of gully cells. As regards statistical modelling, the  
283 probability of gully occurrence was calculated from LR and MARS ensemble models, ~~which were~~  
284 ~~prepared by averaging the score of the 100 model runs.~~ (Kotu and Deshpande, 2015), which were  
285 prepared by averaging the score of the 100 model runs. This procedure was applied in order to  
286 generate a more stable performance of the models and to mitigate the effects of prevalence (i.e.  
287 different proportion of event/non-event cells in the study area) (Svoray et al., 2012). ~~We measured~~  
288 ~~the~~The predictive performance of both “local” (i.e. calibrated and validated in the same watershed)  
289 and “transferred” (i.e. calibrated in one watershed and validated in the other one) statistical models  
290 was measured.

291 The accuracy of the topographic indices and statistical models was assessed by plotting for each  
292 validation sample the receiver operating characteristic (ROC) curve (e.g., Lasko et al., 2005;  
293 Brenning, 2005; Frattini et al., 2010; Cama et al., 2015, 2016) and by calculating the area under the  
294 ROC curve (*AUC*). ROC curve analysis is a cut-off independent technique for assessing the

Formatted: Font color: Text 1

Formatted: Font color: Text 1

Formatted: Font color: Text 1

Formatted: Font color: Text 1

Formatted: Font color: Text 1

Formatted: Font color: Text 1

295 performance of predictive models, which plots all possible values of sensitivity (i.e. true positive  
296 rate, *TPR*) against the corresponding value of 1-specificity (i.e. false positive rate, *FPR*). The ideal  
297 predictive model achieves an *AUC* value close to 1, whereas a value close to 0.5 reveals inaccuracy  
298 in the model (Nandi and Shakoor, 2009). In this experiment, accuracy of the models was interpreted  
299 as acceptable, excellent or outstanding if *AUC* values were higher than 0.7, 0.8 and 0.9, respectively  
300 (Hosmer and Lemeshow, 2000). In both W1 and W2, a group of 100 ROC curves and related *AUC*  
301 values, was obtained (one for each validation sample) for each topographic index and statistical  
302 model. Comparisons between *AUC* groups were performed by using box plots and the Wilcoxon  
303 signed-rank test, setting the level of significance at 0.01.

304 Furthermore, the predictive ability of topographic indices and statistical models was evaluated by  
305 using cut-off dependent performance metrics such as Cohen's kappa index (Cohen, 1960; Landis  
306 and Koch, 1977; Monserud and Leemans, 1992; Geissen et al., 2007; Frattini et al., 2010;  
307 Sterlacchini et al., 2011), sensitivity (or *TPR*) and specificity (i.e. true negative rate, *TNR*). The  
308 Cohen's kappa index ( $\kappa$ ) reflects the degree of agreement between prediction and observation and is  
309 calculated as:

$$311 \kappa = P_{\text{obs}} - P_{\text{exp}} / (1 - P_{\text{exp}}) \quad (6)$$

312 where  $P_{\text{obs}}$  and  $P_{\text{exp}}$  are the observed and the expected proportion of agreement, respectively.  $\kappa$   
313 values were interpreted according to Monserud and Leemans (1992), which evaluated the  
314 agreement between model prediction and observation as: 1.00, perfect; 0.85–0.99, excellent; 0.70–  
315 0.85, very good; 0.55–0.70, good; 0.40–0.55, fair; 0.20–0.40, poor; 0.05–0.20, very poor; <0.05,  
316 null.  
317

318 ~~To calculate  $\kappa$ , *TPR* and *FPR*, we first prepared the average ROC curve from each group of 100~~  
319 ~~validation ROC curves. We then identified the optimal cut off values of these curves by using the~~  
320 ~~Youden's index (*J*) (Youden, 1950; Angileri et al., 2016; Cama et al., 2017; Rotigliano et al., 2019),~~

Formatted: Font color: Text 1, Italian  
(Italy)

Formatted: Font color: Text 1

Formatted: Font color: Text 1, Italian  
(Italy)

Formatted: Font color: Text 1

Formatted: Font color: Text 1, Italian  
(Italy)

Formatted: Font color: Text 1



321 ~~which corresponds to the threshold that maximizes the sum of sensitivity and specificity. Then, by~~  
322 ~~using  $J$  as threshold ( $T$ ) to classify the grid pixels as not susceptible (score  $< T$ ) or as susceptible~~  
323 ~~(score  $> T$ ) to gully erosion, we prepared the contingency tables for each topographic index and~~  
324 ~~ensemble statistical model.~~

325 Firstly, to calculate  $\kappa$ ,  $TPR$  and  $FPR$ , the average ROC curve from each group of 100 validation  
326 ROC curves was prepared. Then, the optimal cut-off values of these curves were identified by using  
327 the Youden's index ( $J$ ) (Youden, 1950; Angileri et al., 2016; Cama et al., 2017; Rotigliano et al.,  
328 2019), which corresponds to the threshold that maximizes the sum of sensitivity and specificity.  
329 Then, by using  $J$  as threshold ( $T$ ) to classify the grid pixels as not susceptible (score  $< T$ ) or as  
330 susceptible (score  $> T$ ) to gully erosion, the contingency tables were prepared for each topographic  
331 index and ensemble statistical model.

### 332 3.5. Gully prediction maps

333 A gully susceptibility map of the study area was obtained from each of the topographic indices and  
334 the four ensemble statistical models which were prepared by averaging the score of 100 MARS and  
335 LR model runs. Susceptibility to gully erosion was then classified into four levels according to  
336 thresholds that were calculated separately in W1 and W2 by using the steps described below, which  
337 were repeated for each topographic index and ensemble statistical model. First,  $J$  was used to  
338 separate the pixels of the 100 validation samples into a low susceptibility dataset (score  $< J$ ) and a  
339 high susceptible dataset (score  $> J$ ). Then, ~~we prepared~~ the average ROC curve and ~~calculated~~ the  
340 Youden index ~~were calculated~~ for ~~both~~ the low susceptibility dataset ( $J_{low}$ ) and ~~for~~ the high  
341 susceptibility dataset ( $J_{high}$ ). Finally, ~~we identified~~ the following four levels of susceptibility to gully  
342 erosion ~~were identified~~: i) low (score  $\leq J_{low}$ ); ii) moderate ( $J_{low} < \text{score} \leq J$ ); iii) high ( $J < \text{score} \leq$   
343  $J_{high}$ ); iv) very high (score  $> J_{high}$ ).

## 344 4. Results

Formatted: Font color: Text 1

Formatted: Font color: Text 1

Formatted: Font color: Text 1

Formatted: Font color: Text 1

Formatted: Font color: Text 1

Formatted: Font color: Text 1

Formatted: Font color: Text 1

Formatted: Font color: Text 1

345 4.1. Predictive performance measured by using a cut-off independent statistic

346 The ability of the topographic indices and statistical models to discriminate between gully and non-  
347 gully cells of the validation samples is graphically represented by the box plots of Fig. 56. Each box  
348 plot reveals the variability of a group of 100 *AUC* values by indicating their quartiles, as well as the  
349 lowest and the highest data still within 1.5 interquartile range of the lower quartile and of the upper  
350 quartile, respectively. Furthermore, descriptive statistics such as mean and standard deviation of  
351 each *AUC* group are reported in Table 1.

352 The *AUC* values reflect excellent ( $AUC > 0.8$ ) to outstanding ( $AUC > 0.9$ ) discrimination ability of  
353 indices and models applied to predict gullies occurred in the studied watersheds. However,  
354 significant differences of accuracy can be detected.

355 *MSPI* performed clearly better than the other indices in both watersheds. In W1, only *SPI* achieved  
356 a similar performance but still significantly lower than that obtained from *MSPI*. In W2, *SPI*  
357 performed better than *TWI* but not significantly different from *CTI* and *MTWI*. *TWI* performed  
358 better than its modified version (i.e. *MTWI*) in W1, whereas the opposite was observed in W2.

359 As regards statistical models, MARS performed better than LR in both watersheds. Accuracy of  
360 MARS and LR is significantly different even in W1, where *AUC* values appear quite similar. A not  
361 significant difference was observed only in W1 between local (i.e. trained in W1) LR and  
362 transferred (i.e. trained in W2) MARS models ( $p$ -value = 0.284). In W1, both MARS and LR local  
363 models (i.e. MARS1 and LR1) exhibited higher accuracy than transferred models (i.e. MARS2 and  
364 LR2). On the other hand, a not significant difference of *AUC* was observed in W2 between local  
365 and transferred LR models ( $p$ -value = 0.5221).

366 The *AUC* values and the Wilcoxon signed-rank test revealed an overall better predictive  
367 performance of the statistical models with respect to the topographic indices, with the exception of  
368 *MSPI*. The latter indeed achieved outstanding accuracy in both watersheds. In W1, *MSPI* exhibited  
369 the same accuracy of transferred MARS and local LR runs and better predictive ability than  
370 transferred LR runs. In W2, *MSPI* achieved higher accuracy than both local and transferred LR runs

Formatted: Font color: Text 1

371 and the same accuracy of MARS1. Only local MARS models performed significantly better than  
372 MSPI.

#### 373 4.2. Predictive performance measured by using cut-off dependent statistics

374 Fig. 67 shows the average ROC curves obtained from the validation of the topographic indices and  
375 statistical models in W1 and W2. These curves were employed to calculate the optimal cut-off ( $T$ )  
376 that maximizes the sum of sensitivity and specificity and which graphically corresponds to the  
377 maximum distance to the diagonal lines plotted in Fig. 68. The value of  $T$ , as well as those of kappa  
378 index ( $\kappa$ ),  $TPR$  and  $TNR$  are reported in Table 2. Kappa values obtained for the five topographic  
379 indices vary from 0.625 to 0.795 indicating a good ( $\kappa > 0.55$ ) to very good ( $\kappa > 0.70$ ) ability to  
380 discriminate between event and non-event pixels. As revealed by  $AUC$  values, the kappa index also  
381 demonstrated that  $MSPI$  achieved the best predictive skill in both watersheds.  $SPI$  reached a  $\kappa$  value  
382 close that of  $MSPI$  in W1. Conversely,  $SPI$  accuracy appears similar to that of  $TWI$  and  $MTWI$  in  
383 W2, where  $CTI$  achieved the second best  $\kappa$  value. As regards sensitivity and specificity,  $MSPI$   
384 obtained the highest values in W1 whereas in W2 a slightly higher  $TPR$  and  $TNR$  was observed for  
385  $MTWI$  and  $TWI$ , respectively.

386 Kappa index revealed approximately the same difference of performance between MARS and LR  
387 models which is highlighted by the  $AUC$  values. Indeed, MARS achieved higher  $\kappa$  values in both  
388 watersheds, with more enhanced difference of accuracy occurring in W2, where LR models are  
389 below the threshold indicating very good performance ( $\kappa > 0.7$ ). The difference of performance  
390 observed in W1 appears related more to a difference in specificity than in sensitivity, which is very  
391 similar for MARS and LR models. On the other hand, in W2, MARS runs exhibit higher values of  
392 both  $TPR$  and  $TNR$ , whereas only transferred models show a similar sensitivity.

393 Kappa,  $TPR$  and  $TNR$  confirm that  $MSPI$  achieves approximately the same accuracy of MARS runs.  
394 Furthermore, these statistics reveal that  $MSPI$  outperforms both LR local and transferred models  
395 which in turn show better discrimination ability when compared to the other topographic indices,  
396 with the exception of  $SPI$ , in W1, and  $CTI$ , in W2.

Formatted: Font color: Text 1, Italian  
(Italy)

Formatted: Font color: Text 1, Italian  
(Italy)

Formatted: Font color: Text 1, Italian  
(Italy)

Formatted: Font color: Text 1, Italian  
(Italy)

Formatted: Font color: Text 1, Italian  
(Italy)

Formatted: Font color: Text 1

Formatted: Font color: Text 1, Italian  
(Italy)

Formatted: Font color: Text 1

Formatted: Font color: Text 1, Italian  
(Italy)

Formatted: Font color: Text 1

397 4.3. Gully prediction maps

398 Fig. 78 shows the gully prediction maps for the sectors of W1 and W2 highlighted in Fig. 3, 4,  
399 obtained from the topographic indices and the ensemble statistical models. To aid the assessment of  
400 the maps, Fig. 89 plots the relative frequency distributions of non-event and event pixels across the  
401 susceptibility levels. The gully erosion susceptibility maps show very low probability of gully  
402 occurrence in most part of the study area, with the exception of few flow lines where susceptibility  
403 level is from moderate to very high. Only maps derived from *MTWI* and *LR*, especially in *W2*,  
404 show slightly larger sectors with moderate to high probability of gully occurrence. This is  
405 confirmed by the bar plots of Fig. 89, which reveal that non-event cells occur with a frequency  
406 higher than 5% only over moderate probability levels of *MTWI* maps and of *LR* maps of *W2*. On  
407 the other hand, although their very low frequency, high and very high susceptibility levels of all the  
408 maps host most of the gully pixels. In particular, the maps derived from *SPI*, *MSPI* and *MARS1*  
409 ensemble model, achieve the highest percentage of gully pixels within the very high level of  
410 susceptibility (Fig. 89).

411 5. Discussion

412 The results of our experiment showed that the spatial distribution of gullies can be effectively  
413 predicted by using either topographic indices or statistical models.  
414 Both cut-off independent and dependent performance metrics revealed that, among the employed  
415 topographic indices, the best accuracy in predicting gully occurrence is achieved by *MSPI* whereas  
416 *MTWI* exhibited similar or worse performance than *SPI*, *CTI* and *TWI*. The ability of the latter  
417 indices to discriminate between gully and non-pixels was evaluated and compared, by identifying  
418 optimal thresholds and by calculating the  $\kappa$  index, in three previous studies (Daggupati et al., 2013;  
419 Sekaluvu et al., 2015; Sheshukov et al., 2018) performed in Kansas. Daggupati et al. (2013)  
420 estimated the thresholds of 30 – 50, 62, and 12, respectively, for *SPI*, *CTI* and *TWI*. Sekaluvu et al.  
421 (2015) and Sheshukov et al. (2018) report that the critical thresholds required by *CTI* to best predict

Formatted: Font color: Text 1

Formatted: Font color: Text 1

Formatted: Font color: Text 1

Formatted: Font color: Text 1

Formatted: Font color: Text 1

Formatted: Font color: Text 1, Italian (Italy)

Formatted: Font color: Text 1

422 the gullies of two watersheds of central Kansas are equal to 79.4 and 25.1. These values are  
423 relatively similar to the *CTI* thresholds estimated by Daggupati et al. (2013) and those calculated in  
424 our experiment (52.8 and 24.3). As regards *SPI*, the thresholds found in our study (270.9 and 127.0)  
425 are of the same order of magnitude of those calculated by Sekaluvu et al. (2015) and Sheshukov et  
426 al. (2018) (501.2 and 158.5), but higher than the values reported by Daggupati et al. (2013).  
427 Furthermore, the *TWI* critical thresholds estimated in our experiment (9.7 and 9.4) are quite similar  
428 to those calculated for the Kansas areas (12.0 – 18.2).

429 By applying the thresholds cited above, Daggupati et al. (2013) found a poor predictive  
430 performance of *CTI* and *TWI* but a fair agreement between observed gullies and prediction obtained  
431 using *SPI* ( $\kappa$ : 0.40 – 0.55). This is in accordance with what ~~we~~ observed in W1 but not in W2,  
432 where *CTI* achieved a higher  $\kappa$  value than *SPI* and *TWI*. A similar result is reported by Sekaluvu et  
433 al. (2015) and Sheshukov et al. (2018), who observed a better accuracy of *CTI*, which achieved a  $\kappa$   
434 value of 0.29 and 0.32 in two watersheds of central Kansas. However, it is worth noting that the  
435 range of  $\kappa$  obtained in our experiment for *SPI*, *CTI* and *TWI* is quite higher (0.63 – 0.77) than the  
436 values calculated in Kansas. This could be explained by considering that the trajectory of our  
437 gullies was adjusted to fit lines of flow concentration extracted from the DEM. This procedure  
438 indeed prevents gullies to intersect cells with very low or null drainage area, which can be caused  
439 by mapping errors or inadequate DEM resolution, and thus may yield a stronger positive  
440 relationship between gully occurrence and contributing area. Furthermore, the higher values of  $\kappa$   
441 achieved by topographic indices in predicting our gullies can be also explained by considering that  
442 validation in this experiment was performed at the pixel scale while a sub-watershed scale was  
443 employed in the studies performed in Kansas (Daggupati et al., 2013; Sekaluvu et al., 2015;  
444 Sheshukov et al., 2018).

445 To explain the better accuracy of *MSPI* with respect to the other indices, ~~we hypothesize~~ it can be  
446 hypothesized that adding *CI* to the *SPI* formula helps in detecting areas of enhanced flow  
447 concentration and, thus, in identifying cells which are likely to host a gully. Moreover, since *MSPI*

Formatted: Font color: Text 1, Italian (Italy)

Formatted: Font color: Text 1

Formatted: Font color: Text 1

Formatted: Font color: Text 1, Italian (Italy)

Formatted: Font color: Text 1

Formatted: Font color: Text 1, Italian (Italy)

Formatted: Font color: Text 1

Formatted: Font color: Text 1, Italian (Italy)

Formatted: Font color: Text 1

Formatted: Font color: Text 1, Italian (Italy)

Formatted: Font color: Text 1

Formatted: Font color: Text 1

448 performs clearly better than *CTI* in both investigated watersheds, ~~we infer it can be inferred~~ that the  
449 contribution of *CI* in increasing the ability to discriminate between non-gully and gully cells is  
450 higher than that provided by *PLANC*. This hypothesis is corroborated by the frequency distributions  
451 of *CI* and *PLANC* measured on gully and non-gully cells, which are revealed by the kernel density  
452 plots of Fig. 910. These plots show that *CI* distributions measured along gully trajectories are  
453 clearly different from those calculated for non-event cells, whereas no such difference can be  
454 observed for *PLANC*. Furthermore, *PLANC* does not improve appreciably the predictive ability of  
455 *CTI* with respect to *SPI*; indeed, *SPI* achieves higher *AUC* values in both studied watersheds and  
456 higher  $\kappa$  value in W1. On the other hand, *CI* did not improve the predictive skill of *TWI*, as *MTWI*  
457 performed better than *TWI* only in W2.

458 As regards statistical modelling of gully occurrence, validation performed in our study area  
459 revealed a better predictive skill of MARS with respect to LR. This results is in line with other  
460 studies, like that of Garosi et al. (2018), which also found a better performance of MARS (*AUC*:  
461 74.5–90.2) with respect to LR (*AUC*: 66.4–85.6) in predicting gully erosion susceptibility in Iran.  
462 MARS provided slightly better accuracy also in another Sicilian watershed (Gómez-Gutiérrez et al.,  
463 2015), where LR has been previously employed to predict the same gully inventory (Conoscenti et  
464 al., 2014). Also Rahmati et al. (2019) observed better accuracy of MARS in predicting the same  
465 gully inventory of this study, although performing validation on pixels selected from the entire  
466 watersheds and employing a quite larger number of predictors, which include land use and bedrock.  
467 The better performance of MARS was somewhat expected given the widely accepted assumption  
468 that gullying is a threshold phenomenon and the ability of MARS to model non-linear relationships  
469 between event occurrence and predictor variables. Indeed, MARS is able to identify, across the  
470 range of the predictors, different linear functions separated by knots which may correspond to  
471 potential thresholds for gully initiation.

472 *AUC* and  $\kappa$  values revealed that, in our study area, statistical models predict the occurrence of  
473 gullies with better accuracy than topographic indices, with the exception of *MSPI*. The latter

Formatted: Font color: Text 1

Formatted: Font color: Text 1

Formatted: Font color: Text 1, Italian  
(Italy)

Formatted: Font color: Text 1

Formatted: Font color: Text 1, Italian  
(Italy)

Formatted: Font color: Text 1

Formatted: Font color: Text 1, Italian  
(Italy)

Formatted: Font color: Text 1

474 exhibited indeed similar or better predictive performance than local LR models and transferred LR  
475 and MARS models, whereas only local MARS2 model runs achieved better accuracy. Due to their  
476 data-driven nature, a better fit of MARS and LR to the observed gully data was expected prior to  
477 performing the experiment. Coefficients of local MARS and LR equations were indeed calculated  
478 on the basis of the observed spatial distribution of gullies within the training areas. Also transferred  
479 models, although calibrated in one watershed and validated in the other one, were expected to  
480 achieve better accuracy than topographic indices, due to the closeness of the two areas and their  
481 similar environmental conditions. Therefore, the difference in performance observed between *MSPI*  
482 and the transferred statistical models suggests that where an inventory of gullies is not available,  
483 reliable maps of gully erosion susceptibility can be prepared by using *MSPI*. This holds in particular  
484 if only topographic data is available at high resolution. Indeed, it is worth considering that  
485 predictive ability of multivariate statistical models can be improved by including variables  
486 reflecting, at high resolution, land use, soil and bedrock characteristics.

487 The gully erosion prediction maps derived from both topographic indices and ensemble statistical  
488 models exhibit an optimal distribution of the susceptibility levels in relation to gullies location.  
489 Indeed, at least 89% of observed non-gully cells fall within the lowest susceptibility level whereas  
490 between 53% (*CTI* map in W2) and 71% (*SPI* map in W1) of gully cells intersect the highest class  
491 of gully occurrence probability. ~~We infer that, in~~In addition to the reliability of the employed  
492 indices and models, ~~it can be inferred that~~ the large agreement observed between prediction maps  
493 and gully spatial distribution is due to the method employed to identify the susceptibility classes,  
494 which was based on the Youden's index (*J*).

## 495 6. Concluding remarks

496 In this experiment, ~~we evaluated~~ the ability of a set of five topographic indices to predict the spatial  
497 distribution of the gullies observed in two adjacent watersheds located in Sicily (Italy). ~~was~~  
498 ~~evaluated~~. Two of these indices, named *MSPI* and *MTWI*, as far as we know, have never been  
499 employed to this aim; they were obtained by multiplying the stream power index (*SPI*) and the

Formatted: Font color: Text 1

Formatted: Font color: Text 1

Formatted: Font color: Text 1

Formatted: Font color: Text 1

500 topographic wetness index (*TWI*), respectively, by the convergence index (*CI*). The predictive  
501 ability of the topographic indices was measured by using both cut-off independent and dependent  
502 statistics and compared to the performance of multivariate statistical models, which use as  
503 predictors the same topographic variables of the five indices (i.e. contributing area, slope steepness,  
504 plan curvature and convergence index).

505 The validation results revealed that topographic indices and statistical models achieved excellent to  
506 outstanding accuracy in predicting the spatial distribution of the gullies observed in our study area.  
507 Statistical models performed better than topographic indices with the exception of *MPSI*. Since the  
508 proposed index showed the best predictive performance among the topographic indices, we inferit  
509 can be inferred that the inclusion of *CI* helps in detecting hollow areas where gullies are more likely  
510 to occur. Furthermore, *MSPi* exhibited similar or better predictive skill than transferred statistical  
511 models (i.e. models calibrated in one watershed and validated in the other one). This suggests that  
512 *MPSI* can be a valid alternative to a data driven approach for identifying potential gully locations in  
513 areas where a gully inventory is not available, which is necessary to calibrate statistical models.

#### 514 Acknowledgments

515 This research was developed in the framework of the project FLUMEN (project number: 318969),  
516 funded by the EU (call identifier: FP7-PEOPLE-2012-IRSES), scientific responsible for the  
517 University of Palermo: Prof. Dr. C. Conoscenti. C. Conoscenti and E. Rotigliano have commonly  
518 shared the whole research phases. This manuscript benefited greatly from the kind suggestions and  
519 comments of the three anonymous reviewers.

#### 520 References

- 521 Angileri, S.E., Conoscenti, C., Hochschild, V., Märker, M., Rotigliano, E., Agnesi, V., 2016. Water erosion  
522 susceptibility mapping by applying stochastic gradient treeboost to the imera Meridionale River basin (Sicily,  
523 Italy). Geomorphology 262, 61–76. <https://doi.org/10.1016/j.geomorph.2016.03.018>  
524 Arabameri, A., Pradhan, B., Pourghasemi, H.R., Rezaei, K., Kerle, N., 2018. Spatial Modelling of Gully Erosion Using  
525 GIS and R Programing: A Comparison among Three Data Mining Algorithms. Appl. Sci. 8, 1369.  
526 <https://doi.org/10.3390/app8081369>  
527 Azareh, A., Rahmati, O., Rafiei-Sardooui, E., Sankey, J.B., Lee, S., Shahabi, H., Ahmad, B. Bin, 2019. Modelling gully-  
528 erosion susceptibility in a semi-arid region, Iran: Investigation of applicability of certainty factor and maximum

Formatted: Font color: Text 1

Formatted: Font color: Text 1

Formatted: Font color: Text 1

Formatted: Font color: Text 1

Formatted: Font color: Text 1, Italian  
(Italy)

Formatted: Font color: Text 1

Formatted: Font color: Text 1, Italian  
(Italy)

Formatted: Font color: Text 1











773 CAPTIONS

774 Fig. 1. Location (a) and topographic map (b) of the watersheds W1 and W2. Flow-chart of  
775 methodology.

776 Fig. 2. Location (a) and topographic map (b) of the watersheds W1 and W2.

777 Fig. 3. Elevation (a), slope steepness (b), lithology (c) and land cover (d) maps of the watersheds  
778 W1 and W2.

779 Fig. 4. Gully maps of the watersheds W1 and W2 and Google Earth views of two gully-prone  
780 sectors of the study area.

781 Fig. 5. An example showing correspondence between gullies and flow pathways.

782 Fig. 6. Box plots showing the variability of the 100 AUC values calculated in W1 and W2 for the  
783 topographic indices and local and transferred statistical models.

784 Fig. 7. Average ROC curves obtained from the validation of the topographic indices and statistical  
785 models in W1 and W2.

786 Fig. 8. Gully erosion susceptibility maps for the sectors of W1 and W2 highlighted in Fig.3. First  
787 and third columns show maps calculated from the topographic indices. Second and fourth columns  
788 show maps calculated from local and transferred statistical models. White pixels were not  
789 investigated because they intersect anthropogenic features (i.e. urban areas, artificial lakes or roads)  
790 or fall within a 10 m buffer around river channels.

791 Fig. 9. Relative frequency distributions of non-event and event pixels across the susceptibility  
792 levels of the gully erosion susceptibility maps.

793 Fig. 10. Kernel density plots of CI and PLANC calculated for gully and non-gully cells of the  
794 watersheds W1 and W2.

795 Table 1. Mean and standard deviation of the 100 AUC values calculated for the topographic indices  
796 and local and transferred statistical models.

797 Table 2. Cut-off (T) dependent statistics calculated in W1 and W2 for the topographic indices and  
798 local and transferred statistical models.

Formatted: No underline, Font color: Text 1

Formatted: Font color: Text 1

Formatted: No underline, Font color: Text 1

Formatted: No underline, Font color: Text 1

Formatted: Font color: Text 1

Formatted: No underline, Font color: Text 1

Formatted: Font color: Text 1

Formatted: No underline, Font color: Text 1

Formatted: No underline, Font color: Text 1

Formatted: Font color: Text 1

Formatted: No underline, Font color: Text 1

Formatted: No underline, Font color: Text 1

Formatted: Font color: Text 1

Formatted: No underline, Font color: Text 1

Formatted: No underline, Font color: Text 1

Formatted: Font color: Text 1

Formatted: No underline, Font color: Text 1

Formatted: No underline, Font color: Text 1

Formatted: Font color: Text 1

Formatted: No underline, Font color: Text 1

Formatted: No underline, Font color: Text 1

Formatted: Font color: Text 1

Formatted: No underline, Font color: Text 1

Formatted: No underline, Font color: Text 1

Formatted: Font color: Text 1

Formatted: No underline, Font color: Text 1

Formatted: Font color: Text 1

Formatted: No underline, Font color: Text 1

Formatted: Font color: Text 1



# 1 Predicting gully occurrence at watershed scale: comparing 2 topographic indices and multivariate statistical models

3 Christian Conoscenti <sup>a,\*</sup>, Edoardo Rotigliano <sup>a</sup>

4 <sup>a</sup>Department of Earth and Marine Sciences (DISTEM), University of Palermo, Via Archirafi 22, 90123 Palermo,  
5 Italy

6

## 7 **Abstract**

8 In this study, the ability of five topographic indices to predict the gully trajectories observed in two  
9 adjacent watersheds located in Sicily (Italy) was evaluated. Two of these indices, named *MSPI* and  
10 *MTWI*, as far as we know, have never been employed to this aim. They were obtained by  
11 multiplying the stream power index (*SPI*) and the topographic wetness index (*TWI*), respectively,  
12 by the convergence index (*CI*). The predictive ability of the topographic indices was measured by  
13 using both cut-off independent (*AUC*: area under the receiver operating characteristic curve) and  
14 dependent statistics (Cohen's kappa index  $\kappa$ , sensitivity, specificity). These statistics were  
15 calculated also for 100 MARS (multivariate adaptive regression splines) and 100 LR (logistic  
16 regression) model runs, which used as predictors the topographic variables (i.e. contributing area,  
17 slope steepness, plan curvature and convergence index) combined into the five indices.  
18 Performance statistics of both topographic indices and statistical models were calculated using 100  
19 random samples of 2 m grid cells, which were extracted only from flow concentration lines. This  
20 was done in order to focus the validation process on where gully erosion is more likely to occur.  
21 *MSPI* achieved the best predictive skill ( $AUC > 0.93$ ;  $\kappa > 0.71$ ) among the topographic indices and  
22 exhibited similar and better accuracy than local (i.e. trained and validated in the same watershed)

23 and transferred (i.e. trained in one watershed and tested in the other one) LR models, respectively.  
24 On the other hand, *MSPI* performed similarly to transferred MARS runs ( $AUC > 0.92$ ;  $\kappa > 0.71$ ) but  
25 slightly worse than local MARS runs ( $AUC > 0.95$ ;  $\kappa > 0.77$ ). Based on the results of this  
26 experiment, it can be inferred that (i) including *CI* helps in detecting hollow areas where gullies are  
27 more likely to occur and (ii) *MPSI* can be a valid alternative to a data driven approach for mapping  
28 gully erosion susceptibility in areas where a gully inventory is not available, which is necessary to  
29 calibrate statistical models.

30

31 *Keywords:* Gully erosion susceptibility; Topographic indices; Multivariate Adaptive Regression  
32 Splines (MARS); Logistic Regression (LR); Geographic Information System (GIS)

33

34 \* Corresponding author. Tel.: +39 09123864670; fax: +39 0916169908. E-mail address:  
35 christian.conoscenti@unipa.it (C. Conoscenti).

36



## 37 **1. Introduction**

38 Gully erosion causes land degradation in a wide range of environmental conditions. The  
39 development of gullies in agricultural watersheds may induce high soil loss and reduction of water  
40 availability, leading to a significant decrease of soil quality and crop yield. Moreover, gully  
41 channels hamper the trafficability of the fields causing extra damages and costs to farmers (Poesen  
42 et al., 2003, 2011).

43 Gullying is a threshold phenomenon that is mainly controlled by rainfall, topography, soil, lithology  
44 and land use. Gullies occur only after a threshold of runoff erosivity and soil erodibility is  
45 exceeded. In addition to rainfall, runoff erosive power depends on topography which regulates  
46 discharge, concentration and velocity of overland flow (e.g., Moore et al., 1988; Desmet et al.,  
47 1999; Poesen et al., 2003; Valentin et al., 2005; Gómez-Gutiérrez et al., 2009a; Daggupati et al.,  
48 2013; Conoscenti et al., 2013). Morphology, density and development of gullies in a given  
49 landscape is also significantly controlled by parent material (Oostwoud Wijdenes et al., 2000;  
50 Vandekerckhove et al., 2001; Poesen et al., 2011). Furthermore, gully occurrence is controlled by  
51 resistance of soil, which is influenced by soil properties such as texture, bulk density, moisture  
52 conditions, organic matter content (Poesen et al., 2003). Soil erosion susceptibility is also related to  
53 crop type and stage, as well as tillage direction and conservation practices (Parker et al., 2007).  
54 Also, several studies have reported triggering of gullies or increasing of gully erosion rates as being  
55 caused by land use changes, intensification of farming activities and overgrazing (Poesen et al.,  
56 2003; Valentin et al., 2005; Zucca et al., 2006; Gómez-Gutiérrez et al., 2009b).

57 Planning of gully erosion control in agricultural watersheds requires either quantifying soil loss and  
58 predicting gully location. Several process-based models have been developed to quantify gully  
59 erosion (e.g., CREAMS, Knisel, 1980; EGEM, Merkel et al., 1988; GLEAMS, Knisel, 1993;  
60 Sidorchuk, 1999; REGEM, Gordon et al., 2007). However, these models require physical input  
61 variables that are difficult to measure at the watershed scale. Soil loss due to gully erosion can be  
62 also evaluated by using empirical models which are based on relationships established between

63 volume and length of the gully channels (e.g., Nachtergaele et al., 2001; Capra and Scicolone, 2002;  
64 Capra et al., 2005; Caraballo-Arias et al., 2014, 2015).

65 Prediction of gully location can be achieved by identifying a topographic threshold that has to be  
66 exceeded for a gully to form. A number of studies have proposed topographic threshold lines  
67 defined on a log-log plot of local slope gradient ( $S$ ) versus upslope contributing area ( $A$ ) measured  
68 at gully heads (e.g., Patton and Schumm, 1975; Montgomery and Dietrich, 1992; Nachtergaele et  
69 al., 2001b; Zucca et al., 2006; Nazari Samani et al., 2009). Both these topographic attributes are  
70 indeed widely considered to play the role of controlling factors in the gully formation process as  
71 they act as proxies for flow velocity and discharge, respectively. The approach based on  $S$ - $A$   
72 threshold lines assumes that for a given  $A$ , a critical  $S$  exists above which runoff erosivity is large  
73 enough to produce gully erosion. The  $S$ - $A$  threshold can be used to predict gullies by classifying a  
74 study area into non-event positions (below the threshold line) and event positions (on or above the  
75 threshold line). However, this approach tends to overestimate the likelihood of gully occurrence  
76 (Svoray et al., 2012; Gómez-Gutiérrez et al., 2015), providing a high number of false positives (i.e.  
77 non-gullied positions classified as gullied).

78 Furthermore, several topographic indices have been employed to predict gully location (e.g.,  
79 Thorne et al., 1986; Moore et al., 1988; Vandaele et al., 1996; Desmet et al., 1999). These models  
80 rely on the assumption that gully formation depends on a combination of primary topographic  
81 attributes (Wilson and Gallant, 2000) which reflect erosivity of concentrated overland flow; gully  
82 erosion occurs when the topographic index exceeds a critical threshold value. Daggupati et al.  
83 (2013), Sekaluvu et al. (2015) and Sheshukov et al. (2018) have compared the ability to  
84 discriminate between gullied and non-gullied areas of several topographic indices, which were  
85 applied using different thresholds. Their analyses revealed that gully predictions were not accurate  
86 without identifying an optimal threshold through local calibration. Indeed, they have observed that a  
87 low threshold causes high number of false positives whereas a high threshold produces high number  
88 of false negatives (i.e. gullied sites predicted as non-gullied).

89 Recently, accurate predictions of gully locations have been achieved by using statistical modeling  
90 and data mining techniques such as logistic regression, classification and regression trees,  
91 multivariate adaptive regression splines, stochastic gradient treeboost, artificial neural network,  
92 random forest, maximum entropy, etc. (e.g., Meyer and Martínez-Casasnovas, 1999; Gómez-  
93 Gutiérrez et al., 2009c; Eustace et al., 2011; Svoray et al., 2012; Conoscenti et al., 2014, 2018;  
94 Dewitte et al., 2015; Angileri et al., 2016; Pourghasemi et al., 2017; Rahmati et al., 2016, 2017a,  
95 2017b; Garosi et al., 2018, 2019; Azareh et al., 2019; Choubin et al., 2019; Javidan et al., 2019).  
96 These techniques are able to analyze and model the relationships between gully locations and  
97 spatial variability of a set of environmental predictors related to topography, land use, parent  
98 materials and soils. Based on the identified statistical relationships, these techniques allow for  
99 calculating a probability of gully occurrence that ranges from 0 to 1, for each position (usually grid  
100 cell) in a given area. However, an important drawback in these procedures, which are data-driven, is  
101 that they generate prediction images which efficiently explain the gully distribution in the study  
102 area but tend to fail when exported to other areas, even if located at a close distance (Conoscenti et  
103 al., 2018).

104 This study focuses on investigating the topographic control of gully erosion caused by concentrated  
105 overland flow at watershed scale. The experiment was carried out in two small agricultural  
106 watersheds located in Sicily (Italy). The main goal of the study was to evaluate and compare the  
107 ability to predict the location of gullies achieved by using a set of topographic indices, which  
108 includes three indices previously proposed for predicting gully location and two modified versions  
109 of them. Predictive models of gully occurrence were prepared also by using logistic regression (LR;  
110 Hosmer and Lemeshow, 2000) and multivariate adaptive regression splines (MARS; Friedman,  
111 1991), two statistical modeling techniques which have been successfully used to this aim in  
112 previous studies (e.g., Vanwallegem et al., 2008; Gómez-Gutiérrez et al., 2009c; Svoray et al.,  
113 2012; Conoscenti et al., 2014, 2018; Dewitte et al., 2015). To further assess the ability to predict  
114 gully occurrence provided by the five topographic indices, their accuracy was compared with that

115 achieved by LR and MARS models.

116

## 117 **2. Materials and Methods**

118 In this study, the topographic analysis was carried out using a LiDAR-derived 2×2 m Digital  
119 Elevation Model (DEM; Regione Siciliana, 2010), with vertical accuracy of 0.1–0.2 m. The GIS  
120 calculations were performed using SAGA-GIS software (Conrad et al., 2015).

121 The calibration of MARS and LR and the validation of both topographic indices and statistical  
122 models were performed using the R software (R Core Team, 2017) with the packages “raster”  
123 (Hijmans, 2017), “usdm” (Naimi, 2015), “splitstackshape” (Mahto, 2018), “pROC” (Robin et al.,  
124 2011), “ROCR” (Sing et al., 2005), “caret” (Wing and Kuhn, 2018) and “earth” (Milborrow, 2018).

125 The flow-chart of Fig. 1 shows a schematic overview of the methodology, which is described in  
126 detail in the following sections.

127

### 128 *2.1. Study area and gully inventory*

129 The experiment was carried out in two adjacent agricultural watersheds located in central-western  
130 Sicily (Fig. 2), approximately 35 km south-east of the city of Palermo. The westernmost watershed  
131 (W1) drains an area of 621.7 ha whereas the easternmost one (W2) covers 901.4 ha. The study area  
132 experiences a typical Mediterranean climate with an average annual rainfall of 711 mm (time  
133 interval: 2002–2017; Camporeale rainfall station; Regione Siciliana – SIAS - Servizio Informativo  
134 Agrometeorologico Siciliano), with a minimum in July (5.6 mm) and a maximum in December  
135 (88.7 mm). Topography of the two investigated watersheds is slightly different (Fig. 3a–b):  
136 elevation ranges from 185 to 576 m a.s.l. in W1 (mean = 303 m) and from 209 to 571 m a.s.l. in W2  
137 (mean = 345 m), whereas average slope gradient is 10.1° (SD = 5.0°) and 9.7° (SD = 6.9°),  
138 respectively. Soils are mostly regosols and vertisols with fine-medium texture (Fierotti, 1988).  
139 Lithologies are mainly eluvial-colluvial deposits, sands of the Late Miocene Terravecchia Fm.,

140 clays of the Middle-Late Miocene Castellana Sicula Fm., silty-clays and sandy-silts of the  
141 Terravecchia Fm. (Fig. 3c). Primary land covers are arable lands (mainly cereal fields) and  
142 vineyards, which occupy 92% of W1 and 80% of W2 (Fig. 3d).

143 Both watersheds are affected by gully erosion which increases soil loss, causes landscape dissection  
144 and hampers the movement of farm machines. Most of the gully channels in the drainage basins are  
145 ephemeral and are usually filled in by tillage within few months after their initiation. Conoscenti et  
146 al. (2018) created a gully inventory of the watersheds by analyzing a Google Earth image acquired  
147 on 3 May 2015 (Fig. 4) and by carrying out field surveys. As their objective was to model gully  
148 erosion due to overland flow concentration, the inventory includes only gullies located on  
149 concentrated flow pathways. The latter were extracted from the DEM, by calculating for each cell  
150 the value of upstream contributing area. To ensure consistency between mapped gullies and  
151 contributing area, gully trajectories have been slightly modified in order to exactly match flow  
152 pathways and to ensure that contributing area increases along each gully from head to mouth (Fig.  
153 5). The inventory includes 115 gullies (83 in W1, 32 in W2) and reveals that gully erosion is more  
154 severe in W1 (gully density =  $0.73 \text{ km}^{-1}$ ) than in W2 ( $0.18 \text{ km}^{-1}$ ). Gullies mostly occur on eluvial-  
155 colluvial deposits and clays. As regards land cover, arable lands host most of the gully trajectories.

## 156 2.2. Topographic indices

157 In this experiment, the ability to predict gully location of five topographic indices was assessed.  
158 These indices, which combine two or more primary topographic attributes (Wilson and Gallant,  
159 2000), including contributing area, slope steepness, plan curvature and convergence index, were  
160 calculated for each grid cell of the DEM, by using terrain analysis tools of SAGA-GIS software  
161 (Conrad et al., 2015).

162 Three topographic indices adopted here, namely stream power index (*SPI*), compound topographic  
163 index (*CTI*) and topographic wetness index (*TWI*), have been employed in previous studies to  
164 predict location of ephemeral gullies in cultivated watersheds (e.g., Vandaele et al., 1996; Parker et

165 al., 2007; Daggupati et al., 2013, 2014; Sekaluvu et al., 2015; Sekaluvu and Sheshukov, 2016;  
166 Sheshukov et al., 2018).

167 The *SPI* (Moore et al., 1988, 1991) is a measure of erosive power of concentrated runoff and is  
168 calculated as:

169

$$170 \quad SPI = A_s \cdot S \quad (1)$$

171

172 where  $A_s$  ( $m^2 m^{-1}$ ) is the specific contributing area and  $S$  ( $m m^{-1}$ ) is the local slope gradient.  $A_s$  and  $S$   
173 are employed as surrogates for flow discharge and velocity.  $A_s$  was extracted from upslope  
174 contributing area ( $A$ ), which in turn was calculated by applying the single flow direction (also  
175 referred to as D8) algorithm (O’Callaghan and Mark, 1984), after filling sinks in the DEM. To  
176 obtain  $A_s$ ,  $A$  has to be divided by the contour width within the pixel (Desmet and Govers, 1996). As  
177 the contour width can be set to the average of the grid cell width (i.e., 2.0 m) and the grid cell  
178 diagonal (i.e., 2.8 m),  $A_s$  was calculated dividing  $A$  by 2.4.

179 The *CTI* (Thorne et al., 1986) is defined as:

180

$$181 \quad CTI = A_s \cdot S \cdot PLANC \quad (2)$$

182

183 where  $PLANC$  ( $m/100 m$ ) is the curvature of the contour line (Hengl and Reuter, 2008).  $PLANC$  is a  
184 measure of local flow convergence and divergence and thus reflects the degree of concentration of  
185 the runoff. *CTI* is employed in the USDA Agricultural Non-Point Source (AGNPS) modelling  
186 system (Bingner and Theurer, 2001) to identify potential ephemeral gully locations throughout a  
187 watershed (Parker et al., 2007; Momm et al., 2012, 2013).

188 *TWI* (Moore et al., 1988; 1991) is a measure of soil saturation and is calculated as:

189

$$190 \quad TWI = \ln (A_s / S) \quad (3)$$

191

192 As *TWI* reflects zones of saturation in a watershed, it could also be an index of the potential location  
193 of ephemeral gullies. Indeed, gully heads often form where soils become very wet and lose their  
194 strength (Moore et al., 1988).

195 In addition to *SPI*, *CTI* and *TWI*, the ability to predict gully locations of other two topographic  
196 indices was explored. These indices are modified versions of *SPI* and *CTI* and are calculated as:

197

$$198 \quad MSPI = A_s \cdot S \cdot CI \quad (4)$$

199

$$200 \quad MTWI = \ln (A_s / S) \cdot CI \quad (5)$$

201

202 where *CI* is the convergence index (Köthe et al., 1996; Kiss, 2004; Thommeret et al., 2010). *CI*  
203 measures to what extent neighboring cells point to the center cell. *CI* is calculated as the average  
204 difference between actual aspect of surrounding cells within a moving square or circular window  
205 and the direction to the center cell, minus 90 degrees. The value ranges from -90 degrees (max  
206 convergence) by 0 (planar slopes) to 90 degrees (max divergence). *CI* provided by SAGA-GIS is  
207 normalized between -100 and 100. Differently from *PLANC*, which depends on local morphology,  
208 *CI* describes the general shape of the landscape up to a scale that depends from the size of the  
209 moving window. In this experiment, the *CI* value of each cell was calculated by averaging the  
210 values obtained varying the search radius of a circular moving window from 1 to 10 cells. As  
211 *PLANC* and *CI* calculated by SAGA-GIS have negative values on concavities (e.g. valley bottoms)  
212 and positive values on convexities (e.g. ridges), a change in the sign of both parameters was  
213 performed before using them to calculate the topographic indices employed to predict gully  
214 location.

215 *MSPI* and *MTWI* could help in predicting gully occurrence as they estimate runoff erosive power  
216 and potential soil saturation, respectively, and incorporate a weighting factor which reflects flow

217 convergence/divergence (i.e. *CI*).

### 218 2.3. Statistical modelling

219 In our experiment, the location of the gullies was also predicted by employing two statistical  
220 techniques, namely logistic regression (LR; Hosmer and Lemeshow, 2000) and multivariate  
221 adaptive regression splines (MARS; Friedman, 1991).

222 LR is a generalized linear model with a logistic link function. LR is among the most common  
223 statistical technique for prediction of gully occurrence (e.g., Meyer and Martínez-Casasnovas, 1999;  
224 Lucà et al., 2011; Conoscenti et al., 2014; Dewitte et al., 2015; Selkimäki and González-Olabarria,  
225 2016). Conversely, MARS has been employed only recently to model gully erosion (Gómez-  
226 Gutiérrez et al., 2009a, 2009c, 2015; Arabameri et al., 2018; Garosi et al., 2018; Conoscenti et al.,  
227 2018). LR and MARS enable modelling of relationships between continuous and/or categorical  
228 independent variables and a dichotomous dependent variable (i.e. event or non-event). Both  
229 techniques consist of an additive combination of terms. LR has a linear structure with constant  
230 coefficients across the entire range of the predictor variables. Conversely, MARS uses piece-wise  
231 linear regressions with breaks at the knots to describe non-linear relationships between event  
232 occurrence and predictors. To reduce the complexity of the models, MARS models were prepared  
233 with terms made of single predictors; as regards LR models, a bilateral stepwise strategy, which  
234 selects only the most significant predictors, was adopted. Please refer to Hosmer and Lemeshow  
235 (2000) and Friedman (1991) for further details about LR and MARS, respectively.

236 LR and MARS models were prepared by using as predictor variables the primary topographic  
237 attributes *S*, *A<sub>s</sub>*, *PLANC* and *CI*. Since both the employed statistical techniques require absence of  
238 multicollinearity, the degree of correlation among these four variables was evaluated before running  
239 the models. To this aim, the variance inflation factor (*VIF*) (Jebur et al., 2014; Heckmann et al.,  
240 2014; Bui et al., 2015; Conoscenti et al., 2016; Cama et al., 2017; Rotigliano et al., 2019; Vargas-  
241 Cuervo et al., 2019), was employed. The results, which were interpreted according to the “rule of  
242 10”, revealed absence of strong correlations among the predictor variables (*VIF* range: 1.0 – 1.1).



243 Calibration of the statistical models was carried out separately in W1 and W2, where 100 learning  
244 samples were prepared by randomly selecting the 25% of the total number of event pixels and the  
245 same number of non-event pixels. This percentage was chosen in order to achieve a compromise  
246 between the attempt to minimize the effects of spatial autocorrelation and the effort to obtain robust  
247 models, by using a sufficiently large number of cases. Since 1928 and 717 gully cells were  
248 identified in W1 and W2, respectively, the W1 learning samples include 964 pixels (i.e. 482 non-  
249 event + 482 event cells, the latter corresponding to 25% of 1928) whereas 358 pixels (i.e. 179 non-  
250 event + 179 event cells, the latter corresponding to 25% of 717) form the W2 samples. The learning  
251 samples were employed to perform 100 LR and 100 MARS model runs in each of the watersheds.  
252 Hereafter, MARS1 and LR1 are used to indicate model runs calibrated in W1 whereas MARS2 and  
253 LR2 indicate model runs calibrated in W2.

#### 254 *2.4. Validation strategy*

255 The ability to predict gully occurrence of topographic indices and statistical models was measured  
256 on a network of flow lines which were identified separately in W1 and W2 by using two different  
257 thresholds of contributing area. The thresholds were set equal to the minimum  $A_s$  of W1 and W2  
258 gully cells, respectively, after discarding values below the 1<sup>st</sup> percentile which were regarded as  
259 outliers. By using this approach, the predictive performance of topographic indices and statistical  
260 models was measured where drainage area is sufficient to trigger gully erosion, given the rainfall,  
261 soil, bedrock and land use characteristics which caused gully erosion in our study watersheds.

262 One hundred validation samples were prepared by randomly selecting pixels from flow lines of  
263 both W1 and W2. Like the calibration samples, also the validation samples include the 25% of the  
264 gully cells and a same number of non-gully cells. The value of the topographic indices was used  
265 directly as a score to predict the distribution of gully cells. As regards statistical modelling, the  
266 probability of gully occurrence was calculated from LR and MARS ensemble models (Kotu and  
267 Deshpande, 2015), which were prepared by averaging the score of the 100 model runs. This  
268 procedure was applied in order to generate a more stable performance of the models and to mitigate

269 the effects of prevalence (i.e. different proportion of event/non-event cells in the study area)  
270 (Svoray et al., 2012). The predictive performance of both “local” (i.e. calibrated and validated in the  
271 same watershed) and “transferred” (i.e. calibrated in one watershed and validated in the other one)  
272 statistical models was measured.

273 The accuracy of the topographic indices and statistical models was assessed by plotting for each  
274 validation sample the receiver operating characteristic (ROC) curve (e.g., Lasko et al., 2005;  
275 Brenning, 2005; Frattini et al., 2010; Cama et al., 2015, 2016) and by calculating the area under the  
276 ROC curve (*AUC*). ROC curve analysis is a cut-off independent technique for assessing the  
277 performance of predictive models, which plots all possible values of sensitivity (i.e. true positive  
278 rate, *TPR*) against the corresponding value of 1-specificity (i.e. false positive rate, *FPR*). The ideal  
279 predictive model achieves an *AUC* value close to 1, whereas a value close to 0.5 reveals inaccuracy  
280 in the model (Nandi and Shakoor, 2009). In this experiment, accuracy of the models was interpreted  
281 as acceptable, excellent or outstanding if *AUC* values were higher than 0.7, 0.8 and 0.9, respectively  
282 (Hosmer and Lemeshow, 2000). In both W1 and W2, a group of 100 ROC curves and related *AUC*  
283 values, was obtained (one for each validation sample) for each topographic index and statistical  
284 model. Comparisons between *AUC* groups were performed by using box plots and the Wilcoxon  
285 signed-rank test, setting the level of significance at 0.01.

286 Furthermore, the predictive ability of topographic indices and statistical models was evaluated by  
287 using cut-off dependent performance metrics such as Cohen’s kappa index (Cohen, 1960; Landis  
288 and Koch, 1977; Monserud and Leemans, 1992; Geissen et al., 2007; Frattini et al., 2010;  
289 Sterlacchini et al., 2011), sensitivity (or *TPR*) and specificity (i.e. true negative rate, *TNR*). The  
290 Cohen’s kappa index ( $\kappa$ ) reflects the degree of agreement between prediction and observation and is  
291 calculated as:

292

$$293 \quad \kappa = P_{\text{obs}} - P_{\text{exp}} / (1 - P_{\text{exp}}) \quad (6)$$

294

295 where  $P_{\text{obs}}$  and  $P_{\text{exp}}$  are the observed and the expected proportion of agreement, respectively.  $\kappa$   
296 values were interpreted according to Monserud and Leemans (1992), which evaluated the  
297 agreement between model prediction and observation as: 1.00, perfect; 0.85–0.99, excellent; 0.70–  
298 0.85, very good; 0.55–0.70, good; 0.40–0.55, fair; 0.20–0.40, poor; 0.05–0.20, very poor; <0.05,  
299 null.

300 Firstly, to calculate  $\kappa$ ,  $TPR$  and  $FPR$ , the average ROC curve from each group of 100 validation  
301 ROC curves was prepared. Then, the optimal cut-off values of these curves were identified by using  
302 the Youden's index ( $J$ ) (Youden, 1950; Angileri et al., 2016; Cama et al., 2017; Rotigliano et al.,  
303 2019), which corresponds to the threshold that maximizes the sum of sensitivity and specificity.  
304 Then, by using  $J$  as threshold ( $T$ ) to classify the grid pixels as not susceptible (score  $< T$ ) or as  
305 susceptible (score  $> T$ ) to gully erosion, the contingency tables were prepared for each topographic  
306 index and ensemble statistical model.

### 307 2.5. Gully prediction maps

308 A gully susceptibility map of the study area was obtained from each of the topographic indices and  
309 the four ensemble statistical models which were prepared by averaging the score of 100 MARS and  
310 LR model runs. Susceptibility to gully erosion was then classified into four levels according to  
311 thresholds that were calculated separately in W1 and W2 by using the steps described below, which  
312 were repeated for each topographic index and ensemble statistical model. First,  $J$  was used to  
313 separate the pixels of the 100 validation samples into a low susceptibility dataset (score  $< J$ ) and a  
314 high susceptible dataset (score  $> J$ ). Then, the average ROC curve and the Youden index were  
315 calculated for both the low susceptibility dataset ( $J_{\text{low}}$ ) and the high susceptibility dataset ( $J_{\text{high}}$ ).  
316 Finally, the following four levels of susceptibility to gully erosion were identified: i) low (score  $\leq$   
317  $J_{\text{low}}$ ); ii) moderate ( $J_{\text{low}} < \text{score} \leq J$ ); iii) high ( $J < \text{score} \leq J_{\text{high}}$ ); iv) very high (score  $> J_{\text{high}}$ ).

## 318 3. Results

319 3.1. Predictive performance measured by using a cut-off independent statistic

320 The ability of the topographic indices and statistical models to discriminate between gully and non-  
321 gully cells of the validation samples is graphically represented by the box plots of Fig. 6. Each box  
322 plot reveals the variability of a group of 100 *AUC* values by indicating their quartiles, as well as the  
323 lowest and the highest data still within 1.5 interquartile range of the lower quartile and of the upper  
324 quartile, respectively. Furthermore, descriptive statistics such as mean and standard deviation of  
325 each *AUC* group are reported in Table 1.

326 The *AUC* values reflect excellent ( $AUC > 0.8$ ) to outstanding ( $AUC > 0.9$ ) discrimination ability of  
327 indices and models applied to predict gullies occurred in the studied watersheds. However,  
328 significant differences of accuracy can be detected.

329 *MSPI* performed clearly better than the other indices in both watersheds. In W1, only *SPI* achieved  
330 a similar performance but still significantly lower than that obtained from *MSPI*. In W2, *SPI*  
331 performed better than *TWI* but not significantly different from *CTI* and *MTWI*. *TWI* performed  
332 better than its modified version (i.e. *MTWI*) in W1, whereas the opposite was observed in W2.

333 As regards statistical models, MARS performed better than LR in both watersheds. Accuracy of  
334 MARS and LR is significantly different even in W1, where *AUC* values appear quite similar. A not  
335 significant difference was observed only in W1 between local (i.e. trained in W1) LR and  
336 transferred (i.e. trained in W2) MARS models ( $p$ -value = 0.284). In W1, both MARS and LR local  
337 models (i.e. MARS1 and LR1) exhibited higher accuracy than transferred models (i.e. MARS2 and  
338 LR2). On the other hand, a not significant difference of *AUC* was observed in W2 between local  
339 and transferred LR models ( $p$ -value = 0.5221).

340 The *AUC* values and the Wilcoxon signed-rank test revealed an overall better predictive  
341 performance of the statistical models with respect to the topographic indices, with the exception of  
342 *MSPI*. The latter indeed achieved outstanding accuracy in both watersheds. In W1, *MSPI* exhibited  
343 the same accuracy of transferred MARS and local LR runs and better predictive ability than  
344 transferred LR runs. In W2, *MSPI* achieved higher accuracy than both local and transferred LR runs

345 and the same accuracy of MARS1. Only local MARS models performed significantly better than  
346 MSPI.

### 347 3.2. Predictive performance measured by using cut-off dependent statistics

348 Fig. 7 shows the average ROC curves obtained from the validation of the topographic indices and  
349 statistical models in W1 and W2. These curves were employed to calculate the optimal cut-off ( $T$ )  
350 that maximizes the sum of sensitivity and specificity and which graphically corresponds to the  
351 maximum distance to the diagonal lines plotted in Fig. 8. The value of  $T$ , as well as those of kappa  
352 index ( $\kappa$ ),  $TPR$  and  $TNR$  are reported in Table 2. Kappa values obtained for the five topographic  
353 indices vary from 0.625 to 0.795 indicating a good ( $\kappa > 0.55$ ) to very good ( $\kappa > 0.70$ ) ability to  
354 discriminate between event and non-event pixels. As revealed by  $AUC$  values, the kappa index also  
355 demonstrated that  $MSPI$  achieved the best predictive skill in both watersheds.  $SPI$  reached a  $\kappa$  value  
356 close that of  $MSPI$  in W1. Conversely,  $SPI$  accuracy appears similar to that of  $TWI$  and  $MTWI$  in  
357 W2, where  $CTI$  achieved the second best  $\kappa$  value. As regards sensitivity and specificity,  $MSPI$   
358 obtained the highest values in W1 whereas in W2 a slightly higher  $TPR$  and  $TNR$  was observed for  
359  $MTWI$  and  $TWI$ , respectively.

360 Kappa index revealed approximately the same difference of performance between MARS and LR  
361 models which is highlighted by the  $AUC$  values. Indeed, MARS achieved higher  $\kappa$  values in both  
362 watersheds, with more enhanced difference of accuracy occurring in W2, where LR models are  
363 below the threshold indicating very good performance ( $\kappa > 0.7$ ). The difference of performance  
364 observed in W1 appears related more to a difference in specificity than in sensitivity, which is very  
365 similar for MARS and LR models. On the other hand, in W2, MARS runs exhibit higher values of  
366 both  $TPR$  and  $TNR$ , whereas only transferred models show a similar sensitivity.

367 Kappa,  $TPR$  and  $TNR$  confirm that  $MSPI$  achieves approximately the same accuracy of MARS runs.  
368 Furthermore, these statistics reveal that  $MSPI$  outperforms both LR local and transferred models  
369 which in turn show better discrimination ability when compared to the other topographic indices,  
370 with the exception of  $SPI$ , in W1, and  $CTI$ , in W2.

### 371 3.3. Gully prediction maps

372 Fig. 8 shows the gully prediction maps for the sectors of W1 and W2 highlighted in Fig. 4, obtained  
373 from the topographic indices and the ensemble statistical models. To aid the assessment of the  
374 maps, Fig. 9 plots the relative frequency distributions of non-event and event pixels across the  
375 susceptibility levels. The gully erosion susceptibility maps show very low probability of gully  
376 occurrence in most part of the study area, with the exception of few flow lines where susceptibility  
377 level is from moderate to very high. Only maps derived from *MTWI* and LR, especially in W2,  
378 show slightly larger sectors with moderate to high probability of gully occurrence. This is  
379 confirmed by the bar plots of Fig. 9, which reveal that non-event cells occur with a frequency  
380 higher than 5% only over moderate probability levels of *MTWI* maps and of LR maps of W2. On  
381 the other hand, although their very low frequency, high and very high susceptibility levels of all the  
382 maps host most of the gully pixels. In particular, the maps derived from *SPI*, *MSPI* and MARS1  
383 ensemble model, achieve the highest percentage of gully pixels within the very high level of  
384 susceptibility (Fig. 9).

## 385 4. Discussion

386 The results of our experiment showed that the spatial distribution of gullies can be effectively  
387 predicted by using either topographic indices or statistical models.

388 Both cut-off independent and dependent performance metrics revealed that, among the employed  
389 topographic indices, the best accuracy in predicting gully occurrence is achieved by *MSPI* whereas  
390 *MTWI* exhibited similar or worse performance than *SPI*, *CTI* and *TWI*. The ability of the latter  
391 indices to discriminate between gully and non-pixels was evaluated and compared, by identifying  
392 optimal thresholds and by calculating the  $\kappa$  index, in three previous studies (Daggupati et al., 2013;  
393 Sekaluvu et al., 2015; Sheshukov et al., 2018) performed in Kansas. Daggupati et al. (2013)  
394 estimated the thresholds of 30 – 50, 62, and 12, respectively, for *SPI*, *CTI* and *TWI*. Sekaluvu et al.  
395 (2015) and Sheshukov et al. (2018) report that the critical thresholds required by *CTI* to best predict

396 the gullies of two watersheds of central Kansas are equal to 79.4 and 25.1. These values are  
397 relatively similar to the *CTI* thresholds estimated by Daggupati et al. (2013) and those calculated in  
398 our experiment (52.8 and 24.3). As regards *SPI*, the thresholds found in our study (270.9 and 127.0)  
399 are of the same order of magnitude of those calculated by Sekaluvu et al. (2015) and Sheshukov et  
400 al. (2018) (501.2 and 158.5), but higher than the values reported by Daggupati et al. (2013).  
401 Furthermore, the *TWI* critical thresholds estimated in our experiment (9.7 and 9.4) are quite similar  
402 to those calculated for the Kansas areas (12.0 – 18.2).

403 By applying the thresholds cited above, Daggupati et al. (2013) found a poor predictive  
404 performance of *CTI* and *TWI* but a fair agreement between observed gullies and prediction obtained  
405 using *SPI* ( $\kappa$ : 0.40 – 0.55). This is in accordance with what observed in W1 but not in W2, where  
406 *CTI* achieved a higher  $\kappa$  value than *SPI* and *TWI*. A similar result is reported by Sekaluvu et al.  
407 (2015) and Sheshukov et al. (2018), who observed a better accuracy of *CTI*, which achieved a  $\kappa$   
408 value of 0.29 and 0.32 in two watersheds of central Kansas. However, it is worth noting that the  
409 range of  $\kappa$  obtained in our experiment for *SPI*, *CTI* and *TWI* is quite higher (0.63 – 0.77) than the  
410 values calculated in Kansas. This could be explained by considering that the trajectory of our  
411 gullies was adjusted to fit lines of flow concentration extracted from the DEM. This procedure  
412 indeed prevents gullies to intersect cells with very low or null drainage area, which can be caused  
413 by mapping errors or inadequate DEM resolution, and thus may yield a stronger positive  
414 relationship between gully occurrence and contributing area. Furthermore, the higher values of  $\kappa$   
415 achieved by topographic indices in predicting our gullies can be also explained by considering that  
416 validation in this experiment was performed at the pixel scale while a sub-watershed scale was  
417 employed in the studies performed in Kansas (Daggupati et al., 2013; Sekaluvu et al., 2015;  
418 Sheshukov et al., 2018).

419 To explain the better accuracy of *MSPI* with respect to the other indices, it can be hypothesized that  
420 adding *CI* to the *SPI* formula helps in detecting areas of enhanced flow concentration and, thus, in  
421 identifying cells which are likely to host a gully. Moreover, since *MSPI* performs clearly better than

422 *CTI* in both investigated watersheds, it can be inferred that the contribution of *CI* in increasing the  
423 ability to discriminate between non-gully and gully cells is higher than that provided by *PLANC*.  
424 This hypothesis is corroborated by the frequency distributions of *CI* and *PLANC* measured on gully  
425 and non-gully cells, which are revealed by the kernel density plots of Fig. 10. These plots show that  
426 *CI* distributions measured along gully trajectories are clearly different from those calculated for  
427 non-event cells, whereas no such difference can be observed for *PLANC*. Furthermore, *PLANC*  
428 does not improve appreciably the predictive ability of *CTI* with respect to *SPI*; indeed, *SPI* achieves  
429 higher *AUC* values in both studied watersheds and higher  $\kappa$  value in W1. On the other hand, *CI* did  
430 not improve the predictive skill of *TWI*, as *MTWI* performed better than *TWI* only in W2.

431 As regards statistical modelling of gully occurrence, validation performed in our study area  
432 revealed a better predictive skill of MARS with respect to LR. This results is in line with other  
433 studies, like that of Garosi et al. (2018), which also found a better performance of MARS (*AUC*:  
434 74.5–90.2) with respect to LR (*AUC*: 66.4–85.6) in predicting gully erosion susceptibility in Iran.  
435 MARS provided slightly better accuracy also in another Sicilian watershed (Gómez-Gutiérrez et al.,  
436 2015), where LR has been previously employed to predict the same gully inventory (Conoscenti et  
437 al., 2014). Also Rahmati et al. (2019) observed better accuracy of MARS in predicting the same  
438 gully inventory of this study, although performing validation on pixels selected from the entire  
439 watersheds and employing a quite larger number of predictors, which include land use and bedrock.  
440 The better performance of MARS was somewhat expected given the widely accepted assumption  
441 that gullying is a threshold phenomenon and the ability of MARS to model non-linear relationships  
442 between event occurrence and predictor variables. Indeed, MARS is able to identify, across the  
443 range of the predictors, different linear functions separated by knots which may correspond to  
444 potential thresholds for gully initiation.

445 *AUC* and  $\kappa$  values revealed that, in our study area, statistical models predict the occurrence of  
446 gullies with better accuracy than topographic indices, with the exception of *MSPI*. The latter  
447 exhibited indeed similar or better predictive performance than local LR models and transferred LR



448 and MARS models, whereas only local MARS2 model runs achieved better accuracy. Due to their  
449 data-driven nature, a better fit of MARS and LR to the observed gully data was expected prior to  
450 performing the experiment. Coefficients of local MARS and LR equations were indeed calculated  
451 on the basis of the observed spatial distribution of gullies within the training areas. Also transferred  
452 models, although calibrated in one watershed and validated in the other one, were expected to  
453 achieve better accuracy than topographic indices, due to the closeness of the two areas and their  
454 similar environmental conditions. Therefore, the difference in performance observed between *MSPI*  
455 and the transferred statistical models suggests that where an inventory of gullies is not available,  
456 reliable maps of gully erosion susceptibility can be prepared by using *MSPI*. This holds in particular  
457 if only topographic data is available at high resolution. Indeed, it is worth considering that  
458 predictive ability of multivariate statistical models can be improved by including variables  
459 reflecting, at high resolution, land use, soil and bedrock characteristics.

460 The gully erosion prediction maps derived from both topographic indices and ensemble statistical  
461 models exhibit an optimal distribution of the susceptibility levels in relation to gullies location.  
462 Indeed, at least 89% of observed non-gully cells fall within the lowest susceptibility level whereas  
463 between 53% (*CTI* map in W2) and 71% (*SPI* map in W1) of gully cells intersect the highest class  
464 of gully occurrence probability. In addition to the reliability of the employed indices and models, it  
465 can be inferred that the large agreement observed between prediction maps and gully spatial  
466 distribution is due to the method employed to identify the susceptibility classes, which was based  
467 on the Youden's index (*J*).

## 468 **5. Concluding remarks**

469 In this experiment, the ability of a set of five topographic indices to predict the spatial distribution  
470 of the gullies observed in two adjacent watersheds located in Sicily (Italy) was evaluated. Two of  
471 these indices, named *MSPI* and *MTWI*, as far as we know, have never been employed to this aim;  
472 they were obtained by multiplying the stream power index (*SPI*) and the topographic wetness index  
473 (*TWI*), respectively, by the convergence index (*CI*). The predictive ability of the topographic

474 indices was measured by using both cut-off independent and dependent statistics and compared to  
475 the performance of multivariate statistical models, which use as predictors the same topographic  
476 variables of the five indices (i.e. contributing area, slope steepness, plan curvature and convergence  
477 index).

478 The validation results revealed that topographic indices and statistical models achieved excellent to  
479 outstanding accuracy in predicting the spatial distribution of the gullies observed in our study area.  
480 Statistical models performed better than topographic indices with the exception of *MPSI*. Since the  
481 proposed index showed the best predictive performance among the topographic indices, it can be  
482 inferred that the inclusion of *CI* helps in detecting hollow areas where gullies are more likely to  
483 occur. Furthermore, *MSPI* exhibited similar or better predictive skill than transferred statistical  
484 models (i.e. models calibrated in one watershed and validated in the other one). This suggests that  
485 *MPSI* can be a valid alternative to a data driven approach for identifying potential gully locations in  
486 areas where a gully inventory is not available, which is necessary to calibrate statistical models.

## 487 **Acknowledgments**

488 This research was developed in the framework of the project FLUMEN (project number: 318969),  
489 funded by the EU (call identifier: FP7-PEOPLE-2012-IRSES), scientific responsible for the  
490 University of Palermo: Prof. Dr. C. Conoscenti. C. Conoscenti and E. Rotigliano have commonly  
491 shared the whole research phases. This manuscript benefited greatly from the kind suggestions and  
492 comments of the three anonymous reviewers.

## 493 **References**

- 494 Angileri, S.E., Conoscenti, C., Hochschild, V., Märker, M., Rotigliano, E., Agnesi, V., 2016. Water erosion  
495 susceptibility mapping by applying stochastic gradient treeboost to the imera Meridionale River basin (Sicily,  
496 Italy). *Geomorphology* 262, 61–76. <https://doi.org/10.1016/j.geomorph.2016.03.018>
- 497 Arabameri, A., Pradhan, B., Pourghasemi, H.R., Rezaei, K., Kerle, N., 2018. Spatial Modelling of Gully Erosion Using  
498 GIS and R Programming: A Comparison among Three Data Mining Algorithms. *Appl. Sci.* 8, 1369.  
499 <https://doi.org/10.3390/app8081369>
- 500 Azareh, A., Rahmati, O., Rafiei-Sardooi, E., Sankey, J.B., Lee, S., Shahabi, H., Ahmad, B. Bin, 2019. Modelling gully-  
501 erosion susceptibility in a semi-arid region, Iran: Investigation of applicability of certainty factor and maximum  
502 entropy models. *Sci. Total Environ.* 655, 684–696. <https://doi.org/10.1016/j.scitotenv.2018.11.235>
- 503 Bingner, R.L., Theurer, F.D., 2001. AGNPS 98: A Suite of water quality models for watershed use, in: Proceedings of  
504 the Sediment: Monitoring, Modeling, and Managing, 7th Federal Interagency Sedimentation Conference. Reno,

505 NV, 25-29 March 2001.

506 Brenning, A., 2005. Spatial prediction models for landslide hazards: review, comparison and evaluation. *Nat. Hazards*

507 *Earth Syst. Sci.* 5, 853–862. <https://doi.org/10.5194/nhess-5-853-2005>

508 Bui, D.T., Tuan, T.A., Klempe, H., Pradhan, B., Revhaug, I., 2015. Spatial prediction models for shallow landslide

509 hazards : a comparative assessment of the efficacy of support vector machines , artificial neural networks , kernel

510 logistic regression , and logistic model tree. *Landslides*. <https://doi.org/10.1007/s10346-015-0557-6>

511 Cama, M., Lombardo, L., Conoscenti, C., Agnesi, V., Rotigliano, E., 2015. Predicting storm-triggered debris flow

512 events: application to the 2009 Ionian Peloritani disaster (Sicily, Italy). *Nat. Hazards Earth Syst. Sci.* 15, 1785–

513 1806. <https://doi.org/10.5194/nhess-15-1785-2015>

514 Cama, M., Conoscenti, C., Lombardo, L., Rotigliano, E., 2016. Exploring relationships between grid cell size and

515 accuracy for debris-flow susceptibility models: a test in the Giampileri catchment (Sicily, Italy). *Environ. Earth*

516 *Sci.* 75. <https://doi.org/10.1007/s12665-015-5047-6>

517 Cama, M., Lombardo, L., Conoscenti, C., Rotigliano, E., 2017. Improving transferability strategies for debris flow

518 susceptibility assessment: Application to the Saponara and Itala catchments (Messina, Italy). *Geomorphology*

519 288, 52–65. <https://doi.org/10.1016/j.geomorph.2017.03.025>

520 Capra, A., Mazzara, L.M., Scicolone, B., 2005. Application of the EGEM model to predict ephemeral gully erosion in

521 Sicily, Italy. *Catena* 59, 133-146 ST-Application of the EGEM model to pre.

522 <https://doi.org/10.1016/j.catena.2004.07.001>

523 Capra, A., Scicolone, B., 2002. Ephemeral gully erosion in a wheat-cultivated area in Sicily (Italy). *Biosyst. Eng.* 83,

524 119–126. <https://doi.org/10.1006/bioe.2002.0092>

525 Caraballo-Arias, N.A., Conoscenti, C., Di Stefano, C., Ferro, V., 2015. A new empirical model for estimating calanchi

526 Erosion in Sicily, Italy. *Geomorphology* 231, 292–300. <https://doi.org/10.1016/j.geomorph.2014.12.017>

527 Caraballo-Arias, N.A., Conoscenti, C., Di Stefano, C., Ferro, V., 2014. Testing GIS-morphometric analysis of some

528 Sicilian badlands. *CATENA* 113, 370–376. <https://doi.org/10.1016/j.catena.2013.08.021>

529 Choubin B., Rahmati O., Tahmasebipour N., Feizizadeh B., Pourghasemi H.R. (2019) Application of Fuzzy Analytical

530 Network Process Model for Analyzing the Gully Erosion Susceptibility. In: Pourghasemi H., Rossi M. (eds)

531 Natural Hazards GIS-Based Spatial Modeling Using Data Mining Techniques. *Advances in Natural and*

532 *Technological Hazards Research*, vol 48. Springer, Cham

533 Cohen, J., 1960. A coefficient of agreement for nominal scales. *Educ. Psychol. Meas.* 20, 37–46.

534 Conoscenti, C., Agnesi, V., Angileri, S., Cappadonia, C., Rotigliano, E., Märker, M., 2013. A GIS-based approach for

535 gully erosion susceptibility modelling: a test in Sicily, Italy. *Environ. Earth Sci.* 70, 1179–1195.

536 <https://doi.org/10.1007/s12665-012-2205-y>

537 Conoscenti, C., Agnesi, V., Cama, M., Caraballo-Arias, N.A., Rotigliano, E., 2018. Assessment of Gully Erosion

538 Susceptibility Using Multivariate Adaptive Regression Splines and Accounting for Terrain Connectivity. *L.*

539 *Degrad. Dev.* 29, 724–736. <https://doi.org/10.1002/ldr.2772>

540 Conoscenti, C., Angileri, S., Cappadonia, C., Rotigliano, E., Agnesi, V., Märker, M., 2014. Gully erosion susceptibility

541 assessment by means of GIS-based logistic regression: a case of Sicily (Italy). *Geomorphology* 204, 399–411.

542 <https://doi.org/10.1016/j.geomorph.2013.08.021>

543 Conoscenti, C., Rotigliano, E., Cama, M., Caraballo-Arias, N.A., Lombardo, L., Agnesi, V., 2016. Exploring the effect

544 of absence selection on landslide susceptibility models: A case study in Sicily, Italy. *Geomorphology* 261, 222–

545 235. <https://doi.org/10.1016/j.geomorph.2016.03.006>

546 Conrad, O., Bechtel, B., Bock, M., Dietrich, H., Fischer, E., Gerlitz, L., Wehberg, J., Wichmann, V., Böhner, J., 2015.

547 System for Automated Geoscientific Analyses (SAGA) v. 2.1.4. *Geosci. Model Dev.* 8, 1991–2007.

548 <https://doi.org/10.5194/gmd-8-1991-2015>

549 Daggupati, P., Douglas-Mankin, K.R., Sheshukov, A.Y., 2013. Predicting ephemeral gully location and length using

550 topographic index models. *Trans. ASABE* 56, 1427–1440. <https://doi.org/10.13031/trans.56.10087>

551 Daggupati, P., Sheshukov, A.Y., Douglas-Mankin, K.R., 2014. Evaluating ephemeral gullies with a process-based

552 topographic index model. *CATENA* 113, 177–186. <https://doi.org/10.1016/j.catena.2013.10.005>

553 Desmet, P.J.J., Govers, G., 1996. Comparison of routing algorithms for digital elevation models and their implications

554 for predicting ephemeral gullies. *Int. J. Geogr. Inf. Syst.* 10, 311–331.

555 <https://doi.org/10.1080/02693799608902081>

556 Desmet, P.J.J., Poesen, J., Govers, G., Vandaele, K., 1999. Importance of slope gradient and contributing area for

557 optimal prediction of the initiation and trajectory of ephemeral gullies. *Catena* 37, 377–392.

558 [https://doi.org/10.1016/S0341-8162\(99\)00027-2](https://doi.org/10.1016/S0341-8162(99)00027-2)

559 Dewitte, O., Daoudi, M., Bosco, C., Van Den Eeckhaut, M., 2015. Predicting the susceptibility to gully initiation in

560 data-poor regions. *Geomorphology* 228, 101–115. <https://doi.org/10.1016/j.geomorph.2014.08.010>

561 Eustace, A.H., Pringle, M.J., Denham, R.J., 2011. A risk map for gully locations in central Queensland, Australia. *Eur.*

562 *J. Soil Sci.* 62, 431–441. <https://doi.org/10.1111/j.1365-2389.2011.01375.x>

563 Fierotti, G., 1988. Carta dei Suoli della Sicilia. Istituto di Agronomia, Università di Palermo e Regione Sicilia,

564 Assessorato Territorio ed Ambiente, Palermo.

565 Frattini, P., Crosta, G., Carrara, A., 2010. Techniques for evaluating the performance of landslide susceptibility models.

566 *Eng. Geol.* 111, 62–72. <https://doi.org/10.1016/j.enggeo.2009.12.004>

567 Friedman, J.H., 1991. Multivariate adaptive regression splines. *Ann. Stat.* 19, 1–141.

- 568 Garosi, Y., Sheklabadi, M., Porghasemi, H.R., Besalatpour, A.A., Conoscenti, C., Van Oost, K., 2018. Comparison of  
569 differences in resolution and sources of controlling factors for gully erosion susceptibility mapping. *Geoderma*  
570 330, 65–78. <https://doi.org/10.1016/j.geoderma.2018.05.027>
- 571 Garosi, Y., Sheklabadi, M., Conoscenti, C., Pourghasemi, H.R., Van Oost, K., 2019. Assessing the performance of GIS-  
572 based machine learning models with different accuracy measures for determining susceptibility to gully erosion.  
573 *Sci. Total Environ.* 664, 1117–1132. <https://doi.org/10.1016/j.scitotenv.2019.02.093>
- 574 Geissen, V., Kampichler, C., López-de Llergo-Juárez, J.J., Galindo-Acántara, A., 2007. Superficial and subterranean  
575 soil erosion in Tabasco, tropical Mexico: Development of a decision tree modeling approach. *Geoderma* 139,  
576 277–287. <https://doi.org/10.1016/j.geoderma.2007.01.002>
- 577 Gómez-Gutiérrez, Á., Conoscenti, C., Angileri, S.E., Rotigliano, E., Schnabel, S., 2015. Using topographical attributes  
578 to evaluate gully erosion proneness (susceptibility) in two mediterranean basins: advantages and limitations. *Nat.*  
579 *Hazards* 79, 291–314. <https://doi.org/10.1007/s11069-015-1703-0>
- 580 Gómez-Gutiérrez, Á., Schnabel, S., Felicísimo, Á.M., 2009a. Modelling the occurrence of gullies in rangelands of  
581 southwest Spain. *Earth Surf. Process. Landforms* 34, 1894–1902. <https://doi.org/10.1002/esp1881>
- 582 Gómez-Gutiérrez, Á., Schnabel, S., Lavado Contador, F., 2009b. Gully erosion, land use and topographical thresholds  
583 during the last 60 years in a small rangeland catchment in SW Spain. *L. Degrad. Dev.* 20, 535–550.  
584 <https://doi.org/10.1002/ldr>
- 585 Gómez-Gutiérrez, Á., Schnabel, S., Lavado Contador, F., 2009c. Using and comparing two nonparametric methods  
586 (CART and MARS) to model the potential distribution of gullies. *Ecol. Modell.* 220, 3630–3637.  
587 <https://doi.org/10.1016/j.ecolmodel.2009.06.020>
- 588 Gordon, L.M., Bennett, S.J., Bingner, R.L., Theurer, F.D., Alonso, C. V., 2007. Simulating ephemeral gully erosion in  
589 AnnAGNPS. *Trans. ASABE*.
- 590 Heckmann, T., Gegg, K., Gegg, a., Becht, M., 2014. Sample size matters: investigating the effect of sample size on a  
591 logistic regression susceptibility model for debris flows. *Nat. Hazards Earth Syst. Sci.* 14, 259–278.  
592 <https://doi.org/10.5194/nhess-14-259-2014>
- 593 Hengl, T., Reuter, H.I., 2008. *Geomorphometry: Concepts, Software, Applications*. Elsevier, Amsterdam.
- 594 Hijmans, R.J., 2017. raster: Geographic Data Analysis and Modeling [WWW Document]. URL [https://cran.r-](https://cran.r-project.org/package=raster)  
595 [project.org/package=raster](https://cran.r-project.org/package=raster)
- 596 Hosmer, D.W., Lemeshow, S., 2000. *Applied logistic regression*, Wiley Series in Probability and Statistics, Wiley  
597 series in probability and statistics: Texts and references section. Wiley. <https://doi.org/10.1198/tech.2002.s650>
- 598 Javidan, N., Kavian, A., Pourghasemi, H.R., Conoscenti, C., Jafarian, Z., 2019. Gully Erosion Susceptibility Mapping  
599 Using Multivariate Adaptive Regression Splines—Replications and Sample Size Scenarios. *Water* 11, 2319, 1–  
600 21. <https://doi.org/10.3390/w11112319>
- 601 Jebur, M.N., Pradhan, B., Tehrany, M.S., 2014. Optimization of landslide conditioning factors using very high-  
602 resolution airborne laser scanning (LiDAR) data at catchment scale. *Remote Sens. Environ.* 152, 150–165.  
603 <https://doi.org/10.1016/j.rse.2014.05.013>
- 604 Kiss, R., 2004. Determination of drainage network in digital elevation models, utilities and limitations. *J. Hungarian*  
605 *Geomathematics* 2, 16–29.
- 606 Knisel, W.G., 1993. GLEAMS: Groundwater loading effects of agricultural management systems. Publication No. 5.  
607 Tifton, Ga.: University of Georgia, Coastal Plains Experiment Station.
- 608 Knisel, W.G., 1980. CREAMS: A field scale model for chemicals, runoff and erosion from agricultural management  
609 systems. *US Dep. Agric. Conserv. Res. Rep.* 26, 474–485.
- 610 Köthe, R., Gehrt, E., Böhner, J., 1996. Automatische Reliefanalyse für geowissenschaftliche Anwendungen—  
611 derzeitiger Stand und Weiterentwicklungen des Programms SARA. *Arbeitshefte Geol.* 1, 31–37.
- 612 Kotu, V., Deshpande, B., 2015. Chapter 2 - Data Mining Process, in: Kotu, V., Deshpande, B. (Eds.), *Predictive*  
613 *Analytics and Data Mining*. Morgan Kaufmann, Boston, pp. 17–36. [https://doi.org/https://doi.org/10.1016/B978-](https://doi.org/https://doi.org/10.1016/B978-0-12-801460-8.00002-1)  
614 [0-12-801460-8.00002-1](https://doi.org/https://doi.org/10.1016/B978-0-12-801460-8.00002-1)
- 615 Landis, J.R., Koch, G.G., 1977. The Measurement of Observer Agreement for Categorical Data. *Biometrics* 33, 159–  
616 174. <https://doi.org/10.2307/2529310>
- 617 Lasko, T.A., Bhagwat, J.G., Zou, K.H., Ohno-Machado, L., 2005. The use of receiver operating characteristic curves in  
618 biomedical informatics. *J. Biomed. Inform.* 38, 404–415. <https://doi.org/10.1016/j.jbi.2005.02.008>
- 619 Lucà, F., Conforti, M., Robustelli, G., 2011. Comparison of GIS-based gully susceptibility mapping using bivariate  
620 and multivariate statistics: Northern Calabria, South Italy. *Geomorphology* 134, 297–308.  
621 <https://doi.org/10.1016/j.geomorph.2011.07.006>
- 622 Mahto, A., 2018. splitstackshape: Stack and Reshape Datasets After Splitting Concatenated Values [WWW Document].  
623 URL <https://cran.r-project.org/package=splitstackshape>
- 624 Merkel, W.H., Woodward, D.E., Clarke, C.D., 1988. Ephemeral gully erosion model (EGEM). *Agric. For. Rangel.*  
625 *Hydrol. Am. Soc. Agric. Eng. Publ.* 07–88, 315–323.
- 626 Meyer, A., Martínez-Casasnovas, J.A., 1999. Prediction of existing gully erosion in vineyard parcels of the NE Spain: a  
627 logistic modelling approach. *Soil Tillage Res.* 50, 319–331. [https://doi.org/10.1016/S0167-1987\(99\)00020-3](https://doi.org/10.1016/S0167-1987(99)00020-3)
- 628 Milborrow, S., 2018. earth: Multivariate Adaptive Regression Splines [WWW Document]. URL [https://cran.r-](https://cran.r-project.org/package=earth)  
629 [project.org/package=earth](https://cran.r-project.org/package=earth)
- 630 Momm, H.G., Bingner, R.L., Wells, R.R., Wilcox, D., 2012. Agnps GIS-based tool for watershed-scale identification

631 and mapping of cropland potential ephemeral gullies. *Appl. Eng. Agric.* 28, 17–29.

632 Momm, H.G., Bingner, R.L., Wells, R.R.W., Rigby, J.R., Dabney, S.M., 2013. Effect of Topographic Characteristics on

633 Compound Topographic Index for Identification of Gully Channel Initiation Locations, in: *Transactions of the*

634 *ASABE*. pp. 523–537. <https://doi.org/10.13031/2013.42673>

635 Monserud, R.A., Leemans, R., 1992. Comparing global vegetation maps with the Kappa statistic. *Ecol. Modell.* 62,

636 275–293. [https://doi.org/https://doi.org/10.1016/0304-3800\(92\)90003-W](https://doi.org/https://doi.org/10.1016/0304-3800(92)90003-W)

637 Montgomery, D.R., Dietrich, W.E., 1992. Channel initiation and the problem of landscape scale. *Science* (80-. ). 255,

638 826–830. <https://doi.org/10.1126/science.255.5046.826>

639 Moore, I.D., Burch, G.J., Mackenzie, D.H., 1988. Topographic effects on the distribution of surface soil water and the

640 location of ephemeral gullies. *Trans. ASAE* 32 32, 1098–1107.

641 Moore, I.D., Grayson, R.B., Ladson, A.R., 1991. Digital terrain modelling: a review of hydrological, geomorphological,

642 and biological applications. *Hydrol. Process.* 4, 3–30.

643 Nachtergaele, J., Poesen, J., Vandekerckhove, L., Oostwoud Wijdenes, D., Roxo, M., 2001a. Testing the Ephemeral

644 Gully Erosion Model (EGEM) in Mediterranean environments, in: Stott, D.E., Mohtar, R.H., Steinhardt, G.C.

645 (Eds.), *Sustaining the Global Farm – Selected Papers from the 10th International Soil Conservation Organization*

646 *Meeting, May 24-29, 1999, West Lafayette, IN*. pp. 1024–1028.

647 Nachtergaele, J., Poesen, J., Vandekerckhove, L., Oostwoud Wijdenes, D., Roxo, M., 2001b. Testing the Ephemeral

648 Gully Erosion Model (EGEM) for two Mediterranean environments. *Earth Surf. Process. Landforms* 26, 17–30.

649 [https://doi.org/10.1002/1096-9837\(200101\)26:1<17::AID-ESP149>3.0.CO;2-7](https://doi.org/10.1002/1096-9837(200101)26:1<17::AID-ESP149>3.0.CO;2-7)

650 Naimi, B., 2015. Uncertainty analysis for species distribution models. *R Software Package*.

651 Nandi, A., Shakoor, A., 2009. A GIS-based landslide susceptibility evaluation using bivariate and multivariate

652 statistical analyses. *Eng. Geol.* 110, 11–20. <https://doi.org/10.1016/j.enggeo.2009.10.001>

653 Nazari Samani, A., Ahmadi, H., Jafari, M., Boggs, G., Ghoddousi, J., Malekian, A., 2009. Geomorphic threshold

654 conditions for gully erosion in Southwestern Iran (Boushehr-Samal watershed). *J. Asian Earth Sci.* 35, 180–189.

655 <https://doi.org/10.1016/j.jseaes.2009.02.004>

656 O’Callaghan, J.F., Mark, D., 1984. The extraction of drainage networks from digital elevation data. *Comput. Vision,*

657 *Graph. Image Process.* 28, 323–344. [https://doi.org/http://dx.doi.org/10.1016/S0734-189X\(84\)80011-0](https://doi.org/http://dx.doi.org/10.1016/S0734-189X(84)80011-0)

658 Oostwoud Wijdenes, D.J., Poesen, J., Vandekerckhove, L., Ghesquiere, M., 2000. Spatial distribution of gully head

659 activity and sediment supply along an ephemeral channel in a Mediterranean environment. *Catena* 39, 147–167.

660 [https://doi.org/10.1016/S0341-8162\(99\)00092-2](https://doi.org/10.1016/S0341-8162(99)00092-2)

661 Parker, C., Thorne, C., Bingner, R., Wells, R., Wilcox, D., 2007. Automated Mapping of Potential For Ephemeral Gully

662 Formation in Agricultural Watersheds, in: *Proceedings of the 2nd Joint Federal Interagency Conference, June 27-*

663 *July 1, 2010, Las Vegas, Nevada. Las Vegas, NV*, pp. 1–12.

664 Patton, P.C., Schumm, S.A., 1975. Gully erosion, northwestern Colorado: a threshold phenomenon. *Geology* 31, 187–

665 199.

666 Poesen, J., Nachtergaele, J., Verstraeten, G., Valentin, C., 2003. Gully erosion and environmental change: importance

667 and research needs. *Catena* 50, 91–133. [https://doi.org/10.1016/S0341-8162\(02\)00143-1](https://doi.org/10.1016/S0341-8162(02)00143-1)

668 Poesen, J., Torri, D., Van Walleghem, T., 2011. Gully Erosion: Procedures to Adopt When Modelling Soil Erosion in

669 Landscapes Affected by Gullying, in: Morgan, P.C., Nearing, M.A. (Eds.), *Handbook of Erosion Modelling*. John

670 Wiley & Sons, Ltd, Chichester, UK, pp. 360–386. <https://doi.org/10.1002/9781444328455.ch19>

671 Pourghasemi, H.R., Yousefi, S., Kornejady, A., Cerdà, A., 2017. Performance assessment of individual and ensemble

672 data-mining techniques for gully erosion modeling. *Sci. Total Environ.* 609, 764–775.

673 <https://doi.org/10.1016/j.scitotenv.2017.07.198>

674 R Core Team, 2017. *R: A Language and Environment for Statistical Computing*.

675 Rahmati, O., Haghizadeh, A., Pourghasemi, H.R., Noormohamadi, F., 2016. Gully erosion susceptibility mapping: the

676 role of GIS-based bivariate statistical models and their comparison. *Nat. Hazards* 82, 1–28.

677 <https://doi.org/10.1007/s11069-016-2239-7>

678 Rahmati, O., Tahmasebipour, N., Haghizadeh, A., Pourghasemi, H.R., Feizizadeh, B., 2017. Evaluating the influence of

679 geo-environmental factors on gully erosion in a semi-arid region of Iran: An integrated framework. *Sci. Total*

680 *Environ.* 579, 913–927. <https://doi.org/10.1016/j.scitotenv.2016.10.176>

681 Rahmati, O., Tahmasebipour, N., Haghizadeh, A., Pourghasemi, H.R., Feizizadeh, B., 2017. Evaluation of different

682 machine learning models for predicting and mapping the susceptibility of gully erosion. *Geomorphology* 298,

683 118–137. <https://doi.org/10.1016/j.geomorph.2017.09.006>

684 Rahmati, O., Kornejady, A., Samadi, M., Deo, R.C., Conoscenti, C., Lombardo, L., Dayal, K., Taghizadeh-Mehrjardi,

685 R., Pourghasemi, H.R., Kumar, S., Bui, D.T., 2019. PMT: New analytical framework for automated evaluation of

686 geo-environmental modelling approaches. *Sci. Total Environ.* 664, 296–311.

687 <https://doi.org/10.1016/j.scitotenv.2019.02.017>

688 Regione Siciliana, 2010. *Modello digitale del terreno (MDT) 2m x 2m Regione Siciliana - ATA 2007-2008 [WWW*

689 *Document]*. URL

690 [http://map.sitr.regione.sicilia.it/gis/services/DEM/DEM\\_2x2\\_2007\\_2008\\_GB/MapServer/WMS/Server](http://map.sitr.regione.sicilia.it/gis/services/DEM/DEM_2x2_2007_2008_GB/MapServer/WMS/Server)

691 Robin, X., Turck, N., Hainard, A., Tiberti, N., Lisacek, F., Sanchez, J.-C., Müller, M., 2011. pROC: an open-source

692 package for R and S+ to analyze and compare ROC curves. *BMC Bioinformatics* 12, 77.

693 Rotigliano, E., Martinello, C., Hernández, M.A., Agnesi, V., Conoscenti, C., 2019. Predicting the landslides triggered

694 by the 2009 96E/Ida tropical storms in the Ilopango caldera area (El Salvador, CA): optimizing MARS-based  
695 model building and validation strategies. *Environ. Earth Sci.* 78, 210. <https://doi.org/10.1007/s12665-019-8214-3>  
696 Sekaluvu, L., Sheshukov, A.Y., 2016. Topographical thresholds for ephemeral gully identification in watersheds with  
697 highly disturbed terrain, in: 2016 American Society of Agricultural and Biological Engineers Annual  
698 International Meeting, ASABE 2016. <https://doi.org/10.13031/aim.20162461481>  
699 Sekaluvu, L., Sheshukov, A.Y., Hutchinson, S.L., 2015. Accuracy of topographic index models at prediction of  
700 ephemeral gullies, in: American Society of Agricultural and Biological Engineers Annual International Meeting  
701 2015. pp. 4432–4439.  
702 Selkimäki, M., González-Olabarria, J.R., 2016. Assessing Gully Erosion Occurrence in Forest Lands in Catalonia  
703 (Spain). *L. Degrad. Dev.* <https://doi.org/10.1002/ldr.2533>  
704 Sheshukov, A.Y., Sekaluvu, L., Hutchinson, S.L., 2018. Accuracy of topographic index models at identifying  
705 ephemeral gully trajectories on agricultural fields. *Geomorphology* 306, 224–234.  
706 <https://doi.org/10.1016/j.geomorph.2018.01.026>  
707 Sidorchuk, A., 1999. Dynamic and static models of gully erosion. *Catena* 37, 401–414. [https://doi.org/10.1016/S0341-](https://doi.org/10.1016/S0341-8162(99)00029-6)  
708 [8162\(99\)00029-6](https://doi.org/10.1016/S0341-8162(99)00029-6)  
709 Sing, T., Sander, O., Beerenwinkel, N., Lengauer, T., 2005. ROCr: visualizing classifier performance in R.  
710 *Bioinformatics* 21, 7881.  
711 Sterlacchini, S., Ballabio, C., Blahut, J., Masetti, M., Sorichetta, a., 2011. Spatial agreement of predicted patterns in  
712 landslide susceptibility maps. *Geomorphology* 125, 51–61. <https://doi.org/10.1016/j.geomorph.2010.09.004>  
713 Svoray, T., Michailov, E., Cohen, A., Rokah, L., Sturm, A., 2012. Predicting gully initiation: comparing data mining  
714 techniques, analytical hierarchy processes and the topographic threshold. *Earth Surf. Process. Landforms* 37,  
715 607–619. <https://doi.org/10.1002/esp.2273>  
716 Thommeret, N., Bailly, J.S., Puech, C., 2010. Extraction of thalweg networks from DTMs: application to badlands.  
717 *Hydrol. Earth Syst. Sci.* 14, 1527–1536. <https://doi.org/10.5194/hess-14-1527-2010>  
718 Thorne, C.R., Zevenbergen, L.W., Grissinger, E.H., Murphey, J.B., 1986. Ephemeral gullies as source of sediments, in:  
719 Proceedings of the 4th Federal Interagency Sedimentation Conference. March 24–27, 1986, Las Vegas, NV, pp.  
720 3,152-3,161.  
721 Valentin, C., Poesen, J., Li, Y., 2005. Gully erosion: Impacts, factors and control. *Catena* 63, 132–153.  
722 <https://doi.org/10.1016/j.catena.2005.06.001>  
723 Vandaele, K., Poesen, J., Marques da Silva, J.R., Desmet, P., 1996. Rates and predictability of ephemeral gully erosion  
724 in two contrasting environments. *Geomorphol. Reli. Proc., Environ.* 2, 83–96.  
725 Vandekerckhove, L., Poesen, J., Oostwoud Wijdenes, D., Gyssels, G., 2001. Short-term bank gully retreat rates in  
726 Mediterranean environments. *Catena* 44, 133–161. [https://doi.org/10.1016/S0341-8162\(00\)00152-1](https://doi.org/10.1016/S0341-8162(00)00152-1)  
727 Vanwalleghem, T., Van Den Eeckhaut, M., Poesen, J., Govers, G., Deckers, J., 2008. Spatial analysis of factors  
728 controlling the presence of closed depressions and gullies under forest: Application of rare event logistic  
729 regression. *Geomorphology* 95, 504–517. <https://doi.org/10.1016/j.geomorph.2007.07.003>  
730 Vargas-Cuervo, G., Rotigliano, E., Conoscenti, C., 2019. Prediction of debris-avalanches and -flows triggered by a  
731 tropical storm by using a stochastic approach: An application to the events occurred in Mocoa (Colombia) on 1  
732 April 2017. *Geomorphology* 339, 31–43. <https://doi.org/https://doi.org/10.1016/j.geomorph.2019.04.023>  
733 Wilson, J.P., Gallant, J.C., 2000. *Terrain Analysis: Principles and Applications*. Wiley & Sons, Inc., Canada.  
734 Wing, J., Kuhn, M., 2018. caret: Classification and Regression Training [WWW Document]. URL [https://cran.r-](https://cran.r-project.org/package=caret)  
735 [project.org/package=caret](https://cran.r-project.org/package=caret)  
736 Youden, W.J., 1950. Index for rating diagnostic tests. *Cancer* 32–35.  
737 Zucca, C., Canu, A., Della Peruta, R., 2006. Effects of land use and landscape on spatial distribution and morphological  
738 features of gullies in an agropastoral area in Sardinia (Italy). *Catena* 68, 87–95.  
739 <https://doi.org/10.1016/j.catena.2006.03.015>  
740  
741

742 CAPTIONS

743 Fig. 1. Flow-chart of methodology.

744 Fig. 2. Location (a) and topographic map (b) of the watersheds W1 and W2.

745 Fig. 3. Elevation (a), slope steepness (b), lithology (c) and land cover (d) maps of the watersheds  
746 W1 and W2.

747 Fig. 4. Gully maps of the watersheds W1 and W2 and Google Earth views of two gully-prone  
748 sectors of the study area.

749 Fig. 5. An example showing correspondence between gullies and flow pathways.

750 Fig. 6. Box plots showing the variability of the 100 *AUC* values calculated in W1 and W2 for the  
751 topographic indices and local and transferred statistical models.

752 Fig. 7. Average ROC curves obtained from the validation of the topographic indices and statistical  
753 models in W1 and W2.

754 Fig. 8. Gully erosion susceptibility maps for the sectors of W1 and W2 highlighted in Fig.3. First  
755 and third columns show maps calculated from the topographic indices. Second and fourth columns  
756 show maps calculated from local and transferred statistical models. White pixels were not  
757 investigated because they intersect anthropogenic features (i.e. urban areas, artificial lakes or roads)  
758 or fall within a 10 m buffer around river channels.

759 Fig. 9. Relative frequency distributions of non-event and event pixels across the susceptibility levels  
760 of the gully erosion susceptibility maps.

761 Fig. 10. Kernel density plots of *CI* and *PLANC* calculated for gully and non-gully cells of the  
762 watersheds W1 and W2.

763 Table 1. Mean and standard deviation of the 100 *AUC* values calculated for the topographic indices  
764 and local and transferred statistical models.

765 Table 2. Cut-off (*T*) dependent statistics calculated in W1 and W2 for the topographic indices and  
766 local and transferred statistical models.

767

Table 1. Mean and standard deviation of the 100 *AUC* values calculated for the topographic indices and local and transferred statistical models.

		MARS1	MARS2	LR1	LR2	SPI	CTI	TWI	MSPI	MTWI
W1	Mean	0.961	0.953	0.952	0.943	0.945	0.902	0.926	0.953	0.913
	Std. Dev.	0.005	0.006	0.006	0.007	0.007	0.010	0.008	0.007	0.009
W2	Mean	0.922	0.946	0.911	0.912	0.891	0.888	0.870	0.927	0.891
	Std. Dev.	0.014	0.011	0.014	0.013	0.018	0.016	0.017	0.012	0.015

Table 2. Cut-off (*T*) dependent statistics calculated in W1 and W2 for the topographic indices and local and transferred statistical models.

		MARS1	MARS2	LR1	LR2	SPI	CTI	TWI	MSPI	MTWI
W1	<i>T</i>	0.952	0.950	0.803	0.794	278.6	52.78	9.696	3245.9	147.8
	$\kappa$	0.797	0.761	0.769	0.728	0.766	0.715	0.715	0.795	0.682
	<i>TPR</i>	0.897	0.880	0.894	0.879	0.883	0.817	0.846	0.889	0.817
	<i>TNR</i>	0.900	0.881	0.874	0.849	0.883	0.897	0.868	0.906	0.865
W2	<i>T</i>	0.865	0.889	0.614	0.741	148.2	24.02	9.646	1024.5	80.00
	$\kappa$	0.714	0.769	0.672	0.659	0.625	0.675	0.627	0.711	0.633
	<i>TPR</i>	0.850	0.913	0.854	0.835	0.831	0.853	0.783	0.902	0.910
	<i>TNR</i>	0.865	0.857	0.819	0.825	0.794	0.822	0.845	0.809	0.724



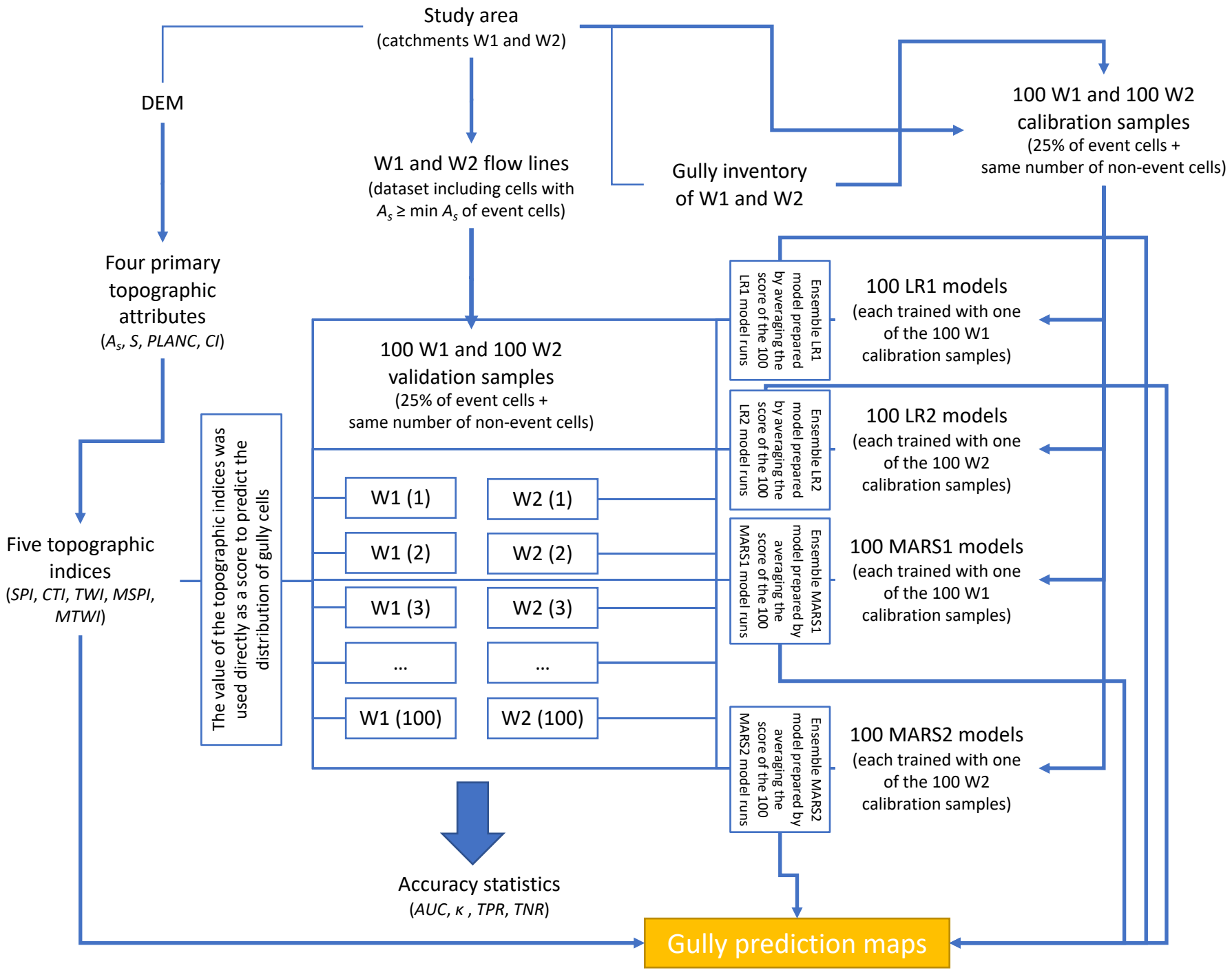


Figure 2 (Color)  
[Click here to download high resolution image](#)

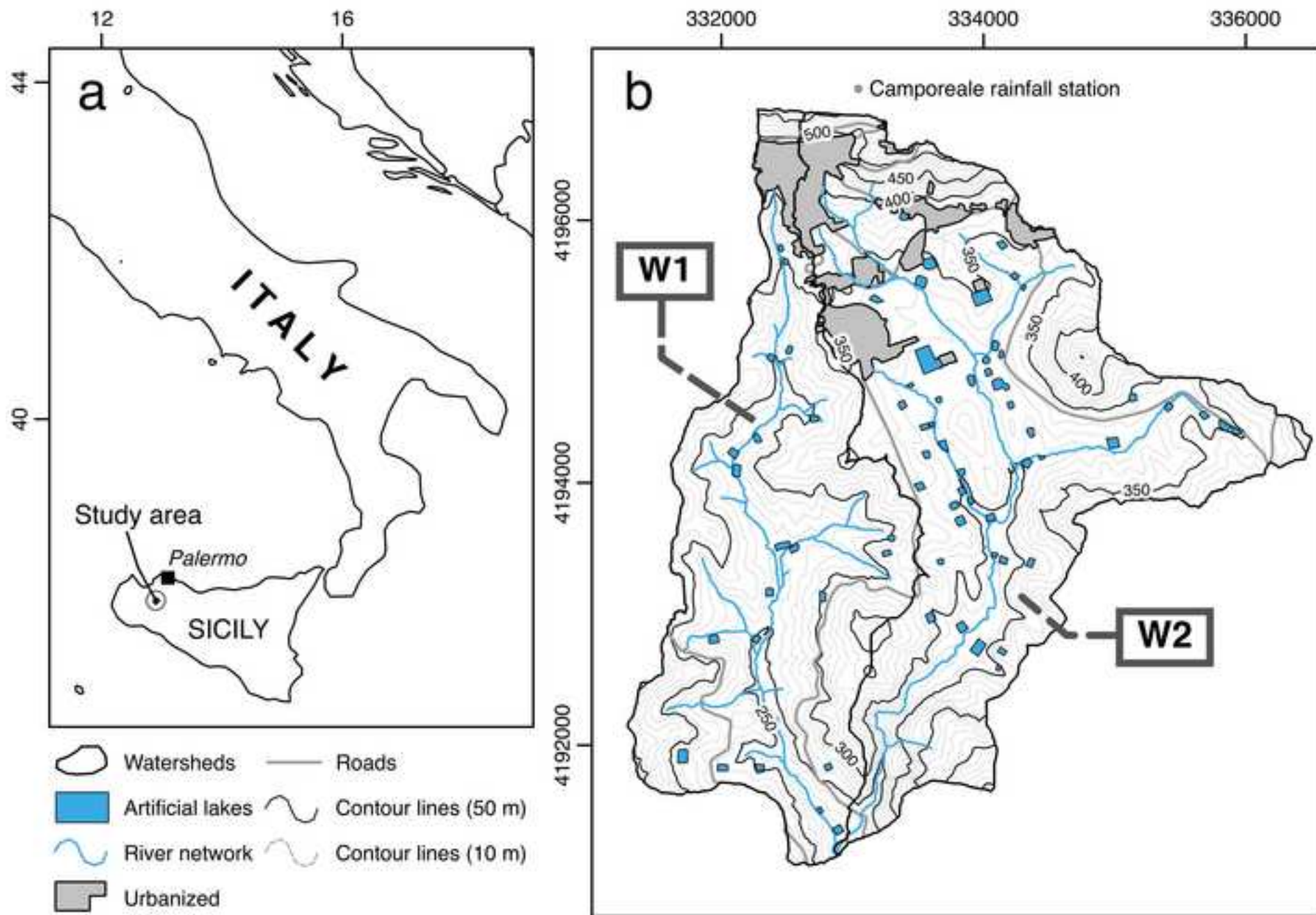


Figure 3 (Color)

[Click here to download high resolution image](#)

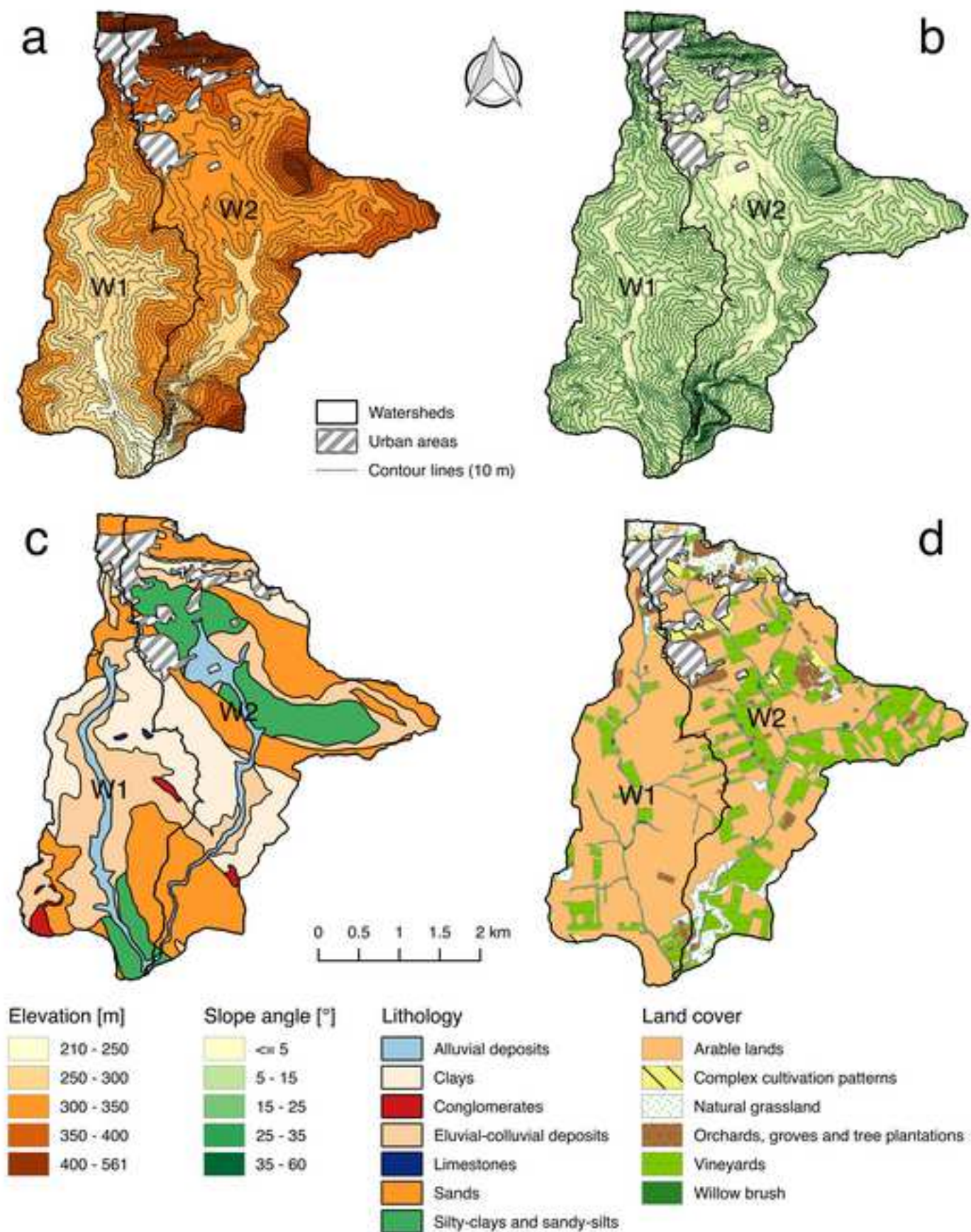


Figure 4 (Color)  
[Click here to download high resolution image](#)

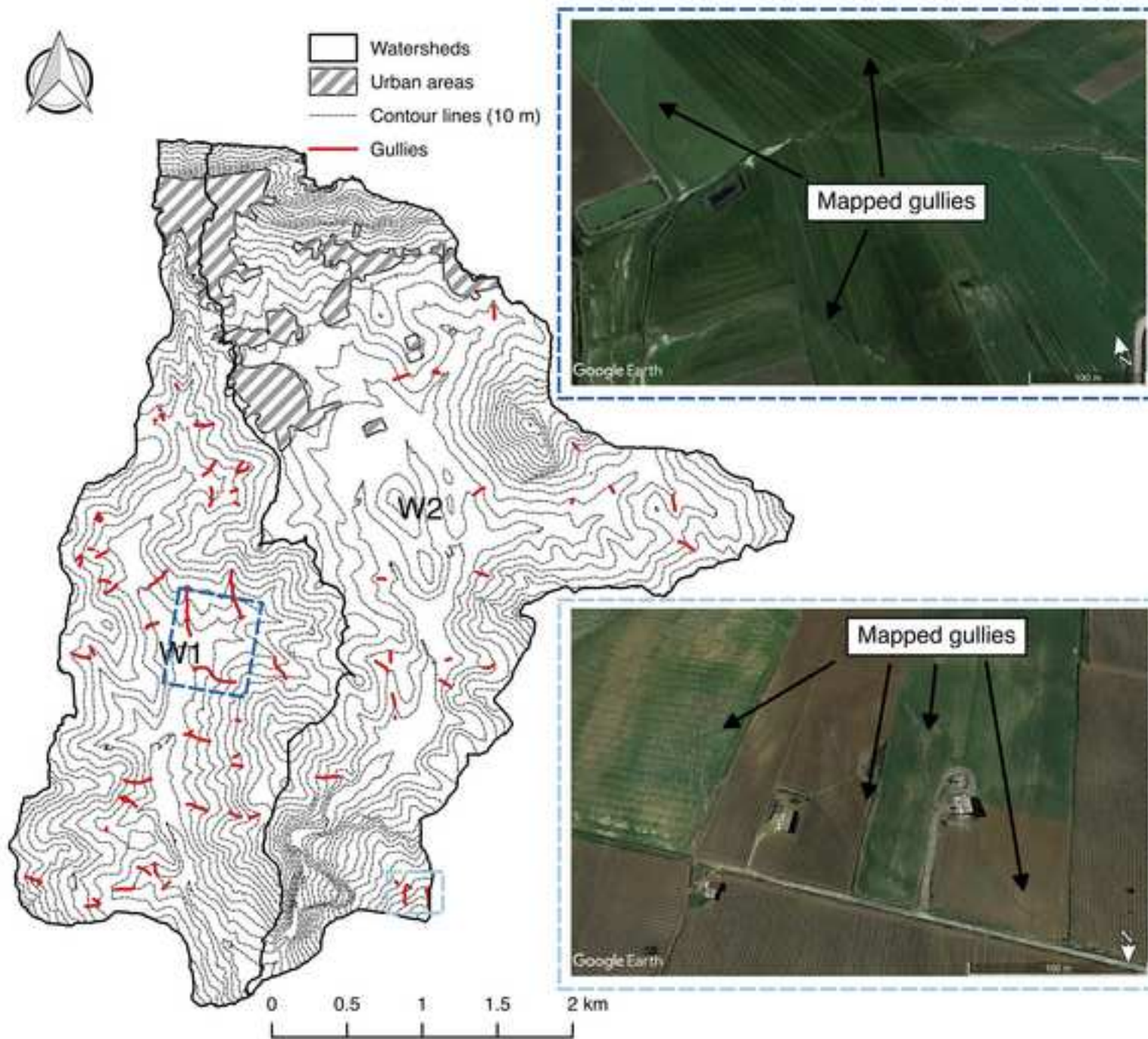
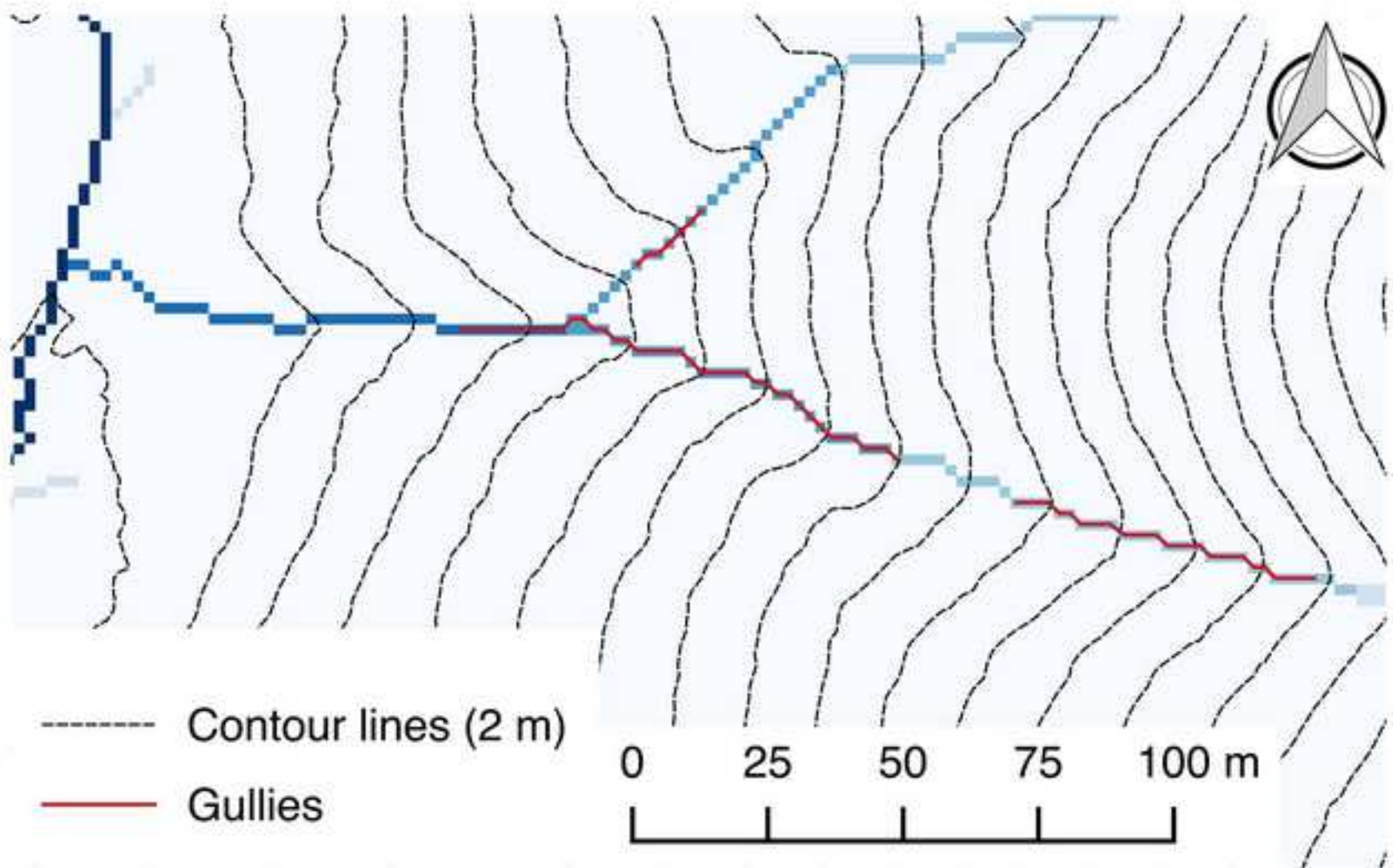


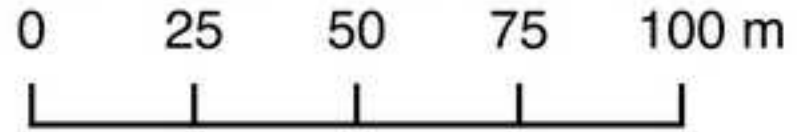
Figure 5 (Color)

[Click here to download high resolution image](#)



--- Contour lines (2 m)

— Gullies



### Contributing area [ha]

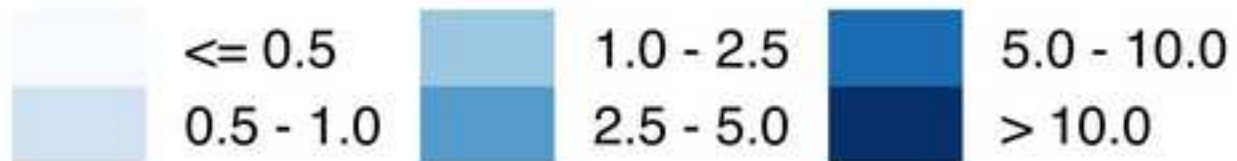


Figure 6 (Color)

Watershed W1

Watershed W2

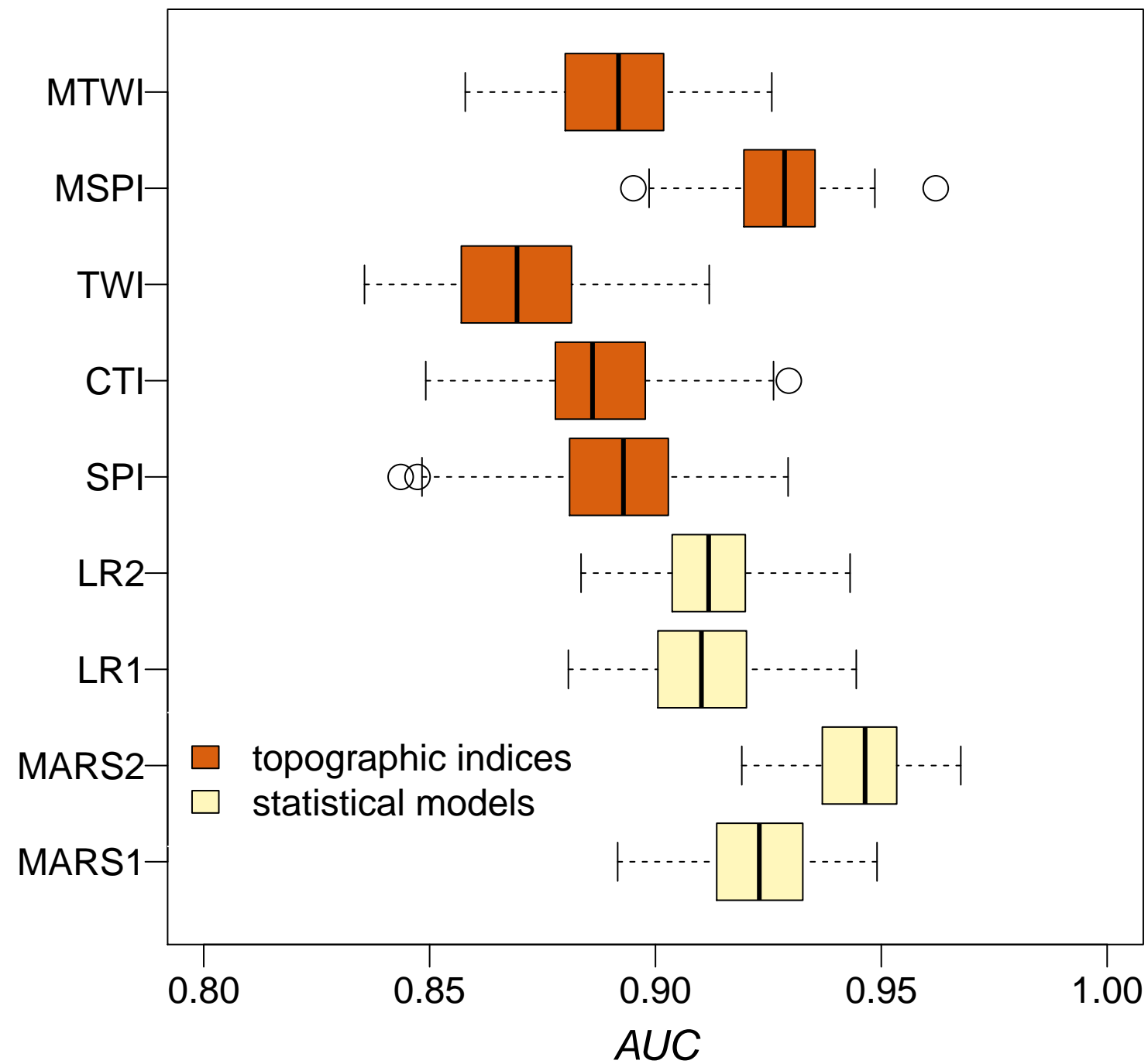
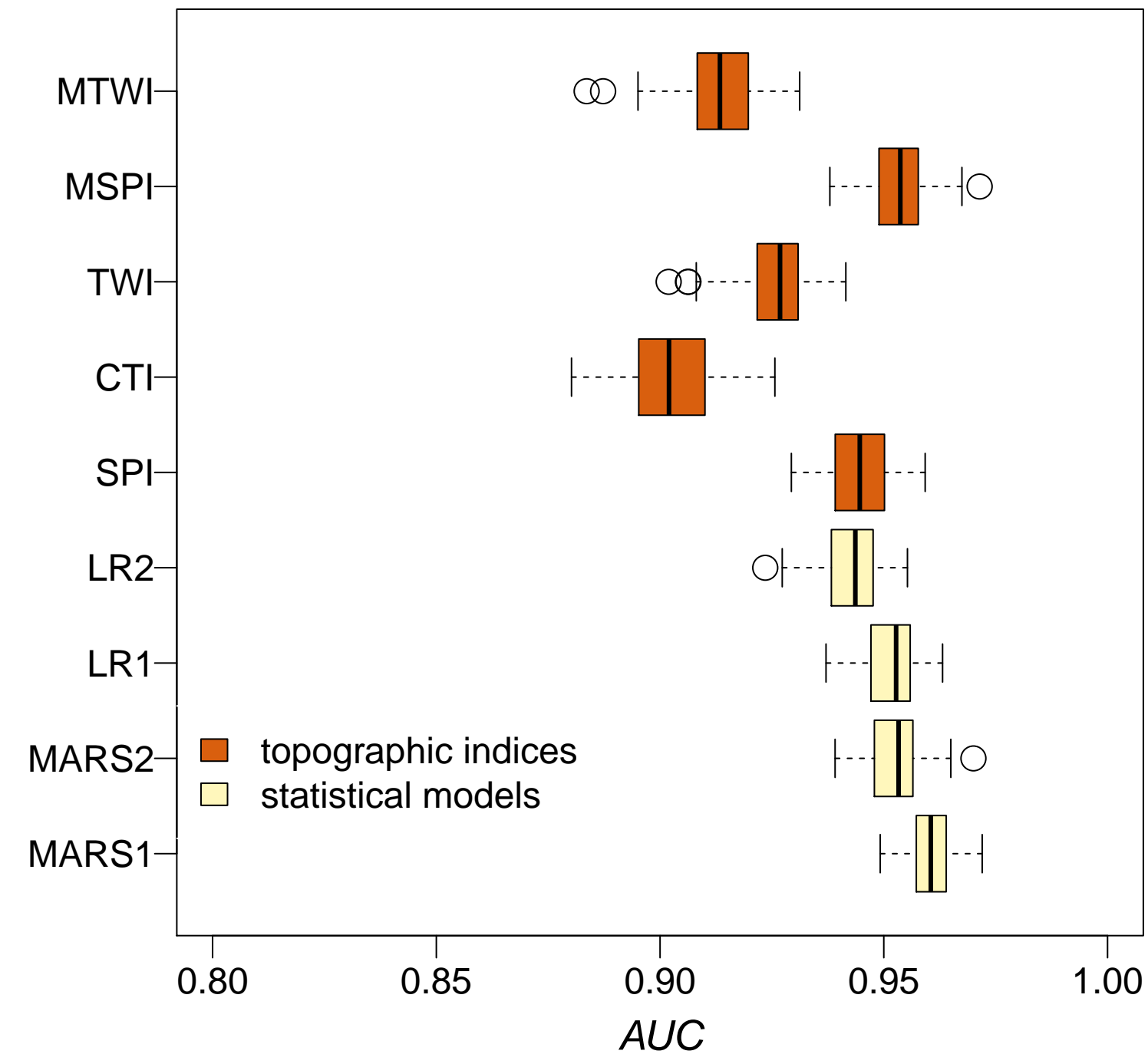


Figure 7 (Color)

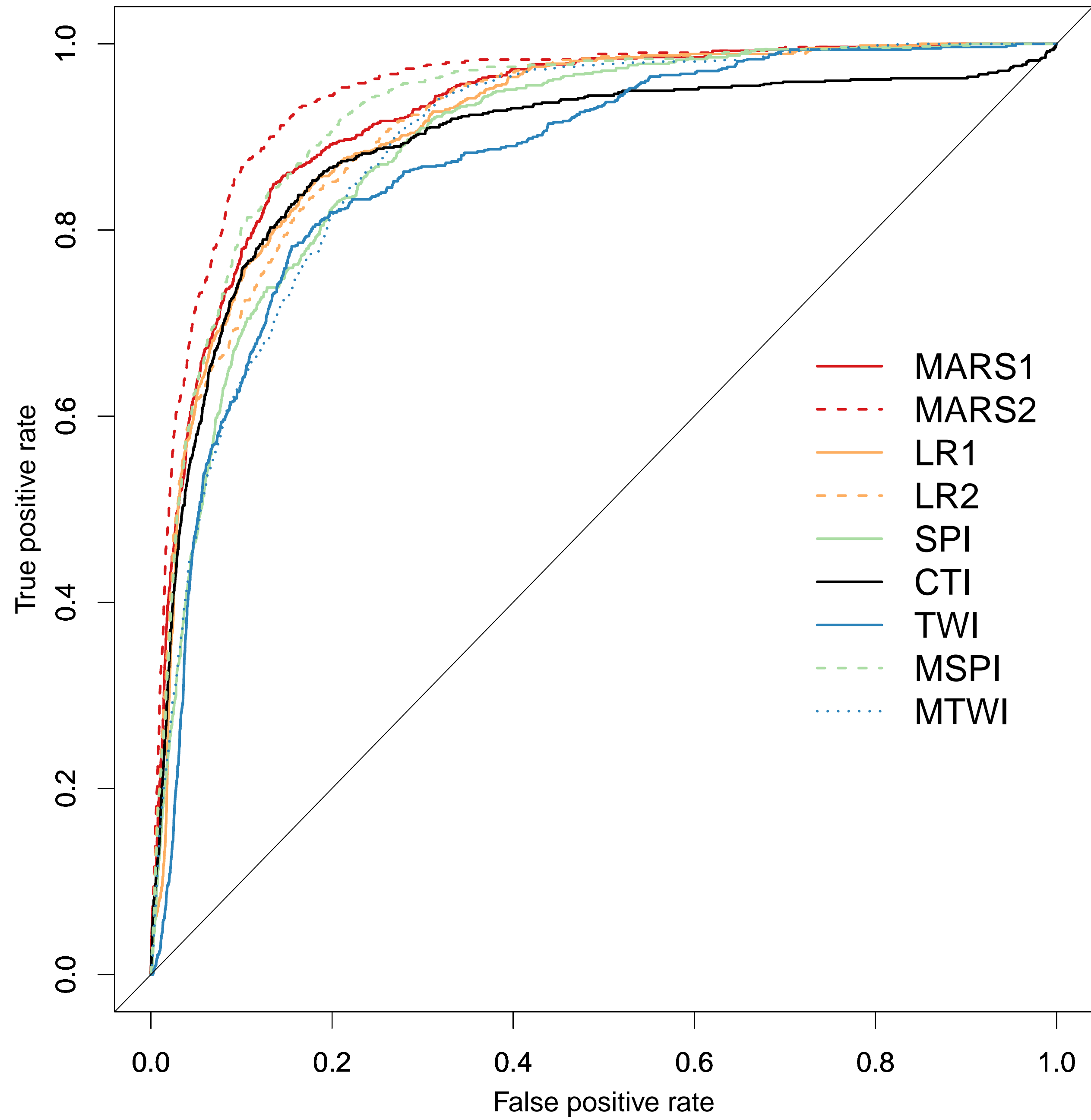
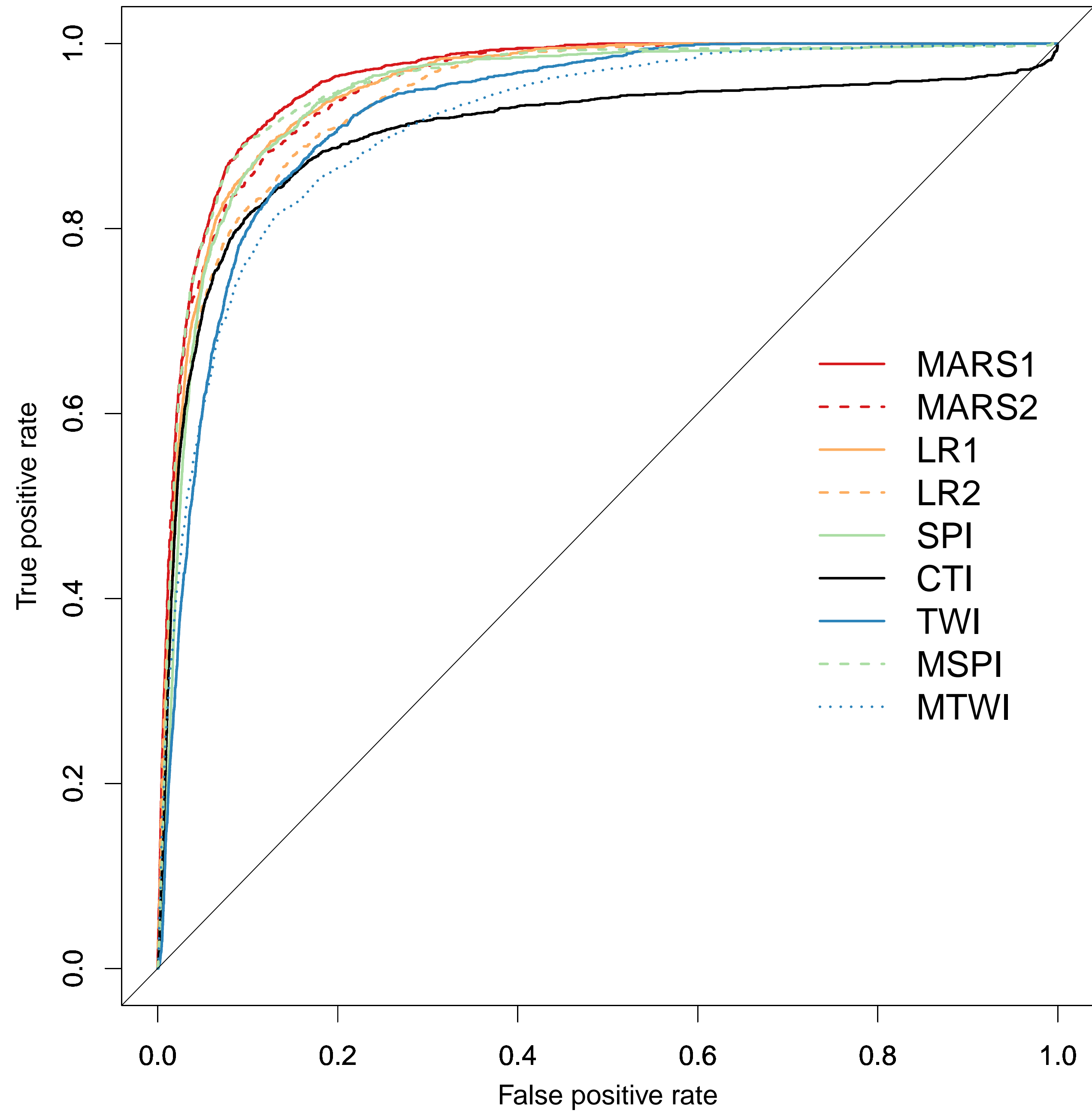
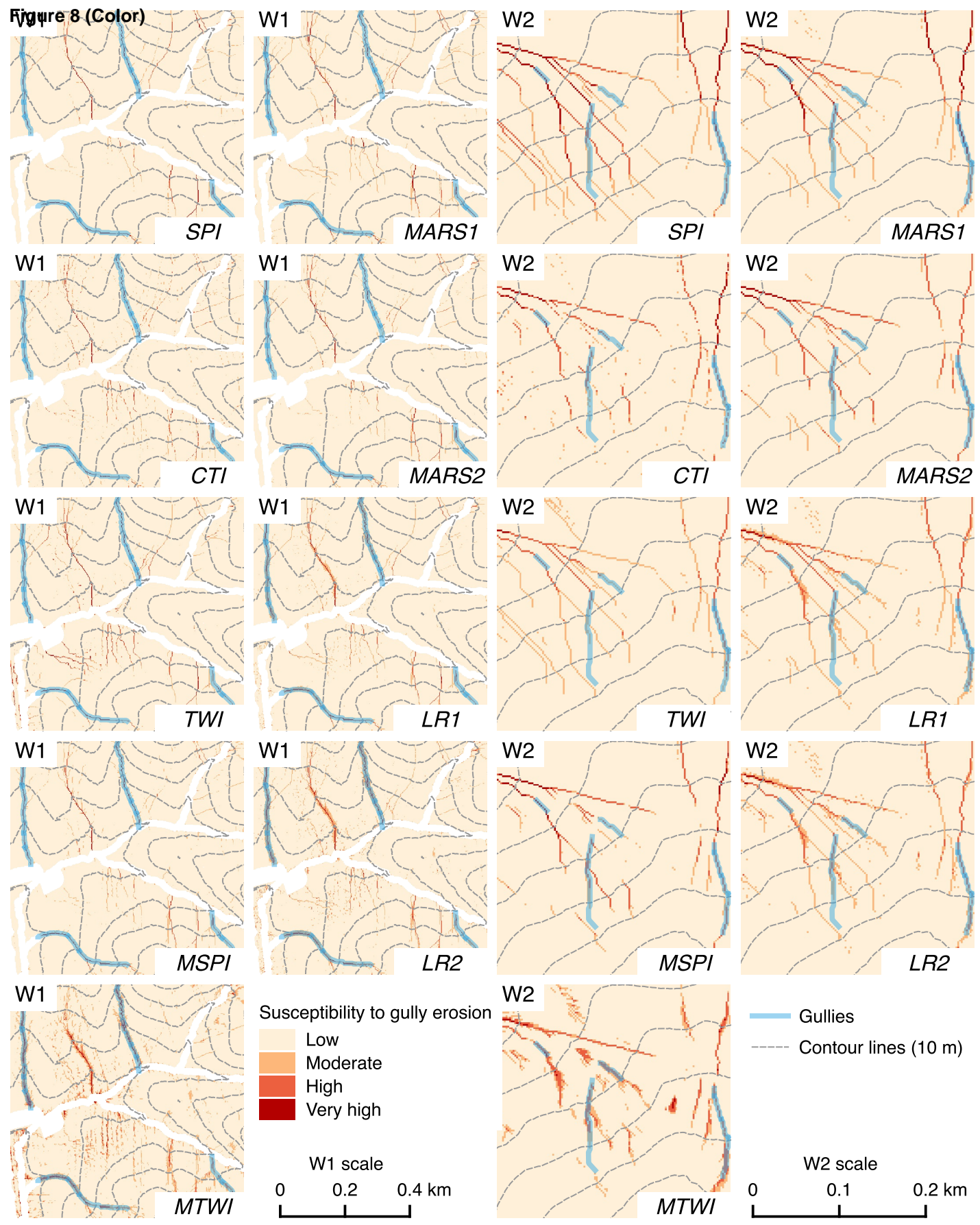


Figure 8 (Color)





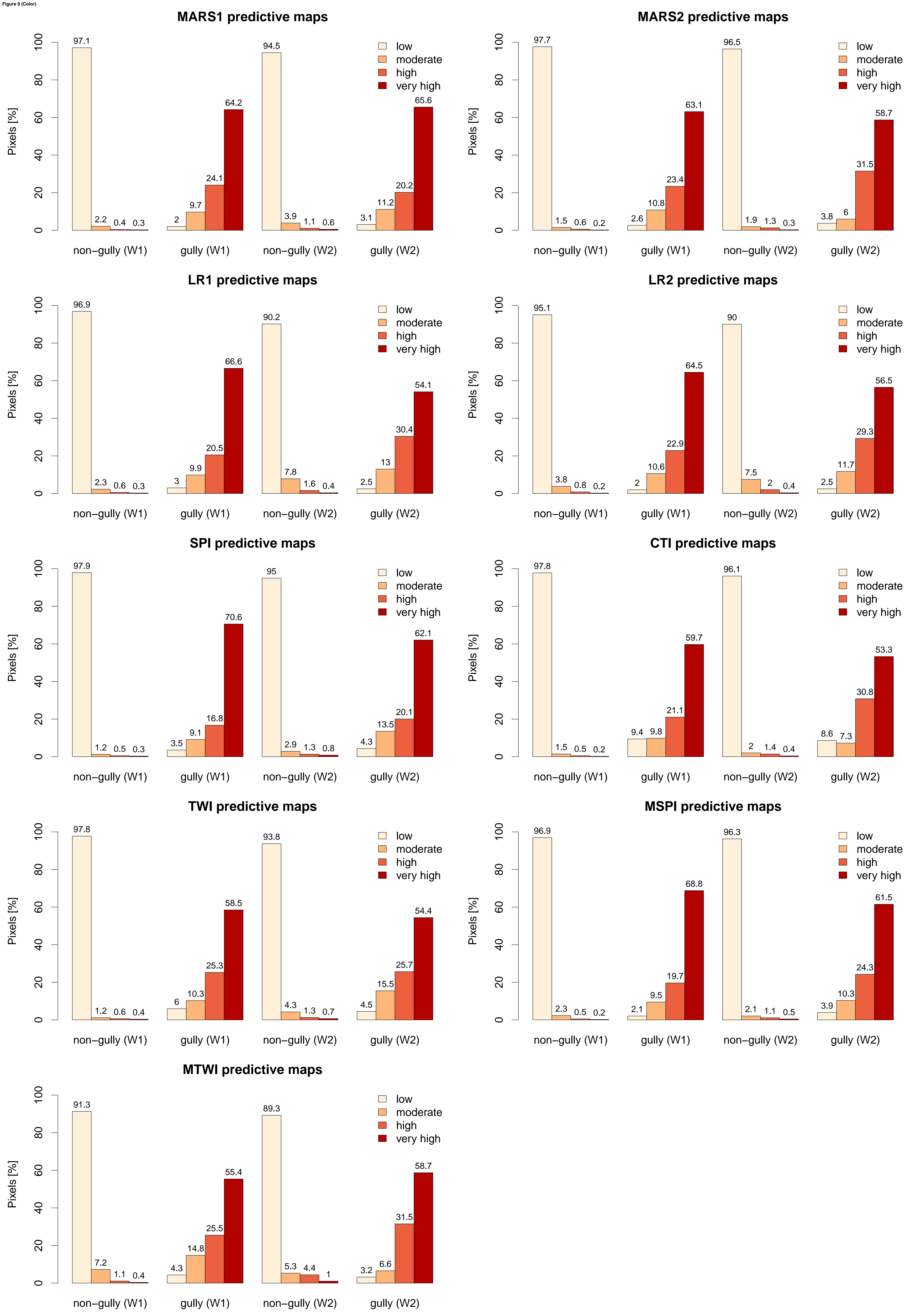
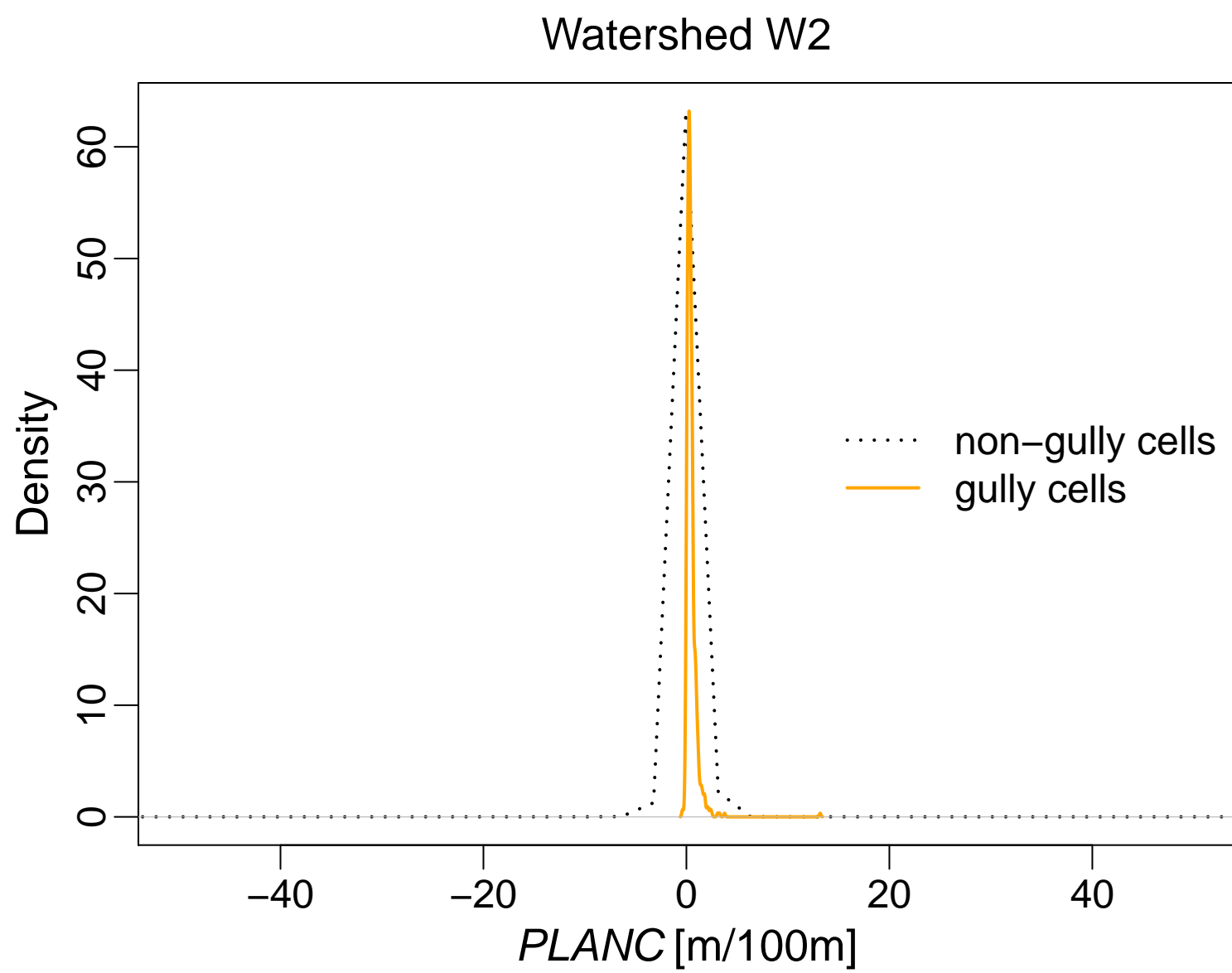
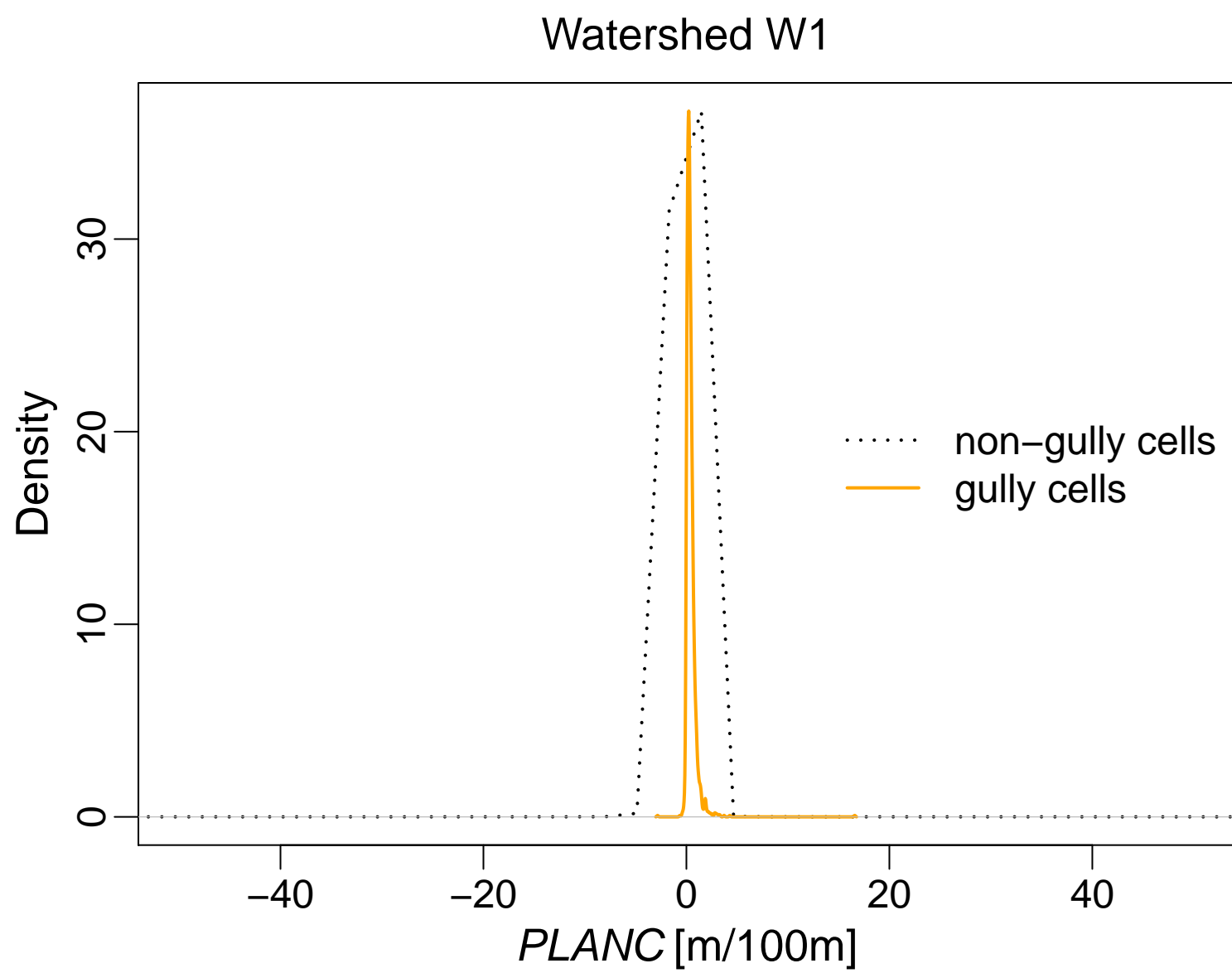
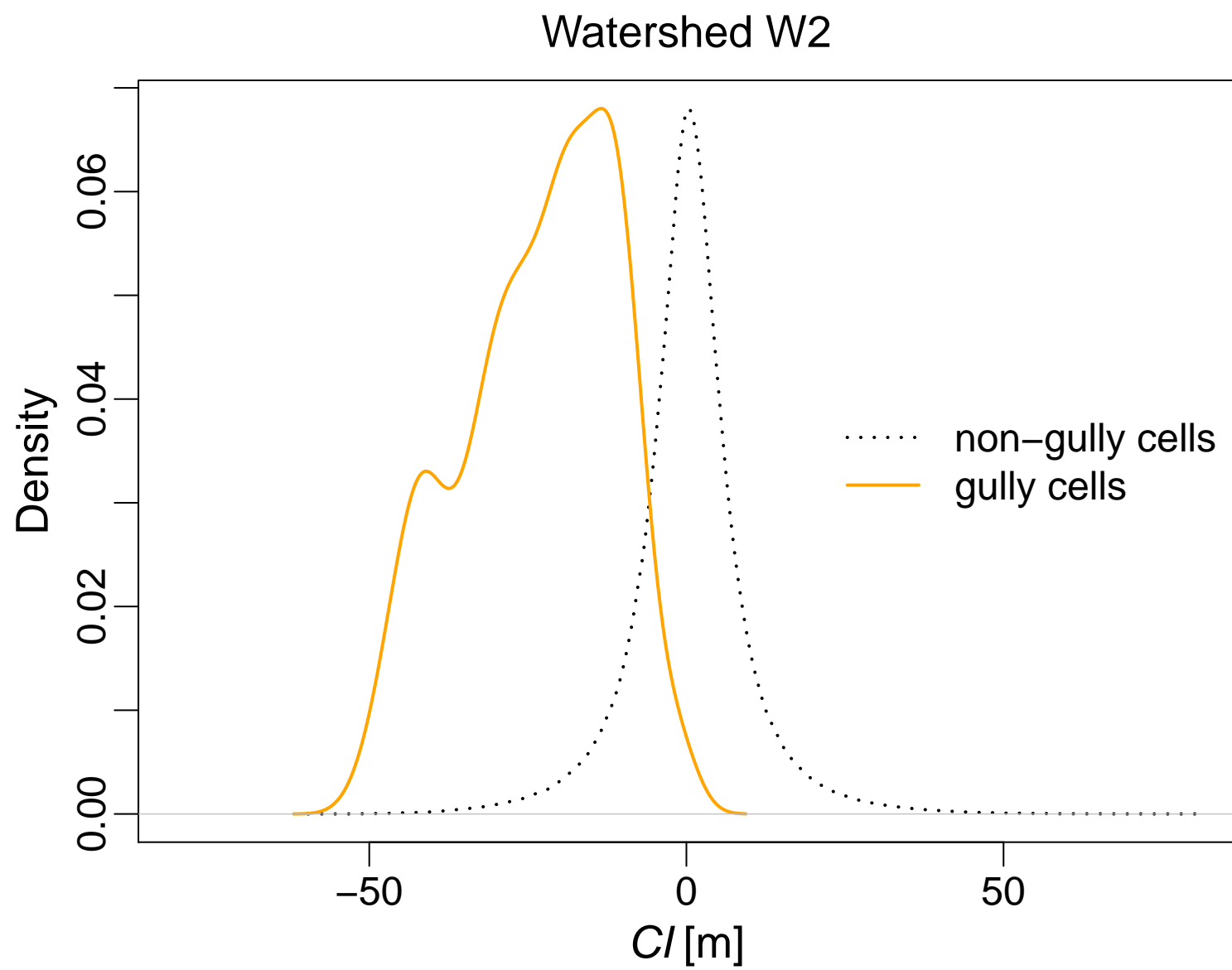
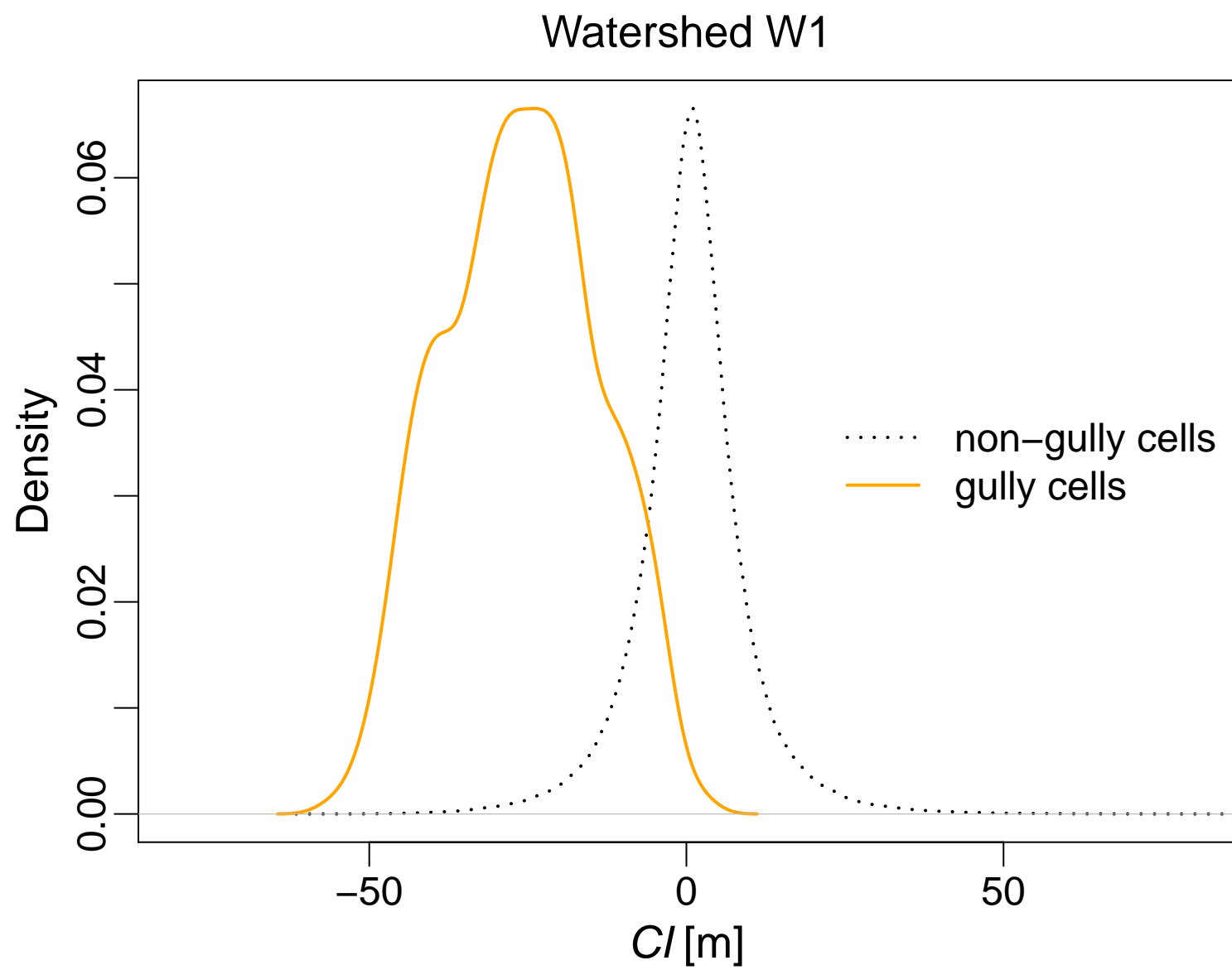


Figure 10 (Color)



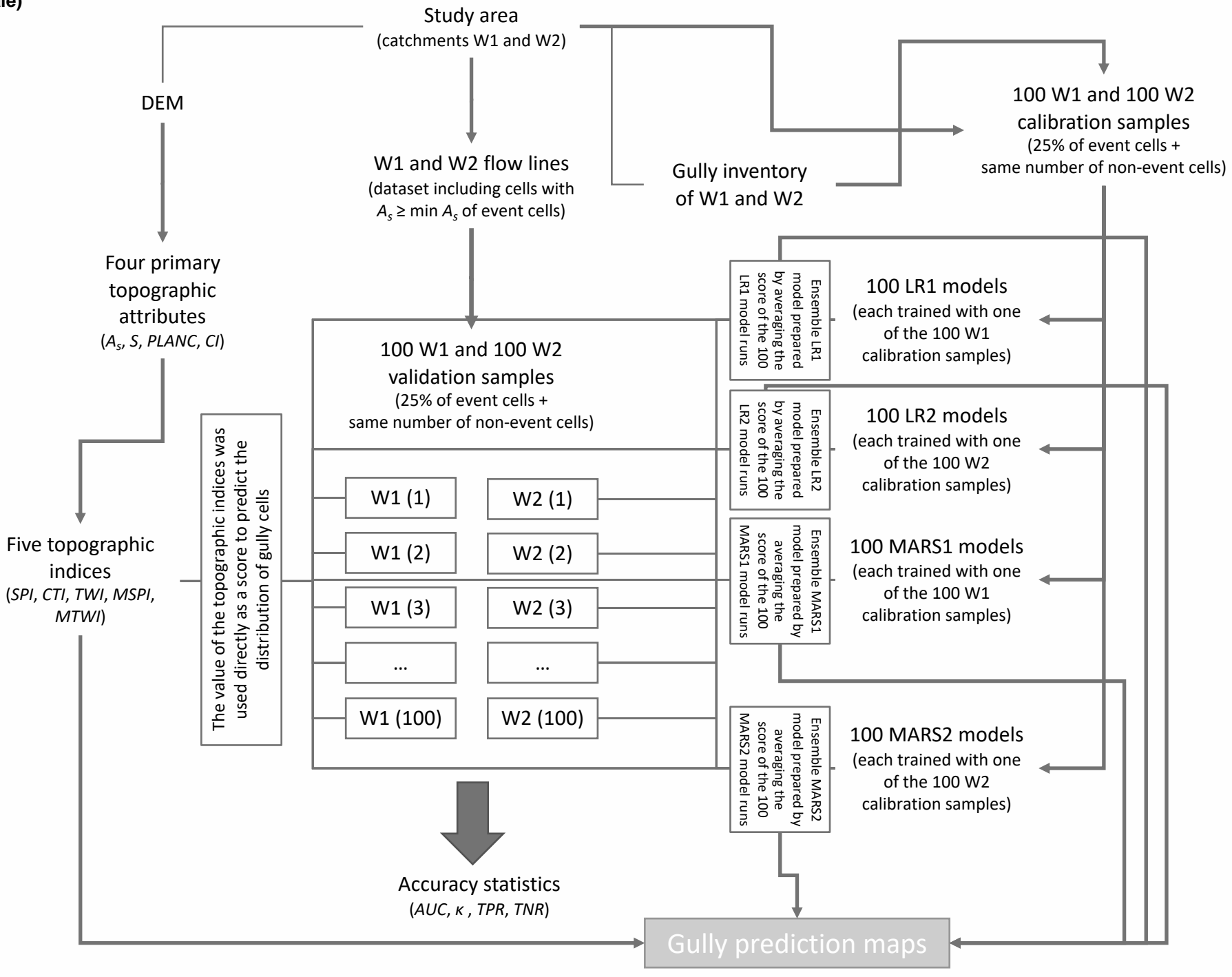


Figure 2 (Greyscale)  
[Click here to download high resolution image](#)

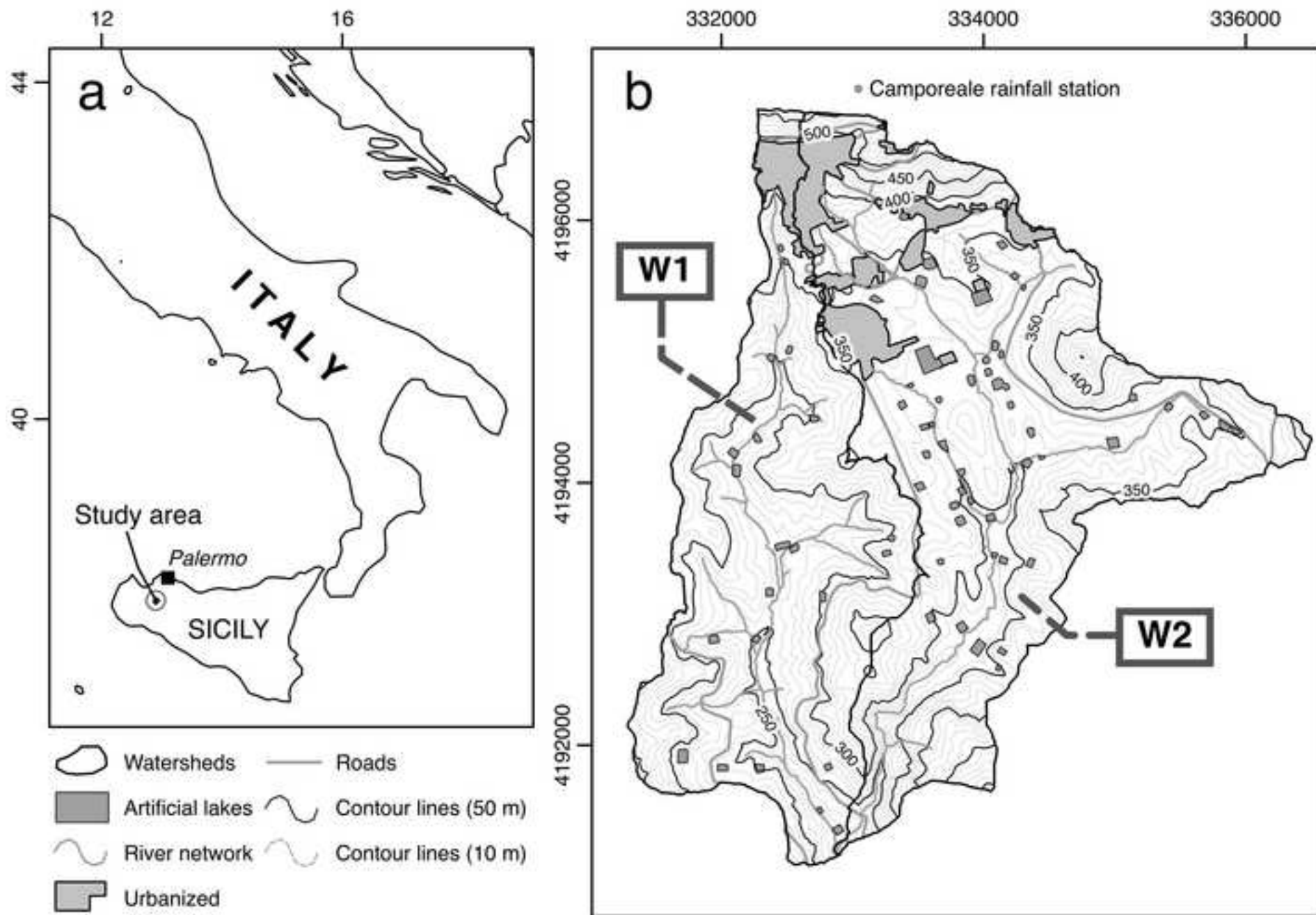


Figure 3 (Greyscale)  
[Click here to download high resolution image](#)

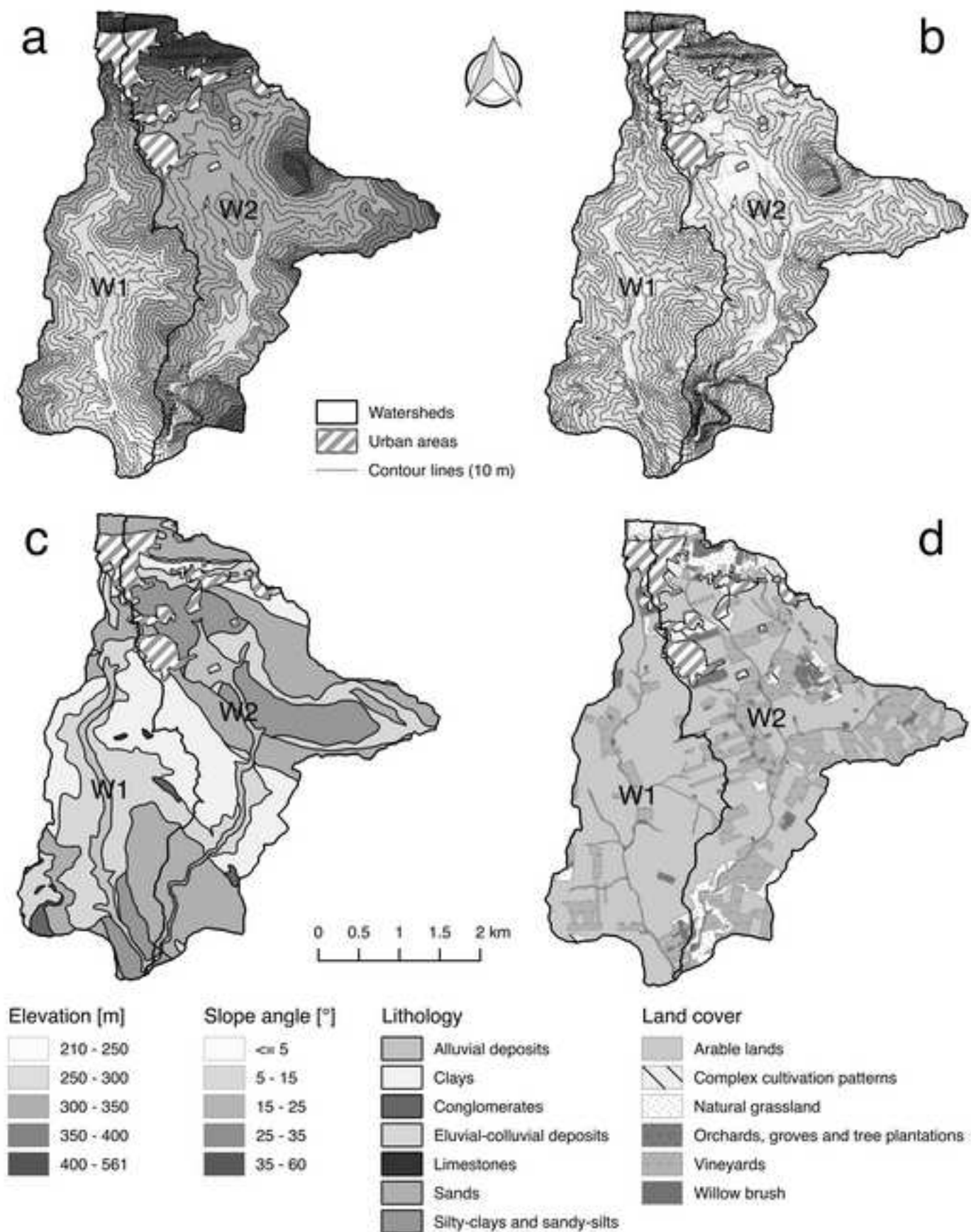


Figure 4 (Greyscale)  
[Click here to download high resolution image](#)

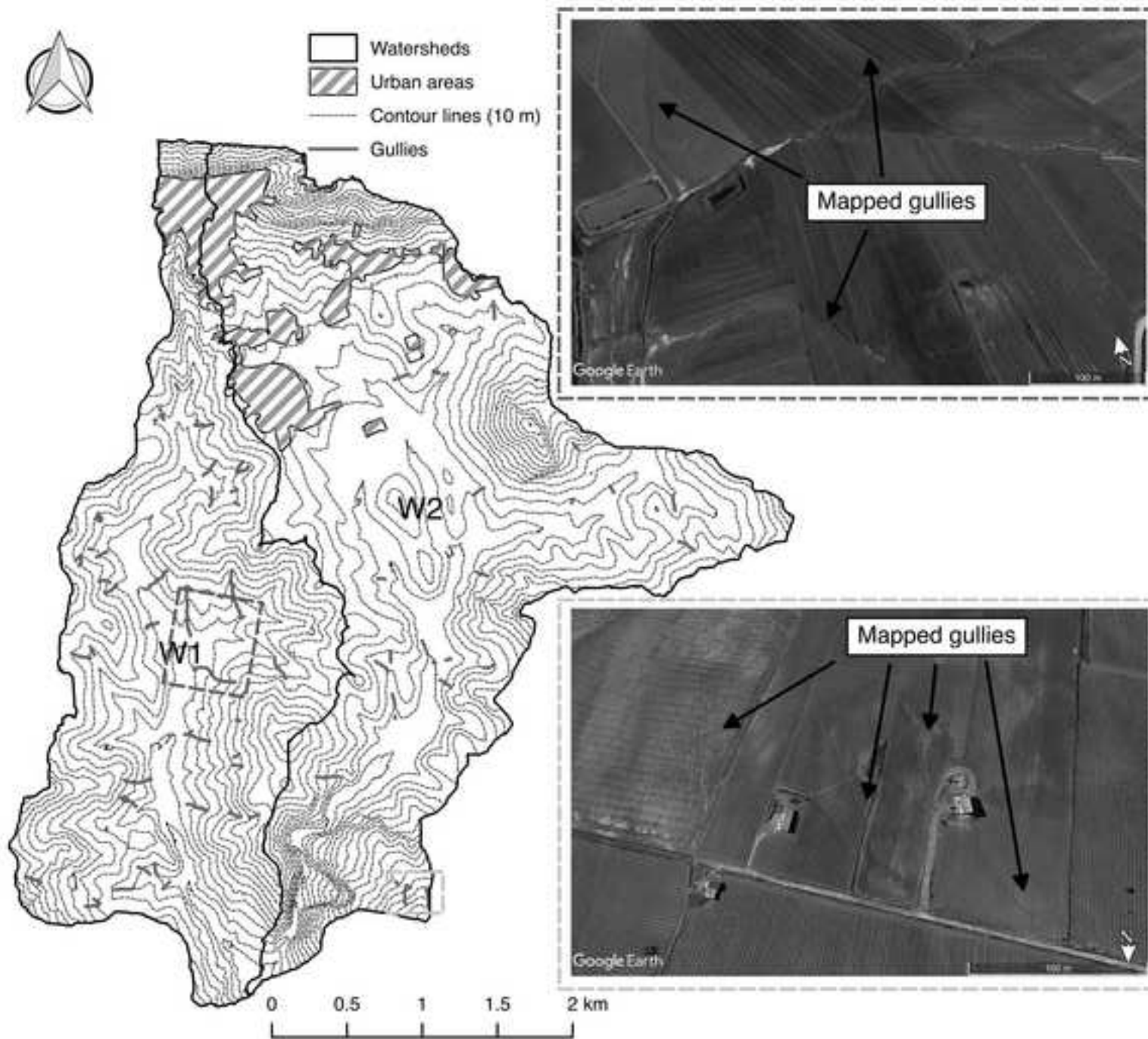
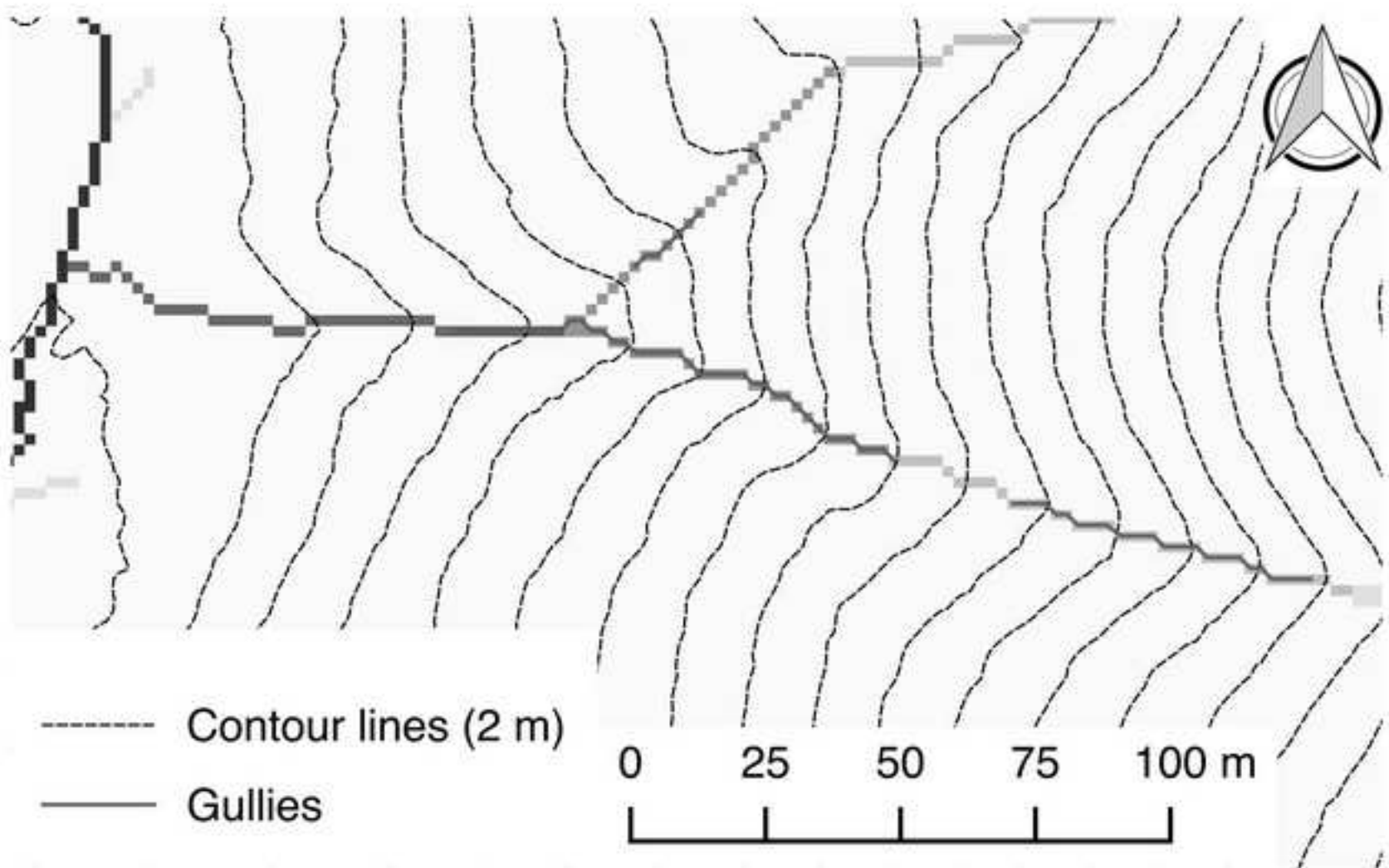


Figure 5 (Greyscale)  
[Click here to download high resolution image](#)



----- Contour lines (2 m)  
—— Gullies

0 25 50 75 100 m

### Contributing area [ha]

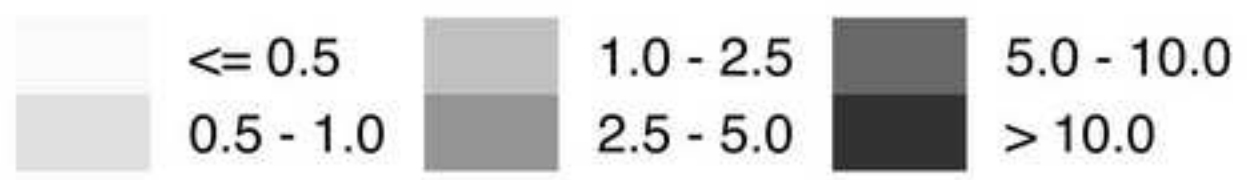
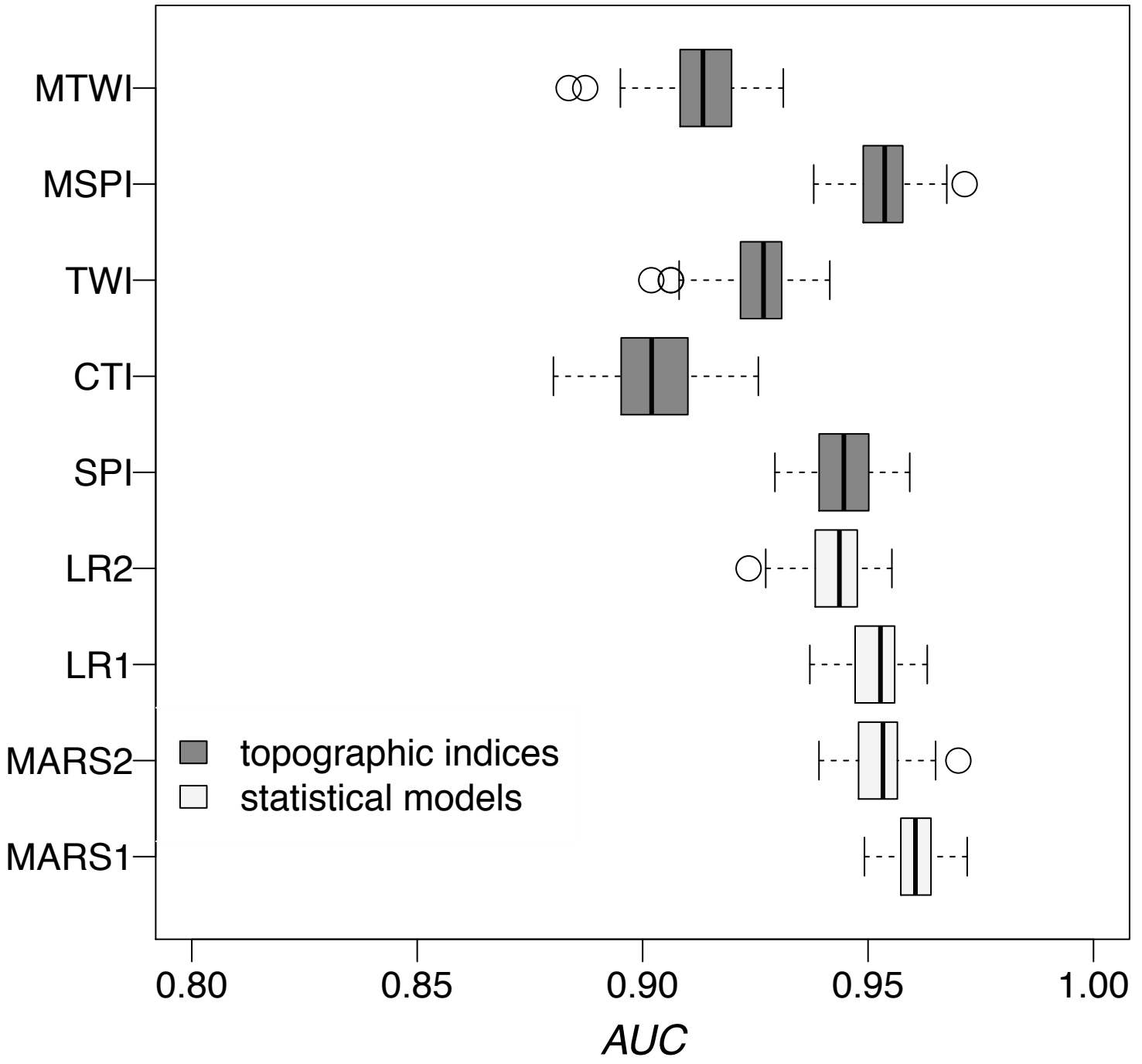


Figure 6 (Greyscale)

### Watershed W1



### Watershed W2

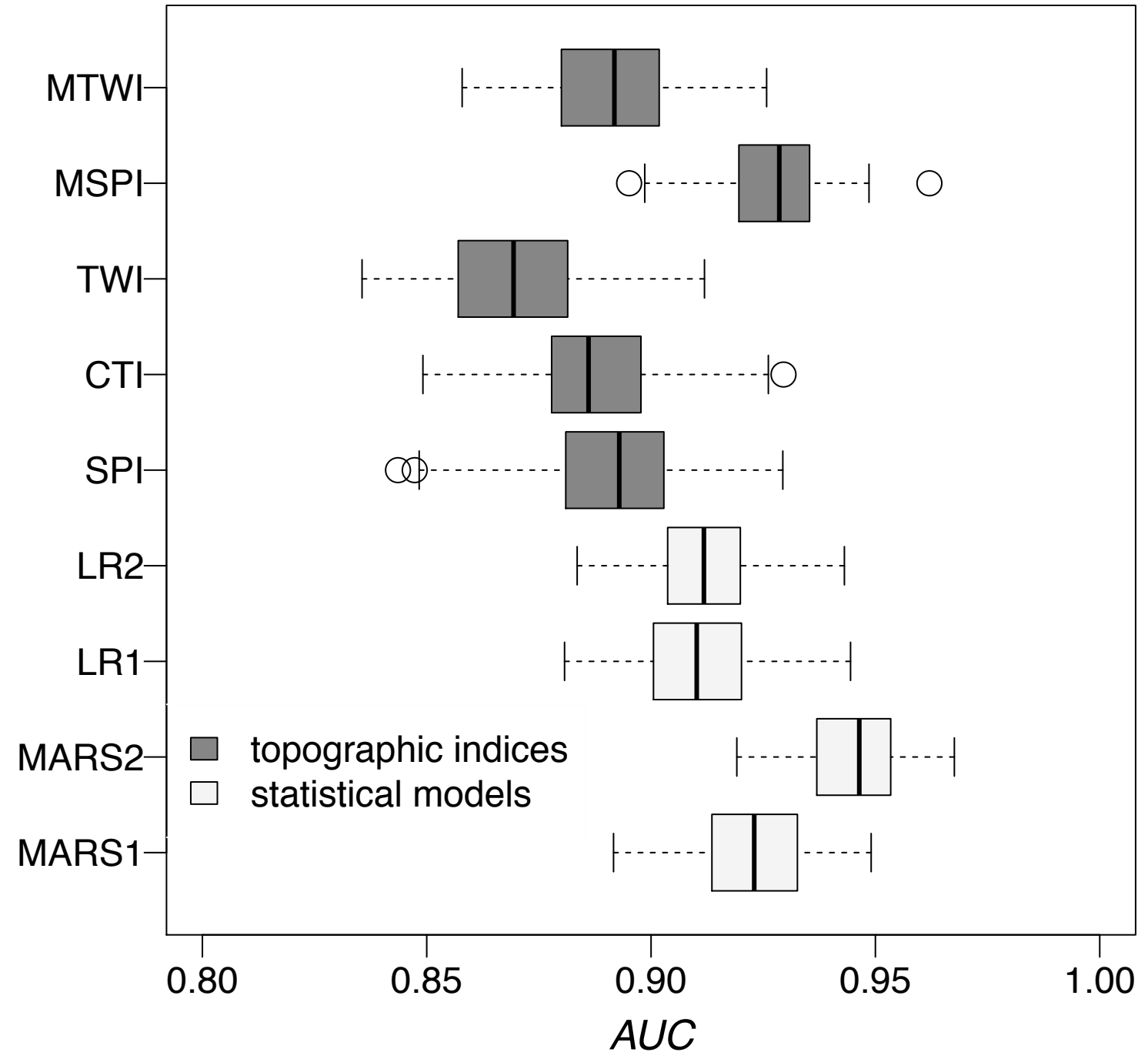




Figure 7 (Greyscale)

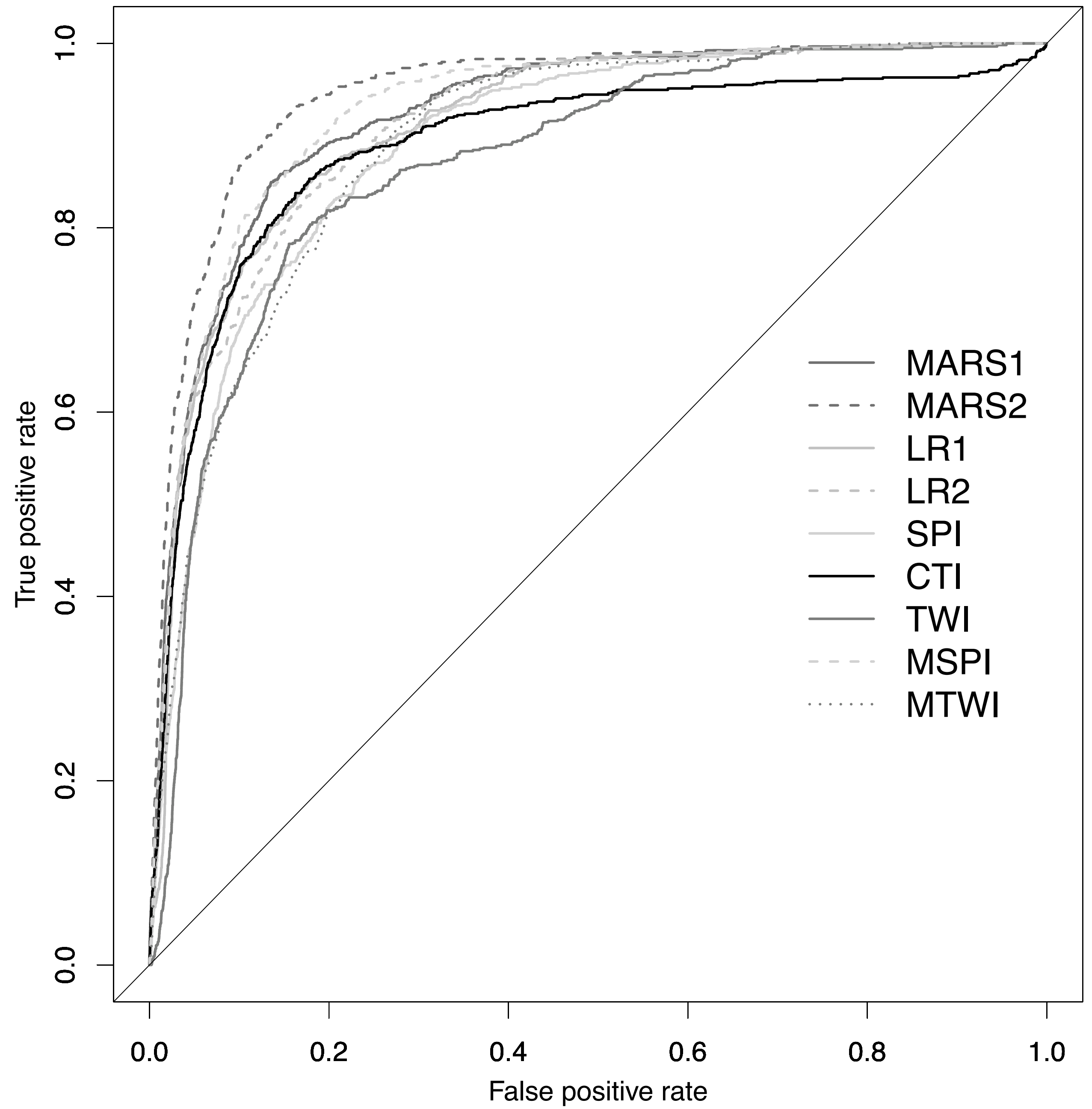
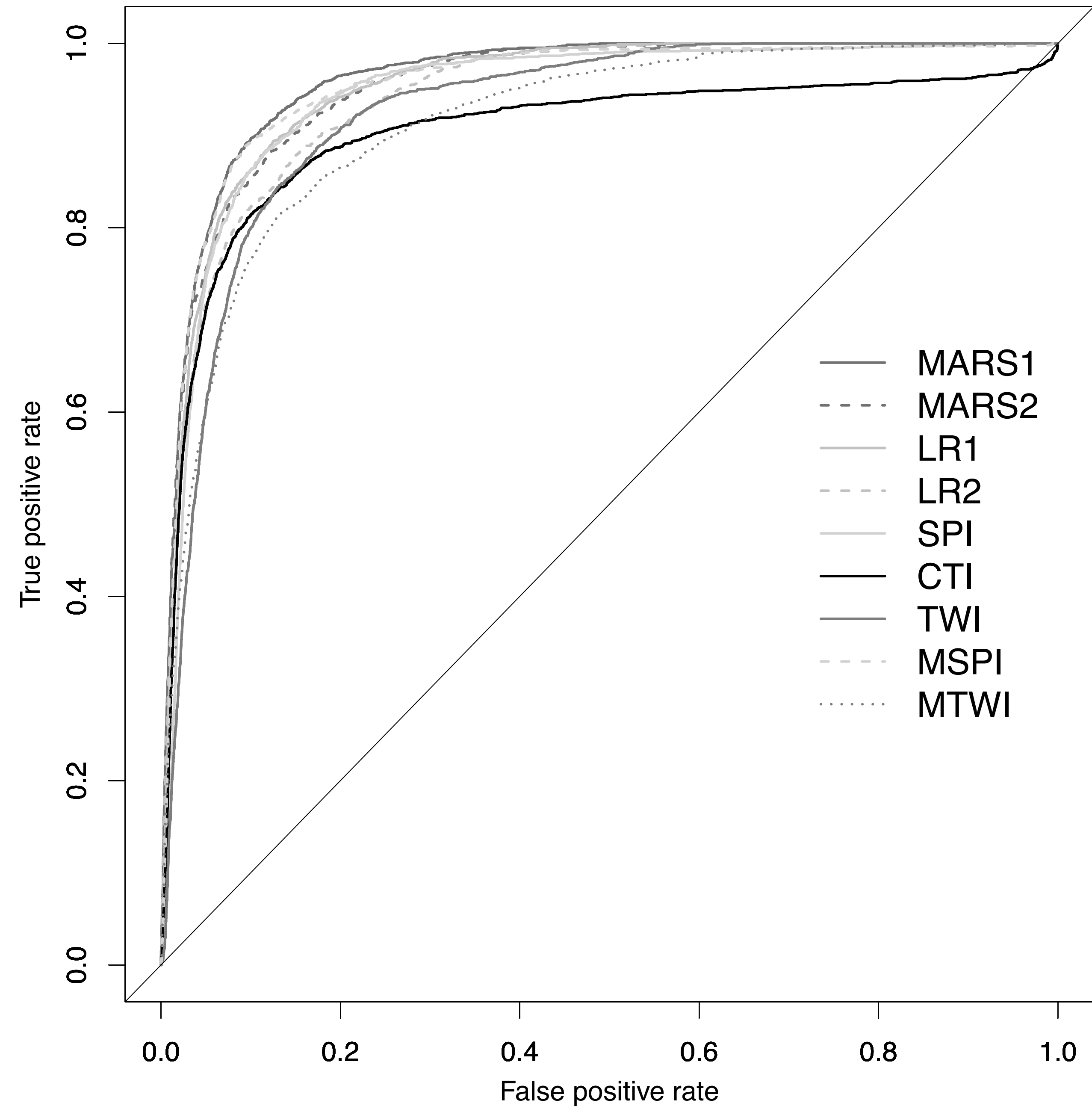
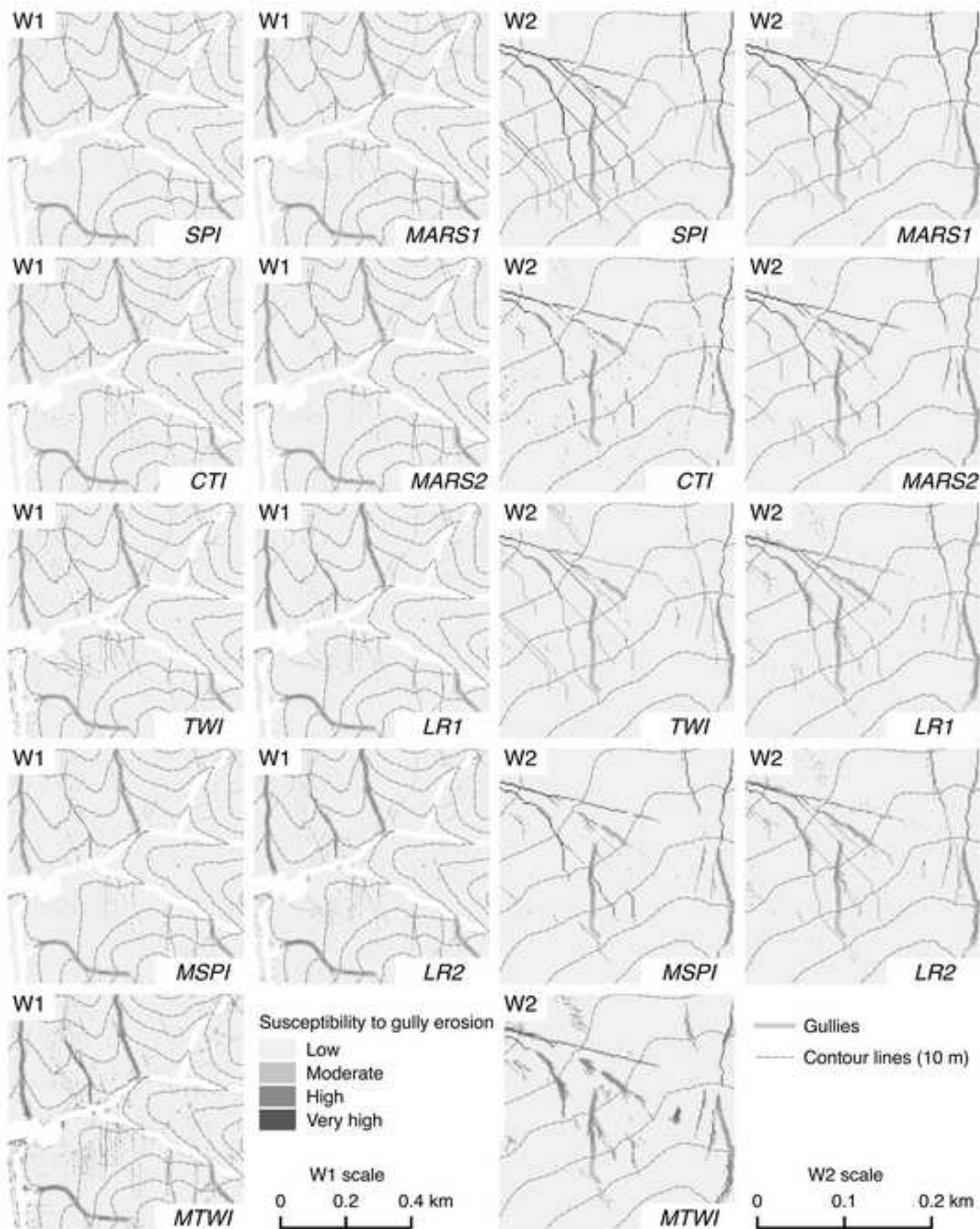
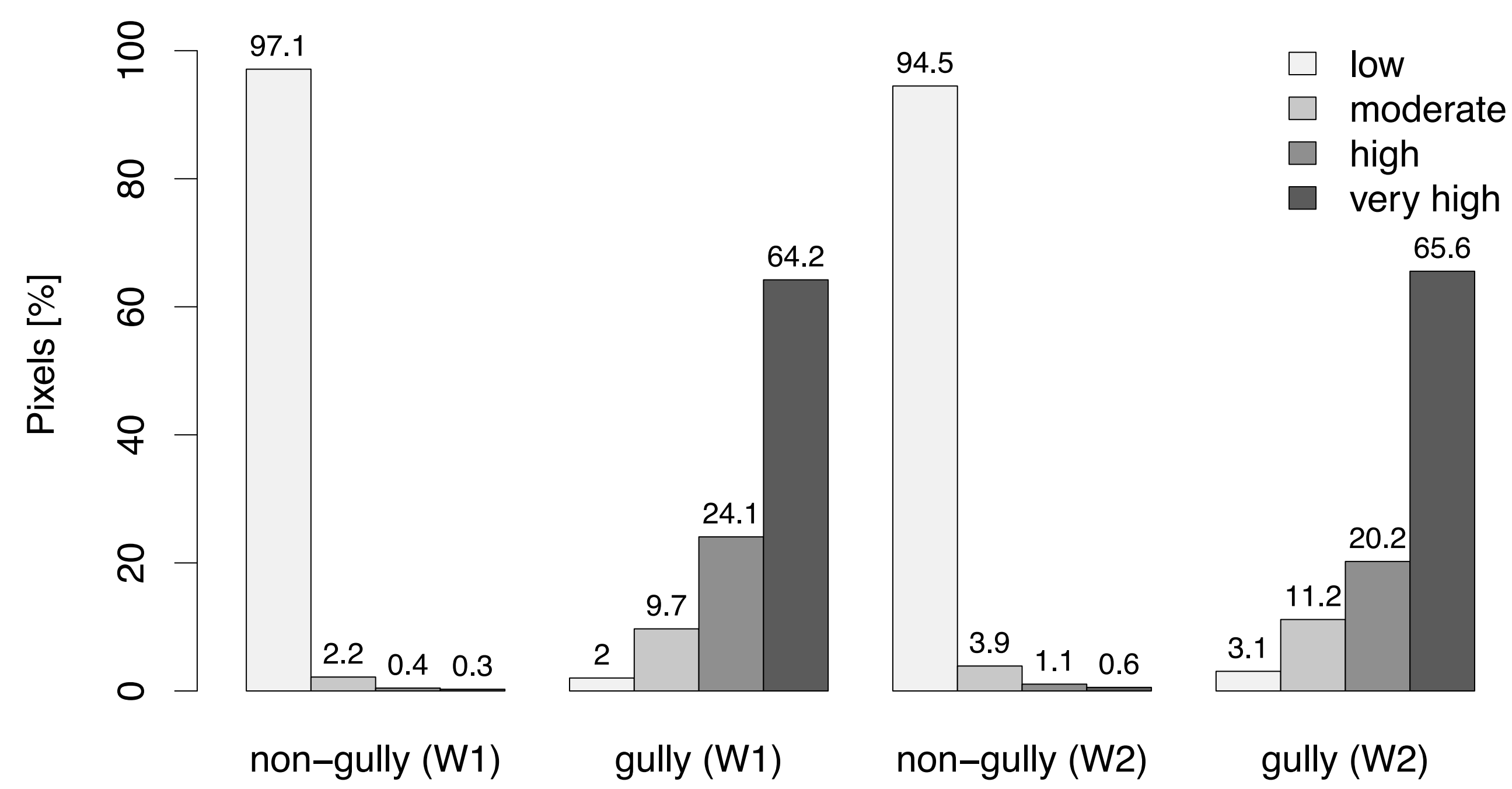
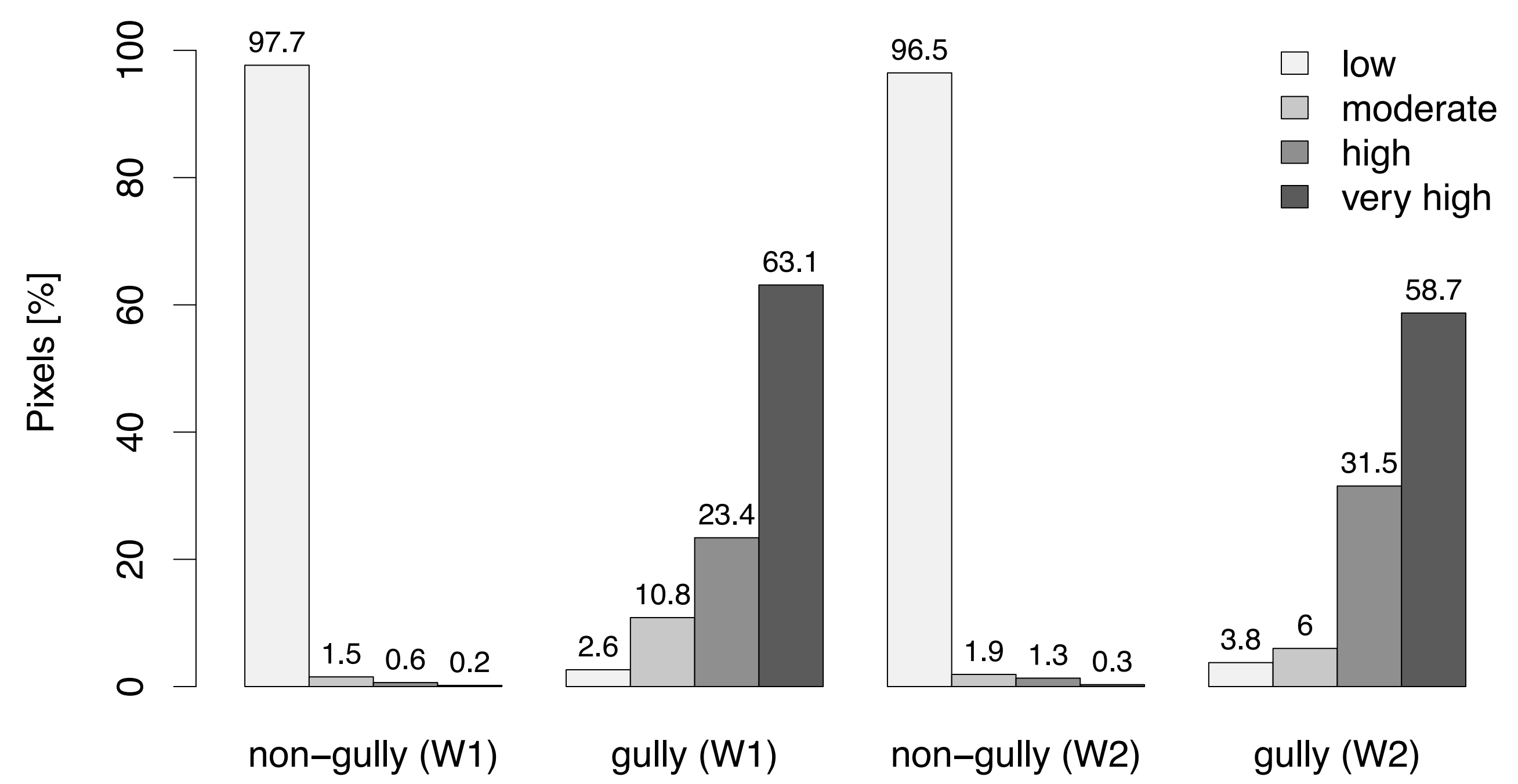
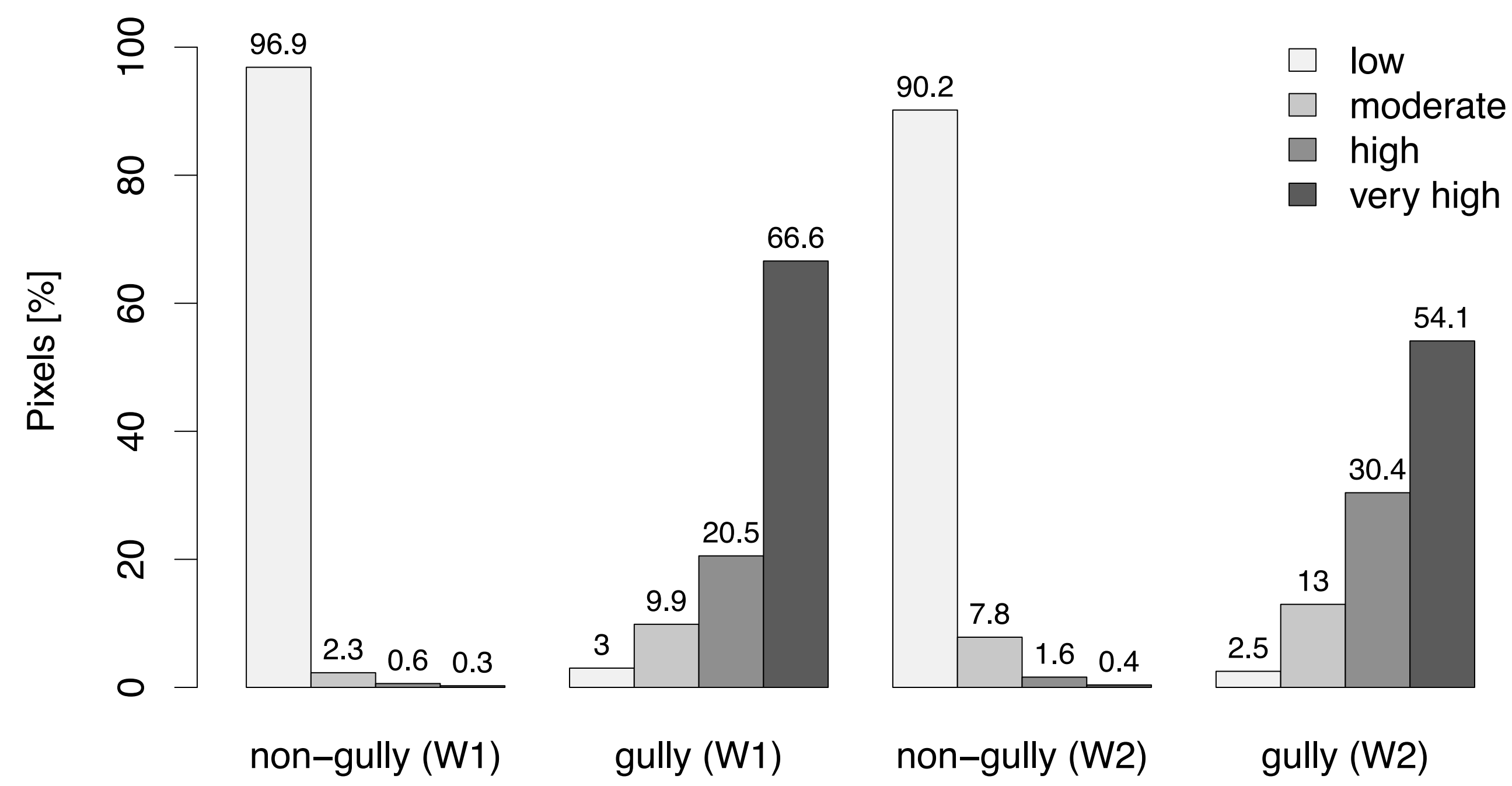
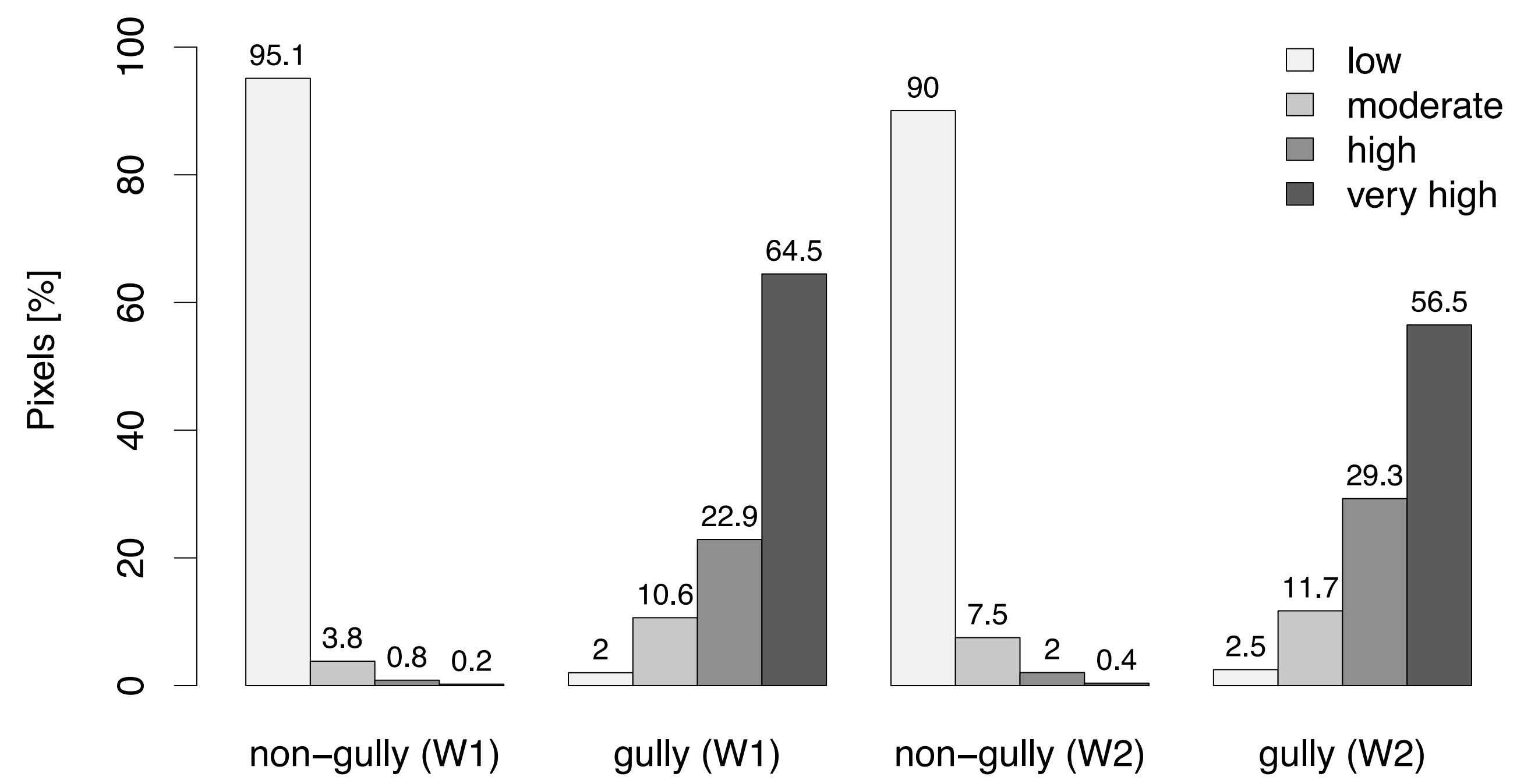
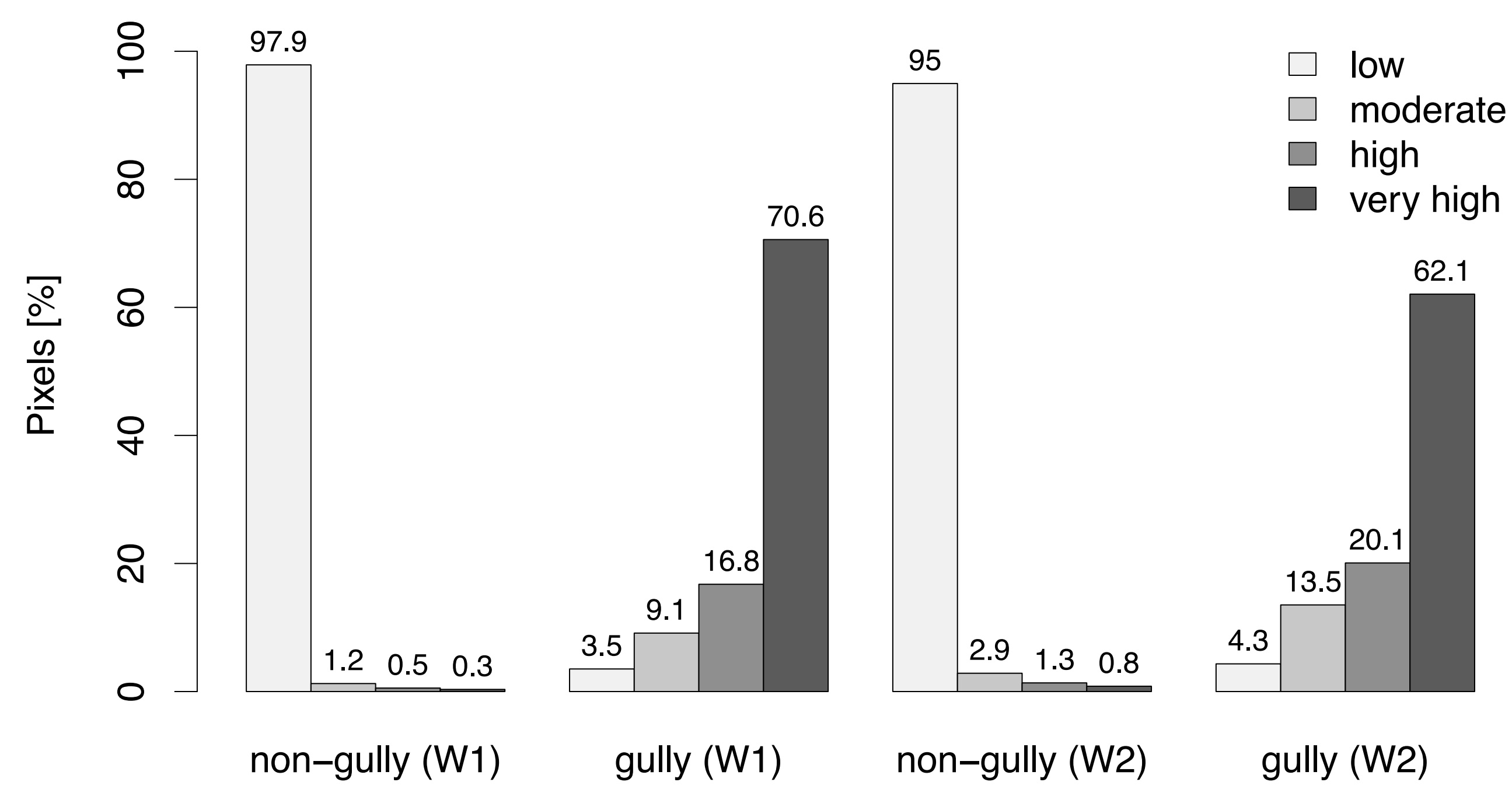
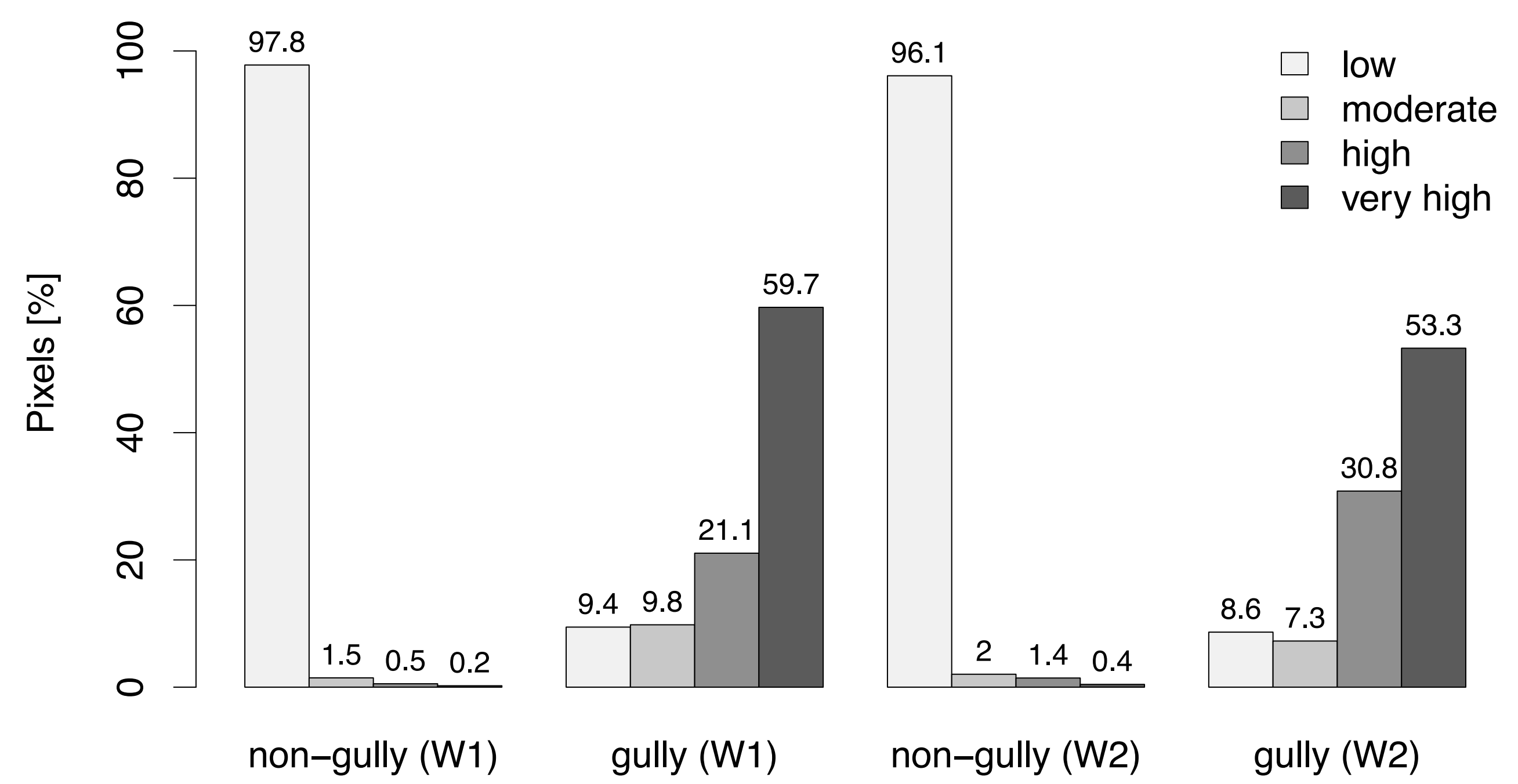
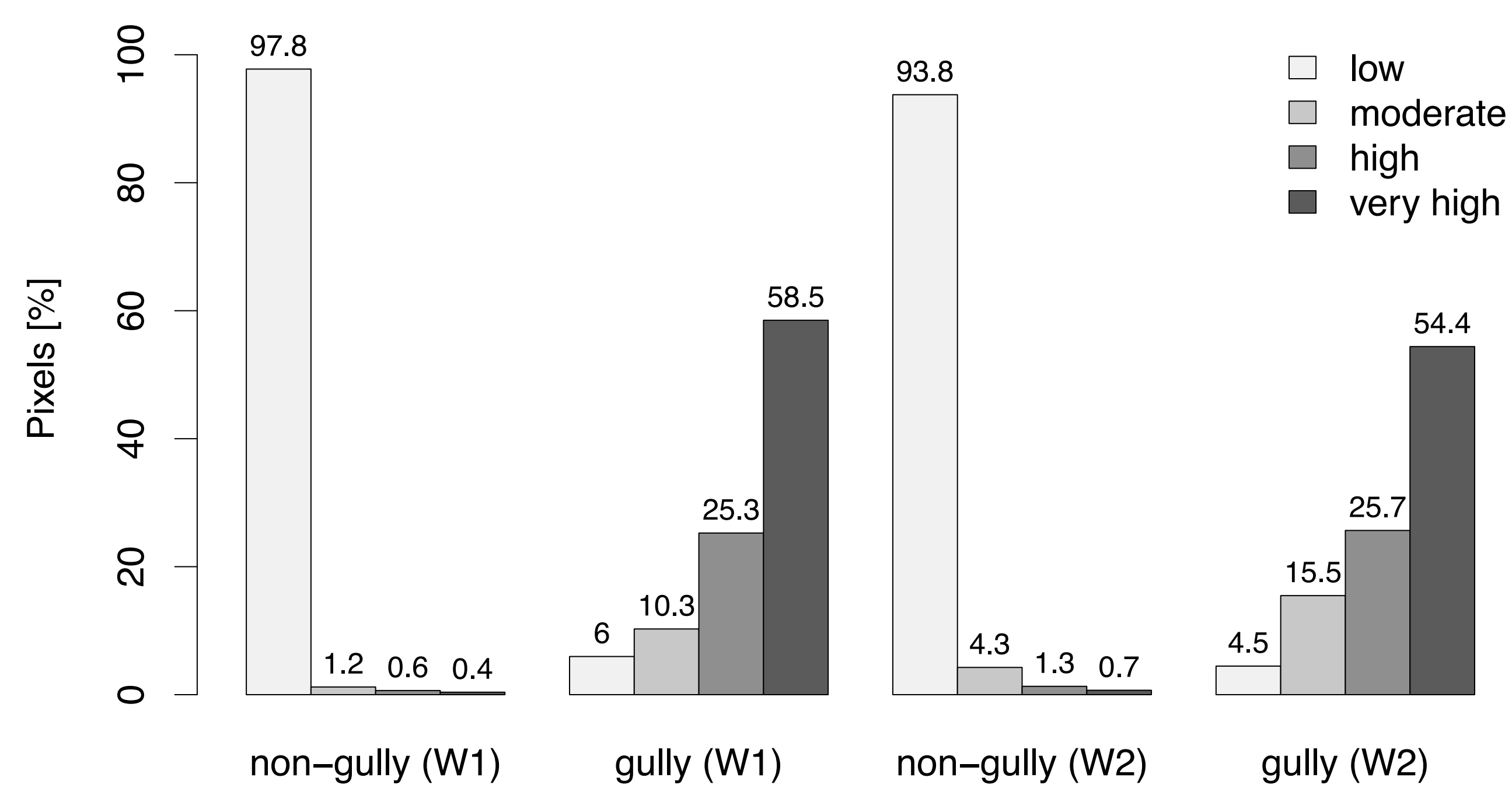
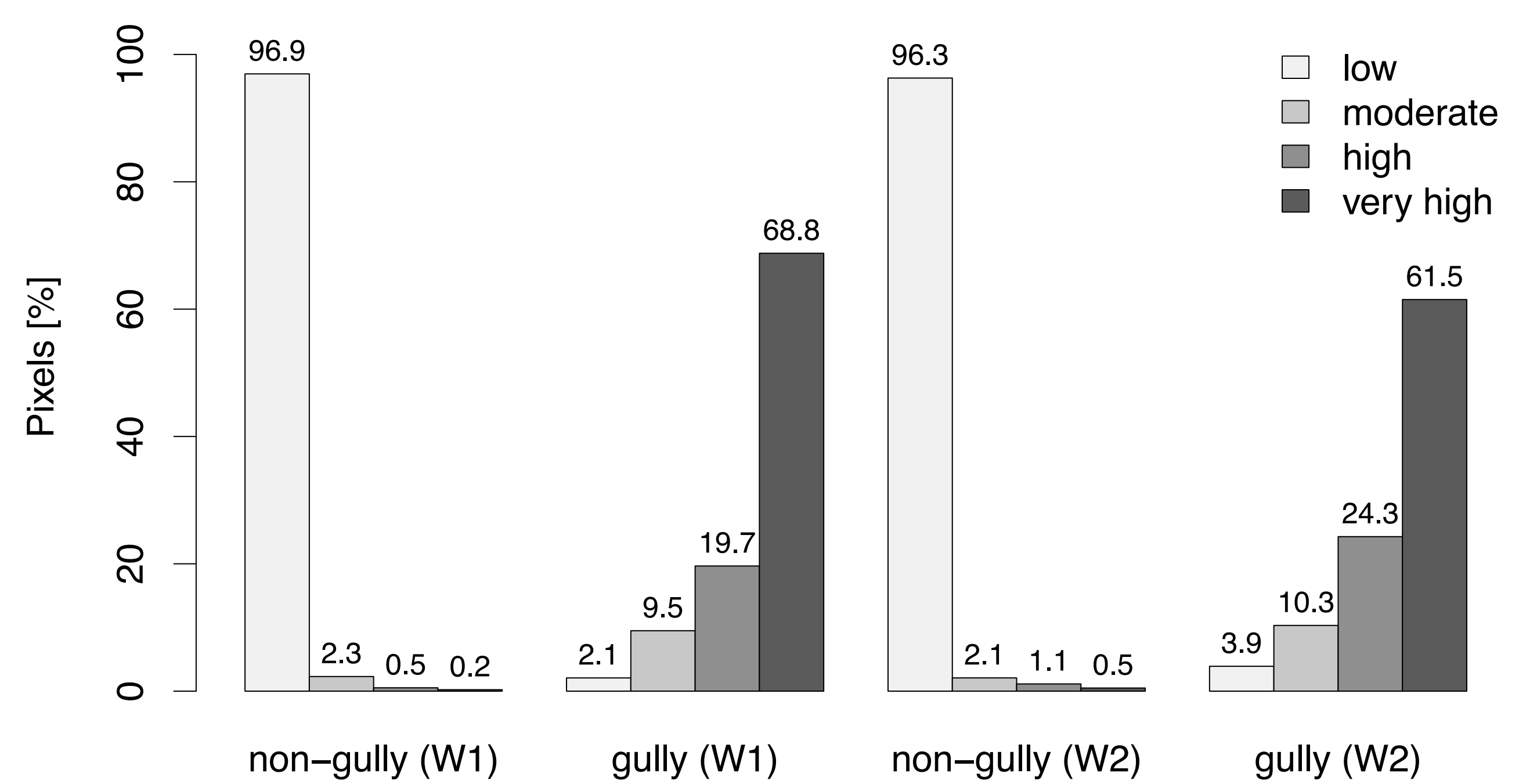
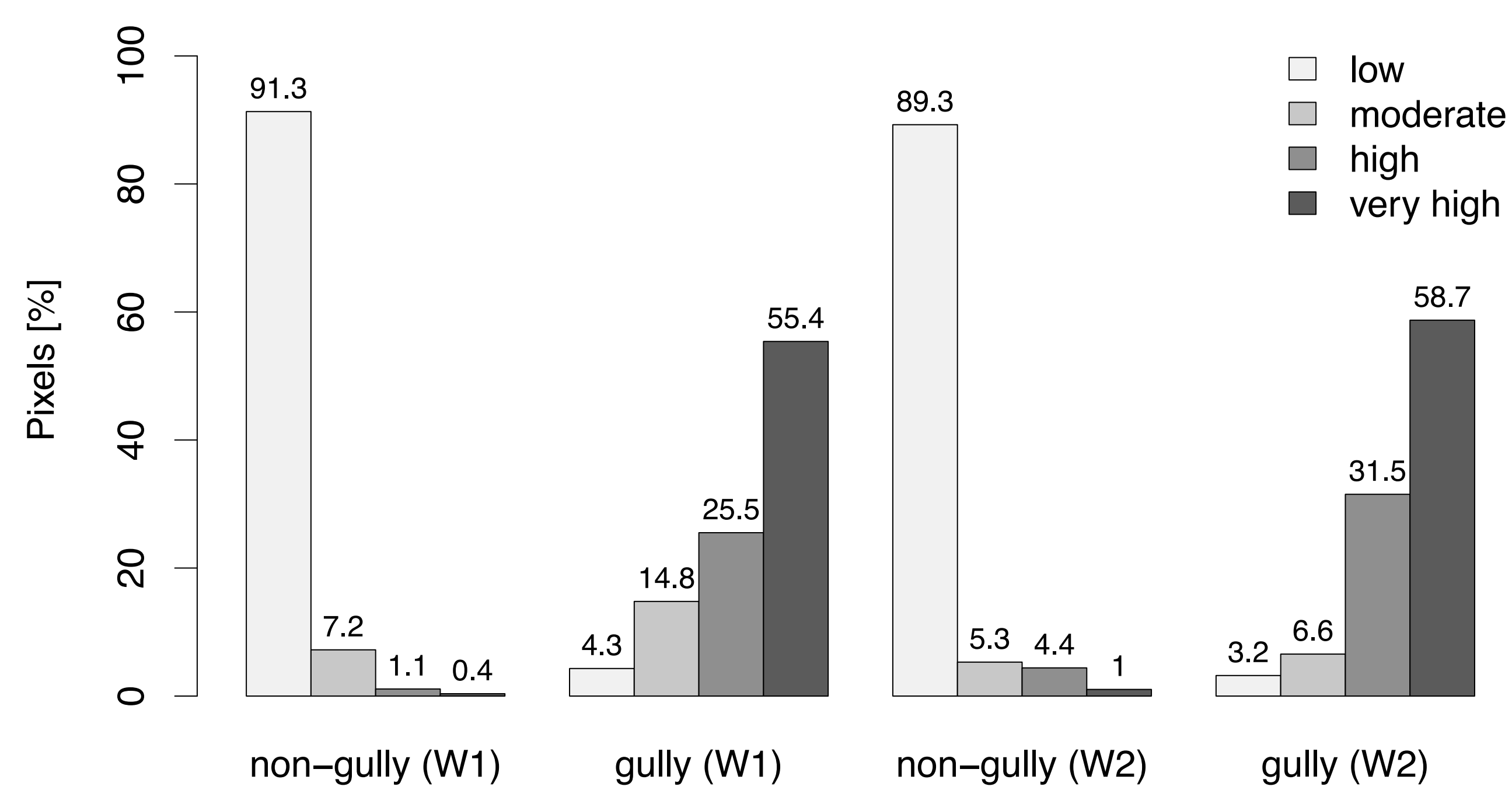


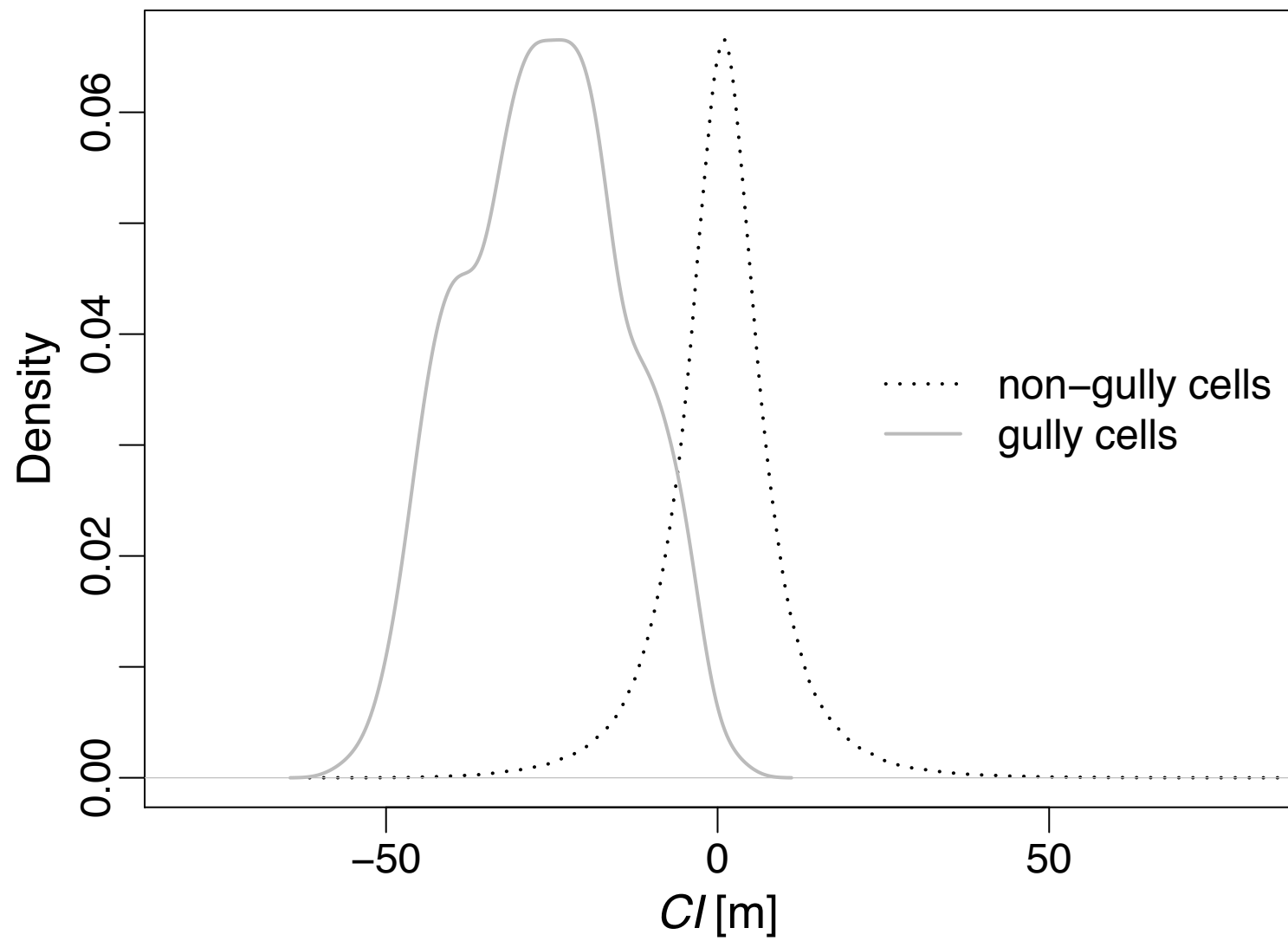
Figure 8 (Greyscale)

[Click here to download high resolution image](#)

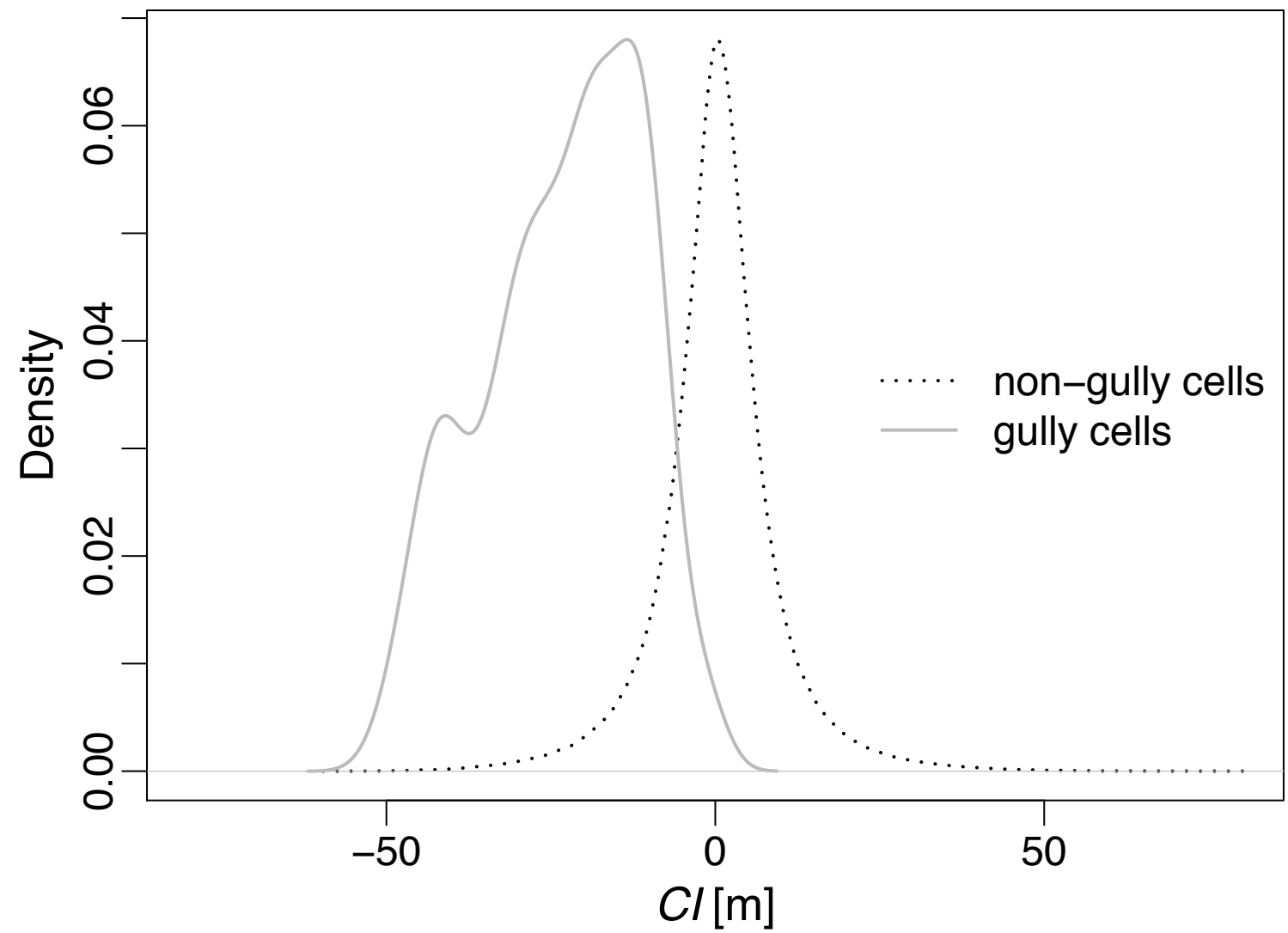


**MARS1 predictive maps****MARS2 predictive maps****LR1 predictive maps****LR2 predictive maps****SPI predictive maps****CTI predictive maps****TWI predictive maps****MSPI predictive maps****MTWI predictive maps**

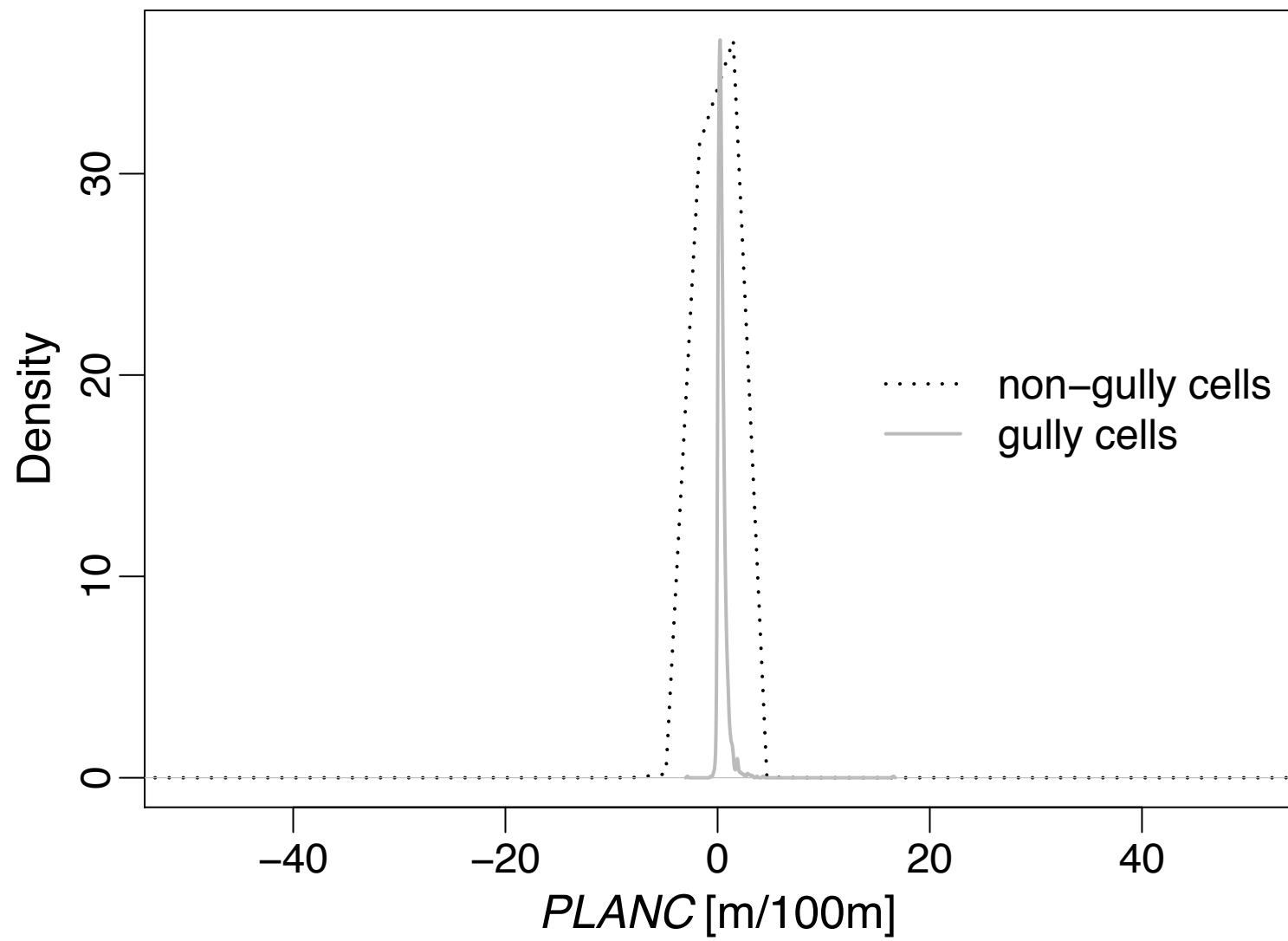
Watershed W1



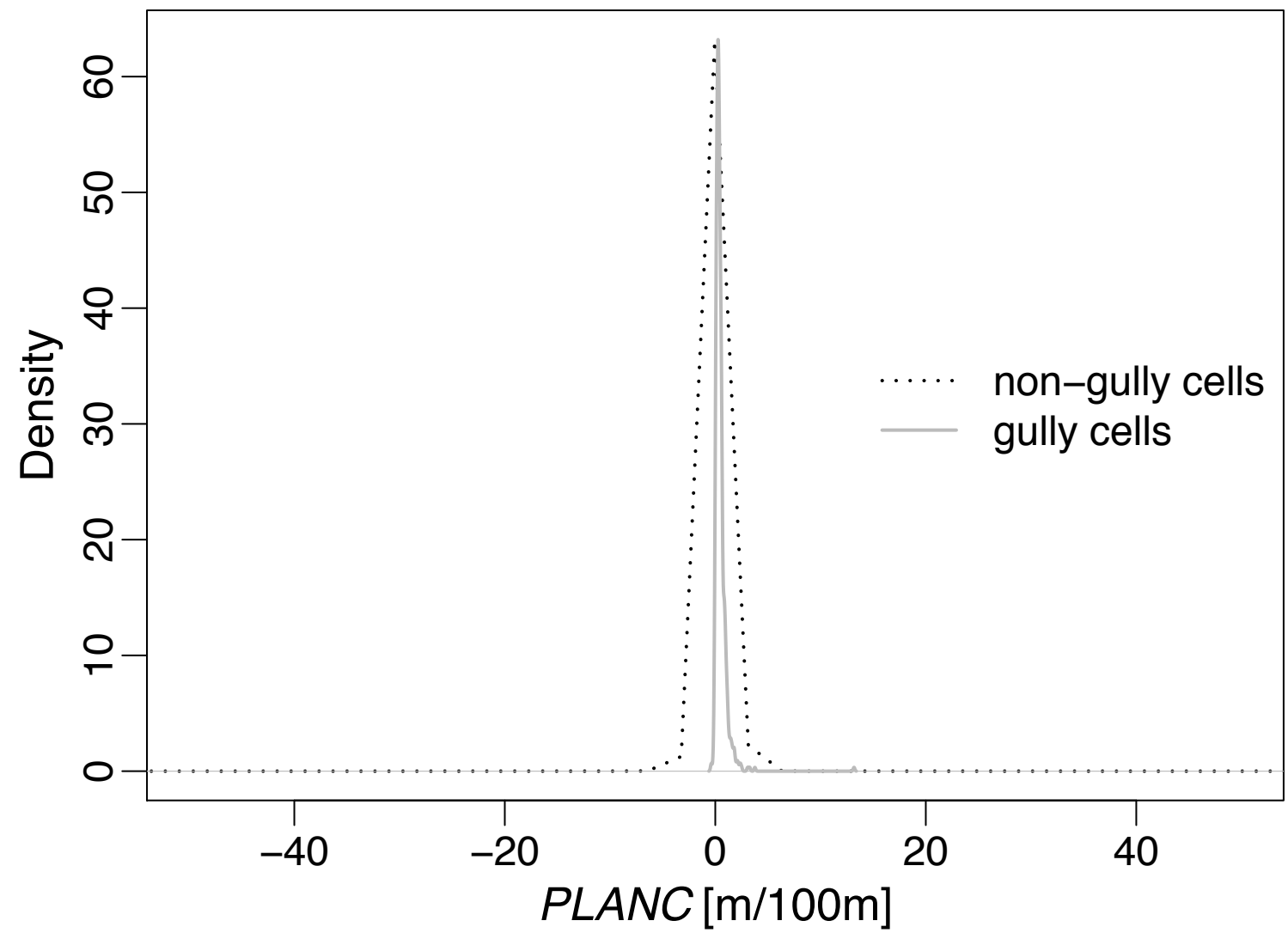
Watershed W2



Watershed W1



Watershed W2



**Declaration of interests**

The authors declare that they have no known competing financial interests or personal relationships that could have appeared to influence the work reported in this paper.

The authors declare the following financial interests/personal relationships which may be considered as potential competing interests: